Stasis, stasis, triple stasis: A theoretical study of cosmological stasis

Keith R. Dienes[1,2,*] Lucien Heurtier,[3,†] Fei Huang,[4,‡] Tim M. P. Tait,[5,§] and Brooks Thomas[6,‖]

[1]*Department of Physics, University of Arizona, Tucson, Arizona 85721 USA*
[2]*Department of Physics, University of Maryland, College Park, Maryland 20742 USA*
[3]*IPPP, Durham University, Durham, DH1 3LE, United Kingdom*
[4]*Department of Particle Physics and Astrophysics, Weizmann Institute of Science, Rehovot 7610001, Israel*
[5]*Department of Physics and Astronomy, University of California, Irvine, California 92697 USA*
[6]*Department of Physics, Lafayette College, Easton, Pennsylvania 18042 USA*

Many theories of physics beyond the Standard Model predict the existence of large or infinite towers of decaying states. In a previous paper [K. R. Dienes *et al.*, Phys. Rev. D **105**, 023530 (2022)], we pointed out that this can give rise to a surprising cosmological phenomenon that we dubbed "stasis" during which the relative abundances of matter and radiation remain constant across extended cosmological eras even though the universe is expanding. Indeed, such stasis epochs are universal attractors, with the universe necessarily entering (and later exiting) such epochs for a wide variety of initial conditions. Matter/radiation stasis is therefore an important and potentially unavoidable feature of many BSM cosmologies. In this paper we extend our arguments to universes containing significant amounts of vacuum energy, and demonstrate that such universes also give rise to various forms of stasis between vacuum energy and either matter or radiation. We also demonstrate the existence of several forms of "triple stasis" during which the abundances of matter, radiation, and vacuum energy all simultaneously remain fixed despite cosmological expansion. We further describe several close variants of stasis which we call "quasi-stasis" and "oscillatory stasis," and discuss the circumstances under which each of these can arise. Finally, we develop a general formalism for understanding the emergence of stasis within BSM cosmologies irrespective of the number or type of different energy components involved. Taken together, these results greatly expand the range of theoretical and phenomenological possibilities for the physics of the early universe, introducing new types of cosmological eras which may play an intrinsic and potentially inevitable role within numerous BSM cosmologies.

I. INTRODUCTION, MOTIVATION, AND BASIC IDEA

Many theories of physics beyond the Standard Model (BSM) predict the existence of infinite towers of unstable states. In theories involving extra spacetime dimensions, such states might be the Kaluza-Klein (KK) states associated with the spectra of quantized momenta in the compactified dimensions. Alternatively, in theories with dark sectors consisting of strongly coupled gauge theories, such states might be the infinite towers of increasingly heavy bound-state resonances. Likewise, in string theory, such towers of states can take the form of not only the Kaluza-Klein and winding-mode states associated with the compactification geometry but also the infinite towers of fundamental string resonances which represent the quantized excitations of the fluctuating strings and branes themselves. In fact, some BSM models can contain mixtures of all of these states, with mass scales that depend on the particular BSM model under study.

In general, such states are likely to be unstable. As a result, they will decay, either to lighter states within the same tower or directly to Standard-Model states. The heavier states will generally decay first since they are likely to have the largest decay widths for a given final state. Likewise, for a given initial state, the largest decay widths will generically arise for decays to the lightest available final states, thereby endowing such states with considerable kinetic energies and rendering them relativistic. Such decay products may therefore be considered as functionally equivalent to radiation. Of course, the detailed properties of such decays will depend on the particular BSM model under study. However, as a general feature, we can expect the different states in our tower to decay *sequentially* to very light states, with the heavier states

---
[*]dienes@arizona.edu
[†]lucien.heurtier@durham.ac.uk
[‡]fei.huang@weizmann.ac.il
[§]ttait@uci.edu
[‖]thomasbd@lafayette.edu

decaying first, then the next-heaviest states, and so forth down the tower. With exceedingly large (or infinite) towers of states, this decay sequence may extend over a significant period of time before finally terminating once the lightest states have decayed.

In Ref. [1], we considered the cosmological implications of such extended decay sequences occurring in the early universe and found that such extended decay sequences can lead to a surprising cosmological phenomenon which we called "stasis." *During this form of stasis, the abundances of matter and radiation in the universe remain constant across extended cosmological epochs even though the universe continues to expand.* At first glance, it might seem that such a phenomenon is impossible. After all, any cosmological epoch consisting of both radiation and matter will transition from radiation dominated to matter dominated, purely as a result of cosmological expansion. This simple observation is a consequence of the fact that the energy density associated with matter scales as a^{-3} where a is the cosmological scale factor, while that of radiation scales as a^{-4}. Thus, as the universe expands, an increasing fraction of the total energy density takes the form of matter rather than radiation, thereby causing the matter abundance to rise and the radiation abundance to fall. However, such a transition from radiation domination to matter domination need not occur if the BSM model in question gives rise to counterbalancing effects which convert matter back into radiation [1–3].

In Ref. [1], we demonstrated that such an extended decay sequence can furnish precisely the sort of counterbalancing effect that is needed, converting matter (in the form of the original infinite towers of heavy states) into radiation (in the form of the decay products, either photons or other highly energetic light states). Indeed, as demonstrated in Ref. [1], this counterbalancing process can persist across many e-folds of cosmological expansion as the decays work their way down the tower. Moreover, this counterbalancing effect can precisely compensate for the effects of cosmological expansion, so that a period of *bona fide* stasis ensues during which the abundances of matter and radiation remain constant throughout this entire epoch. Quite remarkably, this possibility requires no fine-tuning and actually emerges as a *global attractor* within the relevant cosmological framework [1–3]. Moreover, despite this attractor behavior, we demonstrated in Ref. [1] that such matter/radiation stasis epochs ultimately have a finite duration, ending naturally when the lightest states at the bottom of the tower decay. Thus, the universe not only *enters* into a stasis epoch but also *emerges* from it in a natural way. Indeed, a similar kind of stasis between matter and radiation can also arise through the decays of primordial black holes [2,3].

The primary goal of this paper is to extend this discussion to include universes which contain significant amounts of *vacuum energy*. First, we will investigate the extent to which BSM physics can give rise to a two-component stasis within a universe consisting of vacuum energy and matter. We will then seek to understand whether we can similarly achieve a two-component stasis between vacuum energy and radiation. Finally, we will go for broke and ask whether it is possible to have a "triple stasis" in which vacuum energy, matter, and radiation can all simultaneously be in stasis with each other. Equally importantly, we will also investigate whether such forms of stasis require fine-tuning, or whether they follow the example of matter/radiation stasis and also emerge as cosmological attractors. We will also construct a "phase diagram" for stasis which will enable us to understand how all of these different forms of stasis can merge and transition between each other as we change the underlying parameters within our BSM models.

Ultimately, we shall find that all of these new forms of stasis can indeed exist and emerge naturally from BSM physics. This in turn reinforces our belief that the stasis phenomenon is in fact a fairly generic and robust feature in certain types of cosmologies involving BSM physics.

One important subtlety in our work concerns the manner in which we incorporate vacuum energy into our discussion of stasis. At first glance, it might seem that vacuum energy can be treated simply as just another cosmological fluid whose pressure p and energy density ρ are related via the equation of state $p = -\rho$ (i.e., with an equation-of-state parameter $w = -1$). However, as we shall discuss, naïvely taking $w = -1$ leads to a slew of important mathematical and physical complications. For this reason, one important aspect of our work is to develop a method in which we might successfully model vacuum energy. However, as we shall demonstrate here and in Ref. [4], stasis is possible and emerges naturally regardless of the particular manner in which vacuum energy is modeled.

How to model vacuum energy is not the only subtlety we shall encounter. For example, we shall find that there are often multiple ways of performing certain critical calculations. While some methods work best in certain contexts, other methods work best in other contexts. Accordingly, with an eye towards potential future applications of our work, in this paper we shall outline all relevant methods of performing certain calculations and demonstrate how they relate to each other.

This paper is organized as follows. First, in Sec. II A, we review the results of Ref. [1] which focused on stasis between matter and radiation. We do this not only as review, but also in order to establish our overall notation and calculational procedures. In Sec. II B, we then extract certain general lessons from this example—general lessons which will prove critical later in this paper as we expand the scope of our analysis. Then, in Sec. III, we begin our discussion of how vacuum energy may be introduced into this picture. It is here that we discuss the subtleties associated with the introduction of vacuum energy into the stasis framework, but we ultimately demonstrate that a

similar stasis can be achieved between vacuum energy and matter once these subtleties are satisfactorily addressed. In Sec. IV we then demonstrate that a similar pairwise stasis can exist between vacuum energy and radiation. Finally, we conclude our discussion of pairwise stases in Sec. V by outlining various elements of their common algebraic structure.

Section VI in some sense serves as the central focal point of this paper. In this section, pulling together our results from previous sections and extending them in certain critical ways, we demonstrate that we can even achieve a *triple stasis* involving vacuum energy, matter, and radiation simultaneously. As we shall see, this is a highly nontrivial result because the existence of three different pairwise stases between three different energy components does not generally imply the existence of a triple stasis amongst them all simultaneously. Indeed, we shall find that several additional constraints must be satisfied in order to allow such a triple stasis to exist. Fortunately, these constraints are not severe, and many BSM cosmologies give rise to triple stasis as well.

In Sec. VII, we then turn our attention to the attractor behavior associated with these new forms of stasis. We ultimately find that all of the stasis solutions we examine in this paper are indeed global attractors. Likewise, in Sec. VIII, we present a "phase diagram" for the stasis phenomenon and demonstrate how the different types of stasis we have examined in this paper are actually different "phases" of the same stasis phenomenon in different limits of the underlying parameter space.

Along the way we also develop a general formalism which enables a general study of stasis regardless of the number and types of different energy components involved. In this way we also isolate the underlying ingredients that allow stasis to exist. With these insights in hand, in Sec. IX we then investigate what happens when some, but not all, of these ingredients are present. In this way, we discover several new "variants" of the original stasis idea. One of these, discussed in Sec. IX A, is a new theoretical possibility in which the cosmological abundances of different energy components are not strictly constant but instead exhibit highly suppressed time evolution. This too is not seen in the standard cosmological timelines, but may also represent a valid possibility for early-universe physics in certain situations. We shall refer to this phenomenon as *quasi-stasis*. We also discover a different variant of stasis— one in which the abundances are again not constant but instead *oscillate* around their central stasis values. This phenomenon, which we shall call *oscillatory stasis*, is discussed in Sec. IX B. Yet another possibility is discussed in Sec. IX C. We then make concluding remarks and present ideas for further research in Sec. X.

Just as in Ref. [1], our main interest in this paper is the stasis phenomenon itself—i.e., the existence of stable mixed-component cosmological eras—and the manner in which such cosmologies emerge from BSM physics. Needless to say, phenomenological constraints may make it difficult for an epoch of stasis to appear within certain portions of the standard ΛCDM cosmological timeline (particularly those near or after big-bang nucleosynthesis). Indeed, such phenomenological constraints in turn might be used in order to constrain the range of possible BSM theories governing physics at higher energy scales. However, other regions of parameter space may be able to accommodate stasis epochs without difficulty. In this paper we shall therefore study our BSM-inspired realizations of stasis as general theoretical phenomena, and defer discussion of their various phenomenological implications and constraints to future work. That said, the emergence of these different forms of stasis within BSM cosmologies gives rise to a host of new theoretical and phenomenological possibilities for early-universe model-building across the entire cosmological timeline. Such possibilities are therefore ripe for future exploration.

II. MATTER/RADIATION STASIS

In this section we begin by reviewing the results of Ref. [1] concerning the possibility of stasis between matter and radiation. As discussed in the Introduction, our purpose for including this review is two-fold. First, our analyses of each kind of stasis that we shall be discussing in subsequent sections can be patterned after our discussion of this case. This section will therefore introduce the main ideas and establish our notation. But second, we shall find that many of the ingredients of this matter/radiation stasis will become part of the larger triple-stasis structure that we shall eventually construct in Sec. VI. Thus it will be important to recall the details of this case before proceeding further.

A. Algebraic analysis

We begin, as in Ref. [1], by assuming a flat Friedmann-Robertson-Walker (FRW) universe containing two components: a tower of matter states ϕ_ℓ where the indices $\ell = 0, 1, 2, \ldots, N-1$ are assigned in order of increasing mass; and radiation (collectively denoted γ) into which the ϕ_ℓ can decay. This radiation may consist of photons or other highly relativistic particles. We shall let ρ_ℓ and ρ_γ denote the corresponding energy densities and Ω_ℓ and Ω_γ the corresponding abundances. We shall also assume that the dominant decay mode of the ϕ_ℓ is into radiation, and let Γ_ℓ denote the corresponding decay rates. Note that in this section we shall not require that the ϕ_ℓ components be scalars, and indeed any (nonrelativistic) matter fields are acceptable. We shall also implicitly assume that N is large (or potentially even infinite).

Recall that for any energy density ρ_i (where i denotes matter, radiation, or vacuum energy), the corresponding abundance Ω_i is given by

$$\Omega_i \equiv \frac{8\pi G}{3H^2} \rho_i, \qquad (2.1)$$

where H is the Hubble parameter and G is Newton's constant. From this it follows that

$$\frac{d\Omega_i}{dt} = \frac{8\pi G}{3}\left(\frac{1}{H^2}\frac{d\rho_i}{dt} - 2\frac{\rho_i}{H^3}\frac{dH}{dt}\right). \qquad (2.2)$$

We can simplify this expression through the use of the Friedmann "acceleration" equation for dH/dt, which in a universe consisting of only matter and radiation takes the form

$$\begin{aligned}
\frac{dH}{dt} &= -H^2 - \frac{4\pi G}{3}\left(\sum_i \rho_i + 3\sum_i p_i\right) \\
&= -\frac{1}{2}H^2(2 + \Omega_M + 2\Omega_\gamma) \\
&= -\frac{1}{2}H^2(4 - \Omega_M).
\end{aligned} \qquad (2.3)$$

Note that in passing to the second line we have defined the total matter abundance $\Omega_M \equiv \sum_\ell \Omega_\ell$, and in passing to the third line we have imposed the constraint $\Omega_M + \Omega_\gamma = 1$, as suitable for a universe containing only these two energy components. Substituting Eq. (2.3) into Eq. (2.2) we then obtain

$$\frac{d\Omega_i}{dt} = \frac{8\pi G}{3H^2}\frac{d\rho_i}{dt} + H\Omega_i(4 - \Omega_M), \qquad (2.4)$$

whereupon taking $i = M$ (for the total matter abundance) or $i = \gamma$ (for the total radiation abundance) yields

$$\begin{aligned}
\frac{d\Omega_M}{dt} &= \frac{8\pi G}{3H^2}\sum_\ell \frac{d\rho_\ell}{dt} + H\Omega_M(4 - \Omega_M), \\
\frac{d\Omega_\gamma}{dt} &= \frac{8\pi G}{3H^2}\frac{d\rho_\gamma}{dt} + H\Omega_\gamma(4 - \Omega_M).
\end{aligned} \qquad (2.5)$$

These are thus general relations for the time evolution of Ω_M and Ω_γ in terms of $d\rho_\ell/dt$ and $d\rho_\gamma/dt$ in a universe consisting of matter and radiation.

Given the relations in Eq. (2.5), our final step is to insert appropriate "equations of motion" for $d\rho_\ell/dt$ and $d\rho_\gamma/dt$. Since each ϕ_ℓ is assumed to decay into radiation γ with rate Γ_ℓ, and given that each decay process conserves energy, these equations of motion are given by

$$\begin{aligned}
\frac{d\rho_\ell}{dt} &= -3H\rho_\ell - \Gamma_\ell \rho_\ell, \\
\frac{d\rho_\gamma}{dt} &= -4H\rho_\gamma + \sum_\ell \Gamma_\ell \rho_\ell.
\end{aligned} \qquad (2.6)$$

While the final term on each line reflects the effects of the decays, the first term on the right side of each line reflects the redshifting effects of cosmological expansion for matter and radiation respectively. Given these expressions for $d\rho_\ell/dt$ and $d\rho_\gamma/dt$, we find that Eq. (2.5) then takes the form

$$\frac{d\Omega_M}{dt} = -\sum_\ell \Gamma_\ell \Omega_\ell + H(\Omega_M - \Omega_M^2) \qquad (2.7)$$

with $d\Omega_\gamma/dt = -d\Omega_M/dt$.

We are seeking a steady-state "stasis" solution in which Ω_M and Ω_γ are constant. Clearly such a solution will arise if the effects of the ϕ_ℓ decays are precisely counterbalanced by the cosmological expansion. We therefore wish to impose, at the very minimum, the condition that $d\Omega_M/dt = 0$, which from Eq. (2.7) yields the constraint

$$\sum_\ell \Gamma_\ell \Omega_\ell = H(\Omega_M - \Omega_M^2). \qquad (2.8)$$

However, it is not sufficient for this condition to hold only for an instant of time—we want this condition to hold over an extended *interval* of time. In order to achieve this, we shall actually demand something stronger, namely that this condition hold for *all* times t. In imposing this latter constraint we are actually implicitly demanding an *eternal* stasis, one without beginning or end. However, once we understand the conditions that characterize such an eternal stasis state, we shall then discuss the physics that will actually restrict this stasis state to finite duration, essentially introducing not only a natural *entrance* into the stasis state but also a natural *exit* from it.

Demanding that Eq. (2.8) hold for all time requires not only that this equation hold at one given time, but also that both sides of this equation have precisely the same time dependence when the abundances are held fixed (which is the defining property of the stasis configuration we are hoping to understand). Let us therefore assume that Ω_M and Ω_γ are fixed to their stasis values $\bar{\Omega}_M$ and $\bar{\Omega}_\gamma$. Under these stasis conditions, we can actually solve for the Hubble parameter directly via Eq. (2.3), obtaining the exact solution

$$H(t) = \left(\frac{2}{4 - \bar{\Omega}_M}\right)\frac{1}{t} \quad \Rightarrow \quad \bar{\kappa} = \frac{6}{4 - \bar{\Omega}_M} \qquad (2.9)$$

where $\bar{\kappa}$ generally corresponds to the parametrization $H(t) = \bar{\kappa}/(3t)$ during stasis. Indeed, from Eq. (2.9) we verify the standard results that $H(t) = 2/(3t)$ for $\bar{\Omega}_M = 1$ (i.e., for a matter-dominated universe), while $H(t) = 1/(2t)$ for $\bar{\Omega}_M = 0$ (i.e., for a radiation-dominated universe). Substituting Eq. (2.9) into Eq. (2.8) then yields our matter/radiation stasis condition

$$\sum_\ell \Gamma_\ell \Omega_\ell(t) = \frac{\bar{\kappa}}{3} \bar{\Omega}_M (1 - \bar{\Omega}_M) \frac{1}{t}$$

$$= (2 - \bar{\kappa}) \bar{\Omega}_M \frac{1}{t}, \qquad (2.10)$$

where the individual matter abundances $\Omega_\ell(t)$ within this eternal-stasis cosmology are given by

$$\Omega_\ell(t) = \Omega_\ell^* \left(\frac{t}{t_*} \right)^{2-\bar{\kappa}} e^{-\Gamma_\ell(t - t^{(0)})}. \qquad (2.11)$$

Here t_* is some fiducial time within this stasis epoch, while $\Omega_\ell^* \equiv \Omega_\ell(t_*)$ and $\bar{\Omega}_M \equiv \sum_\ell \Omega_\ell(t)$ for all t. By contrast, the quantity $t^{(0)}$ within Eq. (2.11) denotes the (presumed common) production time for the ϕ_ℓ states, and thus serves as the zero of the clock according to which the decay lifetimes of these states are measured.

Of course, given our tower of components ϕ_ℓ, the condition in Eq. (2.10) cannot be strictly satisfied for all times. Thus, we cannot truly have an eternal stasis. For example, regardless of whether the tower of ϕ_ℓ states is finite or infinite, there is an early time immediately after these states are produced at $t^{(0)}$ during which the decay process is just beginning and thus will not yet have grown sufficient to counterbalance cosmological expansion. Indeed, the very presence of a production time $t^{(0)}$ within Eq. (2.11) in some sense invalidates the assumption of a truly eternal stasis. Likewise, there will eventually come a time at which all of the decays will have essentially concluded, at which point we expect our period of stasis to end. However, the critical issue is whether there exist solutions for the spectrum of decay widths $\{\Gamma_\ell\}$ and abundances $\{\Omega_\ell\}$ across our tower of states which will lead to an extended period of stasis *during* the sequential decay process.

Our assertion in this paper is that many well-motivated theories of physics beyond the Standard Model give rise to towers of states with exactly this property. In order to study this question in a general way, we observe—as discussed in the Introduction and in Ref. [1]—that many well-motivated BSM theories give rise to infinite towers of states ϕ_ℓ whose decay widths and initial abundances either exactly or approximately satisfy scaling relations of the forms

$$\Gamma_\ell = \Gamma_0 \left(\frac{m_\ell}{m_0} \right)^\gamma, \qquad \Omega_\ell^{(0)} = \Omega_0^{(0)} \left(\frac{m_\ell}{m_0} \right)^\alpha, \qquad (2.12)$$

where α and γ are general scaling exponents, where the ϕ_ℓ mass spectrum takes the form

$$m_\ell = m_0 + (\Delta m)\ell^\delta \qquad (2.13)$$

with $m_0 \geq 0$, $\Delta m > 0$, and $\delta > 0$ all treated as general free parameters, and where the superscript "(0)" within

Eq. (2.12) denotes the time $t = t^{(0)}$ at which the ϕ_ℓ states are initially produced (thereby setting a common clock for the subsequent ϕ_ℓ decays). For example, if the ϕ_ℓ are the KK excitations of a five-dimensional scalar field compactified on a circle of radius R (or a $\mathbb{Z}_2$ orbifold thereof), we will have either $\{m_0, \Delta m, \delta\} = \{m, 1/R, 1\}$ or $\{m_0, \Delta m, \delta\} = \{m, 1/(2mR^2), 2\}$, depending on whether $mR \ll 1$ or $mR \gg 1$, respectively, where m denotes the four-dimensional scalar mass [5,6]. Alternatively, if the ϕ_ℓ are the bound states of a strongly coupled gauge theory, we have $\delta = 1/2$, where Δm and m_0 are determined by the Regge slope and intercept of the strongly coupled theory, respectively [7]. The same values also describe the excitations of a fundamental string. Thus $\delta = \{1/2, 1, 2\}$ can serve as compelling "benchmark" values. Likewise, the exponent γ is ultimately governed by the particular ϕ_ℓ decay mode. For example, we will have $\gamma = 2d - 7$ if each ϕ_ℓ state decays to photons through a dimension-d contact operator of the form $\mathcal{O}_\ell \sim c_\ell \phi_\ell \mathcal{F}/\Lambda^{d-4}$ where Λ is an appropriate mass scale and where $\mathcal{F}$ is an operator built from photon fields. Thus, values such as $\gamma = \{3, 5, 7\}$ serve as relevant benchmarks. Indeed, $\gamma = 1$ is also relevant in cases in which ϕ_ℓ are scalars decaying into fermions. Finally, α is determined by the original production mechanism for the ϕ_ℓ fields. For example, it is easy to see that $\alpha < 0$ for misalignment production [5,6], while α can generally be of either sign for thermal freeze-out [8].

Our goal will then be to determine for which combinations of these scaling exponents (α, γ, δ) and other dimensionful parameters $(m_0, \Delta m, \Gamma_0, \Omega_0^{(0)})$ an extended stasis state may arise. In this way, through a general study of these scaling exponents and dimensionful parameters, we can survey the effects of many different BSM theories at once. Of course, within the context of this model, we shall assume that $\Omega_M = 1$ at $t = t^{(0)}$ before the decay process has begun. This reflects the fact that no radiation has yet been generated at $t = t^{(0)}$, and that our universe at that time consists of only the initial ϕ_ℓ states. This in turn requires that we choose the overall normalization $\Omega_0^{(0)} = \left[\sum_{\ell=0}^{N-1} (m_\ell/m_0)^\alpha \right]^{-1}$.

For future use, it will prove convenient to define two different dimensionless combinations of the above parameters:

$$\eta \equiv \alpha + \frac{1}{\delta}, \qquad \xi \equiv \frac{2}{\bar{\kappa}} \frac{m_0}{\Gamma_0}. \qquad (2.14)$$

Roughly speaking, we shall find that η describes how the energy density scales per unit mass across the tower, while ξ describes the decay rates of our tower components (as parametrized through Γ_0) relative to the overall rate of cosmological expansion during stasis (as parametrized through $\bar{\kappa}$). Indeed many of our future results will depend directly on these two quantities. Unlike η, however, we

shall find that ξ makes its appearance in our equations only after our system has reached stasis. It is for this reason that ξ has been defined directly in terms of $\bar{\kappa}$ rather than κ itself. Thus ξ has a fixed value during stasis.

Given the scaling relations in Eqs. (2.12) and (2.13), we can now evaluate the conditions for stasis by evaluating the sum which appears on the left side of our constraint equation in Eq. (2.10). Let us first focus on the behavior of $\Omega_\ell(t)$. In Eq. (2.11), we provided an expression for $\Omega_\ell(t)$ in terms of a fiducial time t_* already within stasis, but in order to connect with the abundance-scaling relation in Eq. (2.12) we would like to replace t_* with the production time $t^{(0)}$. However, the expression in Eq. (2.11) assumed an eternal stasis that was already in effect at the fiducial time t_*. Indeed, it is for this reason that we were able to assume within Eq. (2.11) that $\Omega_\ell(t)$ accrues a net gravitational redshift factor $(t/t_*)^{2-\bar{\kappa}}$ between t_* and t. However, as discussed above, these assumptions will no longer be true if t_* is replaced by $t^{(0)}$, since we now expect that stasis will not emerge until some time after $t^{(0)}$.

For simplicity and generality, we shall therefore let $h(t_i, t_f)$ denote the net gravitational redshift factor that accrues between any two times t_i and t_f. We thus have

$$\Omega_\ell(t) = \Omega_\ell^{(0)} h(t^{(0)}, t) e^{-\Gamma_\ell(t - t^{(0)})}. \qquad (2.15)$$

Note that this h-factor is necessarily ℓ-independent since the gravitational redshift affects all components equally. It turns out that there are important subtleties associated with our use of an h-factor in this way, but these subtleties will not affect our results. We shall therefore defer a more detailed discussion of this h-factor until Sec. VI E. However, given Eq. (2.15), we then find that

$$\sum_\ell \Gamma_\ell \Omega_\ell(t) = \Gamma_0 \Omega_0^{(0)} h(t^{(0)}, t)$$
$$\times \sum_\ell \left(\frac{m_\ell}{m_0}\right)^{\alpha + \gamma} e^{-\Gamma_0 \left(\frac{m_\ell}{m_0}\right)^\gamma (t - t^{(0)})}, \qquad (2.16)$$

where we have used the scaling relations in Eq. (2.12).

In order to evaluate this sum, we can pass to a continuum limit in which we have a large number of ϕ_ℓ states. We can therefore imagine that the spectrum of decay times $\tau_\ell \equiv \Gamma_\ell^{-1}$ is nearly continuous, merging to form a continuous variable τ. We can likewise view the discrete spectrum of energy densities ρ_ℓ and abundances Ω_ℓ as continuous functions $\rho(\tau)$ and $\Omega(\tau)$ where the states are now indexed by the continuous τ-variable corresponding to their decay times. This allows us to rewrite our expressions such that ℓ is eliminated in favor of τ. For example, we replace m_ℓ / m_0 with $(\Gamma_0 \tau)^{-1/\gamma}$. We can then convert the ℓ-sum over states to a τ-integral, i.e.,

$$\sum_\ell \Longleftrightarrow \int d\tau \, n_\tau(\tau), \qquad (2.17)$$

where $n_\tau \equiv |d\ell/d\tau|$ is the density of states per unit τ.

Of course, this passage from the sum to the integral involves a number of approximations whose effects are discussed in Ref. [1]. One important observation is that this approximation becomes increasingly accurate for times t which are far from the "boundary" (or "edge") effects associated with the initial entry into or exit from the stasis epoch. For a finite tower ϕ_ℓ with $\ell = 0, 1, ..., N-1$ with $N \gg 1$, this implies that our integral approximation will be especially valid for times t within the range

$$\tau_{N-1} \ll t \ll \tau_0 \qquad (2.18)$$

where of course we recall our original assumption that $t^{(0)} < \tau_{N-1}$, where $t^{(0)}$ is the initial production time for the ϕ_ℓ tower. The requirement that $t \gg \tau_{N-1}$ implies that we are focusing on a time interval after which a sizable number of states at the top of the tower have already decayed from matter to radiation. This allows our integral approximation to capture the general behavior of our system after any initial transient effects have dissipated and the flow of energy density from matter to radiation is well underway.

Evaluating the sums in Eq. (2.16) in this way and assuming $\gamma > 0$ and $\eta > 0$ leads to the result

$$\sum_\ell \Gamma_\ell \Omega_\ell(t) = \frac{\Gamma_0 \Omega_0^{(0)}}{\gamma \delta} \left(\frac{m_0}{\Delta m}\right)^{1/\delta} \Gamma\left(\frac{\eta}{\gamma} + 1\right)$$
$$\times h(t^{(0)}, t) \left[\Gamma_0(t - t^{(0)})\right]^{-1 - \eta/\gamma}, \qquad (2.19)$$

where $\Gamma(z)$ is the Euler gamma function. Likewise, letting t_* continue to denote a fiducial time at which stasis has already developed, we can write [1]

$$h(t^{(0)}, t) = h(t^{(0)}, t_*) h(t_*, t)$$
$$= h(t^{(0)}, t_*) \left(\frac{t}{t_*}\right)^{2 - \bar{\kappa}}. \qquad (2.20)$$

Substituting this result into Eq. (2.19), we see that $\sum_\ell \Gamma_\ell \Omega_\ell$ will scale as $1/t$—as required by Eq. (2.10)—only if we take $t \gg t^{(0)}$ and require

$$\frac{\eta}{\gamma} = 2 - \bar{\kappa}. \qquad (2.21)$$

Equivalently, through Eq. (2.9), this yields

$$\bar{\Omega}_M = \frac{2\gamma - 4\eta}{2\gamma - \eta}. \qquad (2.22)$$

Thus, for $t \gg t^{(0)}$ and for any values of η and γ within the ranges

$$\gamma > 0, \qquad 0 < \eta \le \frac{\gamma}{2}, \qquad (2.23)$$

our system has a stasis configuration during which $\bar{\Omega}_M$ is given in Eq. (2.22). Indeed, it is further shown in Ref. [1] that this state is a *global attractor*, and thus our system will evolve into the stasis state even if it does not begin in stasis at $t = t^{(0)}$. This attractor behavior is discussed further in Sec. VII. The stasis state then ends when the last ϕ_ℓ has decayed. Indeed, it is shown in Ref. [1] that this stasis state will generally last for $\mathcal{N}_s$ e-folds, where

$$\mathcal{N}_s \approx \frac{2\gamma\delta}{4 - \bar{\Omega}_M} \log N. \qquad (2.24)$$

Here N is the number of ϕ_ℓ states in the tower. We thus see that we can adjust the number $\mathcal{N}_s$ of e-folds associated with the stasis epoch simply by adjusting N.

In Fig. 1 we illustrate this matter/radiation stasis by plotting the numerical results that emerge from an exact Boltzmann evolution of our individual abundances within the cosmology defined by the successive decays of our ϕ_ℓ states. In the left panel we plot the individual abundances Ω_ℓ (shown in orange/blue) as well as the corresponding total matter abundance Ω_M (red) as functions of the number $\mathcal{N}$ of e-folds since the initial time of production. The individual abundances $\Omega_\ell(t)$ exhibit complex behaviors, first rising due to cosmological expansion and then falling due to ϕ_ℓ decay. However, as time advances, this happens

in such a way that *the identity of the ϕ_ℓ state with the largest abundance keeps changing* as the decays work their way down the ϕ_ℓ tower. This causes the individual $\Omega_\ell(t)$ abundances to keep crossing each other in an interleaving, cross-hatched fashion, as shown. This cross-hatched behavior for the individual abundances is a hallmark of the stasis state. Indeed, despite the complex behaviors exhibited by the individual abundances $\Omega_\ell(t)$, we see that the system quickly evolves into a stasis state in which their sum Ω_M becomes constant.

In the right panel of Fig. 1 we plot the total matter abundances Ω_M as functions of $\mathcal{N}$ for a variety of different values of (α, γ) satisfying the constraints in Eq. (2.23). In each case we see that the system settles into a prolonged stasis epoch lasting many e-folds, with a corresponding stasis abundance $\bar{\Omega}_M$ predicted by Eq. (2.22). Ultimately, in all cases, the stasis epoch ends as we approach the final decays of the lightest modes.

B. General lessons going forward

Having reviewed the main results of Ref. [1], let us now extract several lessons from this analysis which will serve as critical guideposts for our subsequent work in this paper.

First, we note that our main stasis constraint in Eq. (2.10) has been formulated by demanding that $d\Omega_M/dt = 0$ for all times t during stasis. It is this which led to the constraint equation in Eq. (2.21) and to the result for $\bar{\Omega}_M$ in Eq. (2.22). However, an alternative approach would have been to proceed by demanding the condition
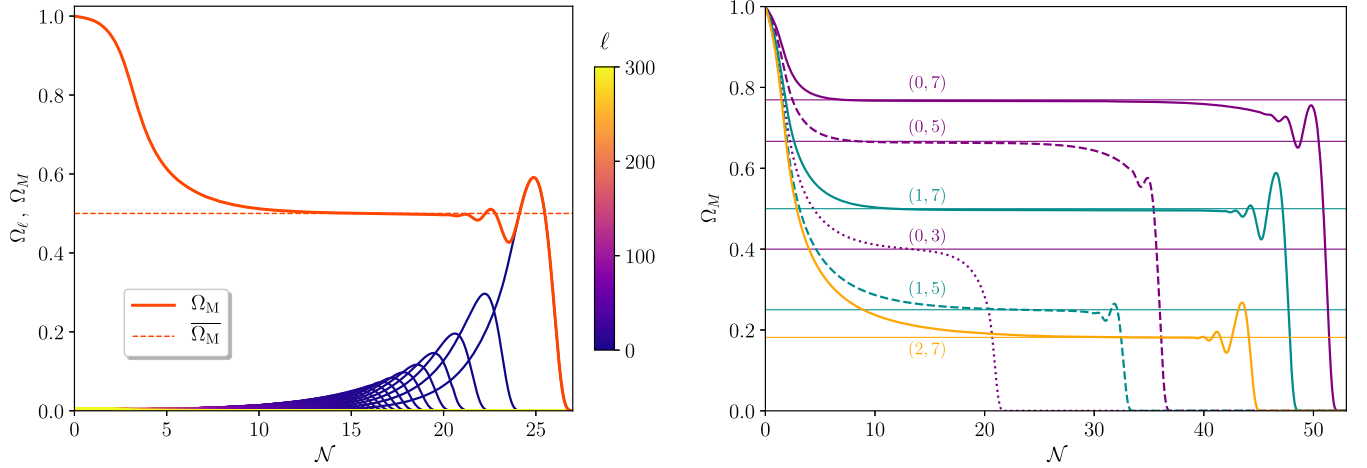

FIG. 1. Matter/radiation stasis. Left panel: the individual matter abundances Ω_ℓ (shown with colors ranging from orange to blue) and the corresponding total matter abundance Ω_M (red), plotted as functions of the number $\mathcal{N}$ of e-folds since the initial time of production. Even though the individual abundances Ω_ℓ exhibit complex behaviors which are affected by cosmological expansion as well as ϕ_ℓ decay, the system quickly evolves into a stasis state in which their sum Ω_M becomes constant. These curves were generated through a direct numerical solution of the Boltzmann equations corresponding to our discrete tower of decaying states without invoking any approximations, and correspond to the parameter choices $(\alpha, \gamma, \delta) = (1, 7, 1)$—for which $\bar{\Omega}_M = 1/2$—with $\Delta m = m_0$, $N = 300$, and $\Gamma_{N-1}/H^{(0)} = 0.01$. Right panel: the total matter abundances Ω_M, plotted as functions of $\mathcal{N}$ for different values of (α, γ) satisfying the constraints in Eq. (2.23). For each plot we have taken $\delta = 1$, $\Delta m = m_0$, $N = 10^5$, and $H^{(0)}/\Gamma_{N-1} = 0.1$. In each case we see that the system settles into a prolonged stasis epoch lasting many e-folds, with a corresponding stasis abundance $\bar{\Omega}_M$ predicted by Eq. (2.22). Ultimately, in all cases, the stasis epoch ends as we approach the final decays of the lightest modes. Both figures are taken from Ref. [1].

$$\sum_\ell \Omega_\ell(t) = \bar{\Omega}_M \qquad (2.25)$$

where each $\Omega_\ell(t)$ is given in Eq. (2.11). This simple condition would then replace the condition in Eq. (2.10). Evaluating the sum within Eq. (2.25) would then lead to an integral that is similar to the one we encountered between Eqs. (2.16) and (2.19), and demanding that the resulting quantity be independent of time would then produce the same results as in Eqs. (2.21) and (2.22).

Of course, these two approaches are not distinct: the former is simply the time derivative of the latter. Indeed, the requirement that $\sum_\ell \Omega_\ell(t)$ be time independent during stasis is ultimately tantamount to the constraint that the quantities in Eq. (2.10) scale as $1/t$ during stasis. We shall therefore refer to these two possible formulations of our stasis constraints as employing either the *differential* approach or the *integral* approach. However, these approaches generally have different advantages. The integral approach is more direct, but it requires having an explicit solution for the abundances $\Omega_\ell(t)$ such as in Eq. (2.11) or Eq. (2.15). For complicated cosmologies, these solutions may not always be easily determined. By contrast, the differential approach does not require this information. Moreover, because the differential approach is the time derivative of the integral approach, it explicitly describes the *flow* of energy densities and abundances between our different energy components. Indeed, as we shall see more explicitly in Sec. VI, the left side of Eq. (2.10) functions as the driving "pump" of energy density from matter to radiation, while the right side depends on the Hubble parameter and thus captures the redshifting effects of cosmological expansion.

Thus, going forward, we shall utilize either the derivative forms of our stasis constraints, as in Eq. (2.10), or the integral forms of such stasis constraints, as in Eq. (2.25), choosing whichever form is calculationally cleaner given the particular stasis scenario under study. Indeed, we shall even occasionally find that a mixture of both approaches is needed in order to obtain certain results.

A second relevant issue concerns whether there are any *further* constraints that should be imposed in order to achieve a stasis epoch. After all, our analysis in Sec. II A merely ensured that the left side of the stasis constraint in Eq. (2.10) has the required $1/t$ scaling dependence. Indeed, this is what gave rise to the constraint in Eq. (2.21). We shall refer to such constraints as *scaling constraints*. However, it might seem that there is an additional constraint that we should also impose, namely that which ensures the correct *prefactor* in Eq. (2.10). In general such prefactor constraints may contain additional information beyond that which emerges from the scaling constraints.

This issue is more subtle than it may at first appear. Given the result in Eq. (2.19), we see that we can write $\sum_\ell \Gamma_\ell \Omega_\ell(t) = C't^{-1}$ where the prefactor C' is given by

$$
\begin{aligned}
C' &\equiv \frac{1}{\gamma\delta}\left(\frac{m_0}{\Delta m}\right)^{1/\delta}\Gamma\left(\frac{\eta}{\gamma}+1\right)h(t^{(0)},t_*)\frac{\Omega_0^{(0)}}{(\Gamma_0 t_*)^{\eta/\gamma}} \\
&= \frac{1}{\gamma\delta}\left(\frac{m_0}{\Delta m}\right)^{1/\delta}\Gamma\left(\frac{\eta}{\gamma}+1\right)\Omega_0(\tau_0)e^{\Gamma_0(\tau_0-t^{(0)})}. \qquad (2.26)
\end{aligned}
$$

In writing Eq. (2.26) we have used Eq. (2.21) in order to simplify our expressions, and we have likewise defined $\tau_0 \equiv \Gamma_0^{-1}$. In this connection, we note that in passing to the second line of Eq. (2.26) the value of C' has become independent of the choice of t_*, as it must, since t_* is only a fiducial time with no physical significance.

In principle the result for C' in Eq. (2.26) bears no relation to the desired prefactor $(2-\bar{\kappa})\bar{\Omega}_M$ in Eq. (2.10). However, if we calculate $\bar{\Omega}_M$ by directly evaluating the sum in Eq. (2.25) by similarly utilizing our integral approximation and imposing the constraint in Eq. (2.21), we find that $\sum_\ell \Omega_\ell(t) = C$ where C is the same expression as in Eq. (2.26) except that the argument of the Euler gamma function is now given by η/γ rather than $\eta/\gamma + 1$. Using the identity $\Gamma(1+z) = z\Gamma(z)$, we can therefore bundle these results together in order to find that our two prefactors are related to each other via

$$C' = \left(\frac{\eta}{\gamma}\right)C = (2-\bar{\kappa})C. \qquad (2.27)$$

Of course, this is only a *relative* relation between C and C'—one which is independent of their individual absolute sizes. However, it eliminates all of the complicated factors such as those in Eq. (2.26) which arose from our conversion of the discrete sum to an integral, and it is also consistent with Eq. (2.10).

Given these results, the final remaining step is to demonstrate that either of our two prefactors C or C' takes the correct *absolute* size—i.e., that

$$C = \bar{\Omega}_M, \qquad (2.28)$$

or that

$$C' = \left(\frac{\eta}{\gamma}\right)\bar{\Omega}_M = (2-\bar{\kappa})\bar{\Omega}_M, \qquad (2.29)$$

where $\bar{\Omega}_M$ is the matter abundance that ultimately emerges during stasis. In conjunction with Eq. (2.27), this would then guarantee the correct prefactors in Eq. (2.10). Indeed, from Eq. (2.29) and the definition of C' above Eq. (2.26), we find that

$$\sum_\ell \Gamma_\ell \Omega_\ell(t) = \left(\frac{\eta}{\gamma}\right)\bar{\Omega}_M \frac{1}{t} \qquad (2.30)$$

during stasis. However, this final absolute-prefactor constraint in Eq. (2.28) or (2.29) is unlike the others. Whereas

our overall scaling constraint and *relative*-prefactor constraint are independent of the specific approximations involved in passing from Eq. (2.16) to Eq. (2.19) [or equivalently in obtaining a precise value for the discrete sum $\sum_\ell \Omega_\ell(t)$], the *absolute*-prefactor constraint in Eq. (2.28) or (2.29) is highly sensitive to the details of these approximations.

Fortunately, as discussed in Ref. [1], we need not worry about this absolute-prefactor constraint because it basically functions as an overall normalization constraint, and the proper normalizations of these sums are ultimately guaranteed by the attractor behavior of this system. Indeed, even if this overall normalization constraint is not initially satisfied, the system will inevitably flow towards the stasis attractor solution in which the proper overall normalization comes into balance. This feature is illustrated explicitly in Fig. 1 and in Ref. [1].

It is important to understand how this balancing occurs. *A priori*, the individual abundances are given in Eq. (2.15) where $h(t^{(0)}, t)$ represents the net gravitational redshift factor that accrues between the original production time $t^{(0)}$ and any later time t. Thus, $h(t^{(0)}, t)$ carries with it an explicit time dependence. Indeed, because this factor is ℓ independent, this same factor also appears within the total sum $\sum_\ell \Omega_\ell(t)$. However, once our system settles into a stasis configuration, $h(t^{(0)}, t)$ factorizes as in Eq. (2.20) where t_* is any fiducial time during stasis. The factor $(t/t_*)^{2-\bar{\kappa}}$ within Eq. (2.20) is then cancelled as part of the overall scaling constraints, leaving behind the time-independent factor $h(t^{(0)}, t_*)$ which appears in Eq. (2.26). This factor thus represents the part of the net redshift that occurs between $t^{(0)}$ and t_*, and its value has already been dynamically adjusted during the prestasis epoch so as to ensure that $C = \bar{\Omega}_M$.

Phrased somewhat differently, we may define

$$h(t) \equiv h(t^{(0)}, t) \left(\frac{t}{t_*}\right)^{-2+\bar{\kappa}}. \tag{2.31}$$

In general, this quantity is time dependent and evolves significantly during the time interval from $t^{(0)}$ to t_* prior to the emergence of stasis. However, upon reaching t_*, we know that our system has entered the stasis regime. The quantity $h(t)$ is then a constant, and from Eq. (2.20) we see that this constant is what we have been calling $h(t^{(0)}, t_*)$. Indeed, during the prestasis epoch when $h(t)$ was still evolving, this quantity was heading towards (and ultimately assumed) precisely the value $h(t^{(0)}, t_*)$ needed to ensure that $C = \bar{\Omega}_M$. We will discuss these h-factors in further detail in Sec. VI E.

There is also one additional constraint that is worthy of note. As indicated below Eq. (2.16), it was necessary to assume in passing from Eq. (2.16) to Eq. (2.19) that $\gamma > 0$ and that

$$\eta > 0. \tag{2.32}$$

Indeed, if our initial parameters had satisfied $\eta = 0$, we would have obtained a logarithmic (rather than power-law) dependence on t, and there would have been no hope of achieving a true stasis in such a case because of the resulting logarithmic drift.

Of course $\gamma > 0$ is a perfectly natural assumption for our underlying model, since this implies that our decay widths grow with ℓ—i.e., that the more massive ϕ_ℓ states decay more rapidly than do the lighter ϕ_ℓ states. By contrast, it is not *a priori* required that $\eta > 0$ (or equivalently that $\alpha + 1/\delta > 0$). In principle, this therefore becomes an additional constraint that must be imposed on our model in order to avoid logarithmic drift and achieve stasis. However, it turns out that this constraint is already guaranteed by Eq. (2.21): since purely matter-dominated and radiation-dominated universes have $\bar{\kappa} = 2$ and $\bar{\kappa} = 3/2$ respectively, any universe exhibiting a two-component stasis between matter and radiation must necessarily have $3/2 < \bar{\kappa} < 2$. Eq. (2.21) then implies that $\eta > 0$. The constraint $\eta > 0$ is also already implicit within Eq. (2.23).

Thus, to summarize, we see that in general there are several kinds of constraints that must be satisfied in order to achieve stasis:

(i) overall scaling constraints such as that in Eq. (2.21);

(ii) *relative* prefactor constraints such as that in Eq. (2.27);

(iii) *absolute* prefactor constraints such as that in Eq. (2.28) or (2.29) which ensure the correct overall normalizations; and

(iv) constraints such as that in Eq. (2.32) which ensure that there is no logarithmic drift, and that a true power-law time dependence emerges from our sums over states, ultimately to be cancelled through cosmological redshifting effects.

In general, the absolute-prefactor constraints will be satisfied as a consequence of the attractor behavior associated with our stasis solutions when these solutions are indeed attractors. However, *a priori*, each of the other constraints is generally capable of yielding new restrictions on our model or independent information concerning the properties of the resulting stasis. Of course, for the case of the pairwise matter/radiation stasis we have examined here, we have found that the relative-prefactor and logarithm-avoidance constraints are already satisfied whenever the overall scaling constraint is satisfied. In other words, matter/radiation stasis may be viewed as an over-constrained system which nevertheless gives rise to stasis solutions because these different constraints happen to be redundant (or subsumed within each other) without providing additional information. However, as we shall shortly see, this will not always be the case.

We close this section with one final comment. Throughout this section, we have been referring to

Eq. (2.21) as a *constraint* equation. In reality, however, this equation is not a constraint on our scaling exponents (α, γ, δ) so much as a *prediction* for the value of κ during the resulting stasis. Indeed, so long as our scaling exponents are chosen to lie within the ranges specified in Eq. (2.23), we see that Eq. (2.21) simply allows us to calculate the corresponding value of $\bar{\kappa}$, and this in turn allows us [via Eq. (2.9)] to determine the stasis abundance $\bar{\Omega}_M$, as in Eq. (2.22). Thus, so long as our scaling exponents are chosen to lie within the ranges specified in Eq. (2.23), we will *always* obtain a stasis. We see, then, that our desire to achieve matter/radiation stasis does not impose any actual constraints on our model beyond those in Eq. (2.23); indeed, stasis emerges quite robustly for all values of the relevant parameters within these ranges. We shall nevertheless often refer to Eq. (2.21) and its cousins as constraint equations in what follows.

III. VACUUM-ENERGY/MATTER STASIS

We now turn our attention to one of the main tasks of this paper: the inclusion of *vacuum energy* into the stasis discussion. In this section we begin by exploring the possibility of a stasis between vacuum energy and matter, and the ways in which this might arise from BSM physics. Of course, we know that any epoch in which both matter and vacuum energy are present and which is initially matter-dominated will evolve—simply as the result of cosmological expansion—into a vacuum-energy-dominated epoch. This is because the matter energy density falls like $\rho_M \sim a^{-3}$ as the universe expands, while the vacuum-energy density ρ_Λ remains constant. Achieving stasis between matter and vacuum energy therefore requires a mechanism to counterbalance this effect and convert vacuum energy back to matter.

A. Modeling vacuum energy and the transition to matter

To study this, we begin with a discussion of how we might introduce vacuum energy into our analysis. As we shall see, this issue turns out to be surprisingly subtle and requires some care.

By definition, vacuum energy has equation-of-state parameter $w = -1$. Indeed, such a state is pure potential energy (this is the "vacuum energy") and no kinetic energy. One natural approach towards studying a stasis involving vacuum energy and matter would therefore be to repeat the analysis in Sec. II for matter/radiation stasis, only replacing the equation of state of the initial ϕ_ℓ components from $w = 0$ to $w = -1$ until the moment they each undergo some sort of transition to matter. We would then replace the posttransition equation of state in Sec. II from $w = 1/3$ (radiation) to $w = 0$.

Of course, it would also be necessary to identify a mechanism for this "transition"—i.e., to identify a general process through which vacuum energy can be converted into matter, in much the same way as the process of particle decay converted matter into radiation in Sec. II. However, it is not difficult to identify such a process. Let us consider the coherent state consisting of the zero-momentum modes of a scalar field ϕ of mass m. At early times, when the Hubble parameter is large (with $3H \gg 2m$), this field is severely overdamped and thus has little kinetic energy. This is therefore a situation in which the energy of the field can be considered pure potential energy (vacuum energy), with equation-of-state parameter $w \approx -1$. However, as the universe expands, the Hubble parameter generally drops. As a result, the field eventually becomes underdamped (with $3H \lesssim 2m$) and begins to experience damped oscillations. In general, these oscillations quickly virialize, whereupon the energy of this field is split equally between potential and kinetic energy. The corresponding equation-of-state parameter is then $w = 0$, and the corresponding energy density behaves as matter as far as issues pertaining to cosmological expansion are concerned.

We thus see that the overdamped/underdamped transition at $3H(t) = 2m$ provides a natural mechanism for converting vacuum energy to matter, in exactly the same way as particle decay at $t = 1/\Gamma$ provided a natural mechanism in Sec. II for converting matter into radiation. Of course, near the transition time, our field has a nonzero kinetic energy and thus has neither $w = -1$ nor $w = 0$. Indeed, during such a transition period, the energy density of our field can be interpreted as a mixture of vacuum energy and matter. However, our main point is that an overdamped/underdamped transition has the net effect of converting vacuum energy to matter. In the following discussion, for the purpose of calculational simplicity, we shall idealize this transition by disregarding the "transient" effects that arise near $3H(t) \approx 2m$, and instead approximate our scalar field as having $w = -1$ whenever $3H(t) > 2m$ and $w = 0$ otherwise.

Given this understanding, we might attempt to generate a long-lived vacuum-energy/matter stasis by initially assuming a tower of coherent overdamped scalar fields ϕ_ℓ with masses m_ℓ and equations of state $w_\ell = -1$, in complete analogy with the initial configuration in Sec. II. We would then allow these ϕ_ℓ states to undergo successive transitions to an underdamped phase as the falling Hubble parameter $H(t)$ crosses the successive critical transition points $2m_\ell/3$. Such underdamping transitions would then proceed down the ϕ_ℓ tower, just as before, and potentially establish a stasis epoch along the way. Indeed, at any moment, the lighter fields would still be in the overdamped phase while the heavier fields will have already transitioned to the underdamped phase.

This approach would clearly be the most straightforward analog of the scenario discussed in Sec. II. Ultimately, however, this approach does not work. The reason is simple: such a system begins as pure vacuum energy, with

a total equation-of-state parameter $w_{\text{tot}} = -1$. Such a universe therefore has a Hubble parameter which is constant and never falls. As a result, there is no possibility of any fields becoming underdamped, and likewise no possibility of any subsequent transitions from vacuum energy to matter. Indeed, such a system simply remains "stuck" in its initial state, with no subsequent dynamics at all. There is thus no way in which a true stasis can develop in such a theory—we simply have the total initial abundances $\Omega_\Lambda = 1$ and $\Omega_M = 0$ in perpetuity. Of course, this is itself a kind of degenerate "stasis," but it is uninteresting for our purposes.

We shall therefore need to modify this naïve picture in such a way that our system will actually evolve away from its initial state, with ensuing cascading overdamped/underdamped transitions that convert vacuum energy to matter. There are several approaches we might follow in order to achieve this:

(i) We could begin by positing that the initial state of our system also includes some additional nonvacuum-energy component. Such an additional energy component would then introduce a nontrivial time dependence for the Hubble parameter, and this would in turn eventually trigger the cascading overdamped/underdamped transitions that we require. Unfortunately, doing this requires that our model now include extra components beyond our initial tower of states ϕ_ℓ. While there is nothing wrong with this (and indeed such additional components may ultimately be well motivated on phenomenological grounds), the introduction of such extra components beyond our tower of ϕ_ℓ states is not in the spirit of our previous analysis and would introduce arbitrary new features and parameters into our model.

(ii) A second option—indeed, one which is more "minimal" and which does not introduce new fields—would be to *deform* our model slightly by imagining that our overdamped ϕ_ℓ fields actually have a small kinetic energy (i.e., a "slow roll") in addition to their potential energies. For algebraic simplicity, we can incorporate this kinetic energy into our model by imagining that each of our ϕ_ℓ fields has an arbitrary common fixed equation-of-state parameter w in the range $-1 < w < 0$ prior to becoming underdamped (after which we can assume that each field transitions to having $w = 0$, as above). For example, we might consider w to be extremely close to (but slightly greater than) -1. Our model would then proceed exactly as before, with sharp overdamped/underdamped transitions occurring when $3H(t) = 2m_\ell$. Indeed, in such a model, nonzero values of the quantity $w + 1$ would essentially function as a "regulator" which allows us to avoid the difficulties associated with taking $w = -1$. We could then define our case of interest—namely

that with "vacuum energy"—as the $w \to -1$ limit of this model. Indeed, as we shall find, the $w \to -1$ limit is typically well behaved even if the precise $w = -1$ endpoint is not.

(iii) Finally, we could consider the full equations of motion for the scalar fields ϕ_ℓ without any approximations. These equations are those of a damped driven oscillator in which the Hubble damping terms carry a nontrivial time dependence. Within an arbitrary universe that has not yet reached stasis, such equations of motion lack analytical solutions, so this approach would necessarily be numerical.

The latter two approaches have complementary strengths and weaknesses. Within the $w > -1$ approach we are positing a relatively simple behavior for the ρ_ℓ energy densities, and thus this model can be understood and solved analytically. Moreover, taking $w > -1$ as a regulator successfully allows us to avoid having an initial Hubble parameter which remains constant, thereby allowing the dynamics of our system to "start" on its own. Indeed, we shall find that this model yields results in the $w \to -1$ limit which match much of what we expect from a naïve treatment in which we simply allow the vacuum-energy component to have $w = -1$ at the outset but in which the dynamics is somehow "started" in other ways. Finally, this model has the side benefit of allowing us to study the prospects for achieving stasis for arbitrary w. In this way we could thereby understand how the properties of the resulting stasis, if any, depend on w.

Unfortunately, this model, while suitable for understanding overall cosmological features associated with stasis, lacks a microscopic (particle-physics) Lagrangian description. By contrast, the full scalar-dynamics model has a *bona fide* realization in terms of the physics of a scalar field evolving in an external cosmology (i.e., subject to Hubble friction). Such a model is thus the rigorous setting for the $3H = 2m$ transition that allows us to convert from overdamped to underdamped behavior, or equivalently from vacuum energy to matter. Although this model cannot be solved analytically outside the stasis regime, a numerical analysis is possible. Of course, within this approach, the equation-of-state parameter w for each field during the overdamped phase is not an input parameter over which we have direct control, but is instead an *output* of the numerical simulation. Indeed, w may not even be constant, nor will it necessarily be the same for each field. In a similar way, the value of w for each field *after* the field becomes underdamped will not be strictly zero, but will also continue to have a nontrivial time dependence. Thus, within this model it is only an approximation to assert that the underdamped phase results in pure "matter," just as it is an approximation to state that the overdamped phase is pure "vacuum energy" with fixed $w = -1$.

In this paper we shall adopt the general-w model (as described in the second list item above), allowing w to lie

anywhere within the range $-1 < w < 0$. As we have discussed, this will enable us to study the stasis phenomenon analytically. This in turn will also allow us to determine the conditions for stasis and ultimately study the behavior of this model as $w \to -1$. However, we shall study the full dynamical-scalar model in Ref. [4], and we shall find that stasis emerges within the dynamical-scalar model as well. Indeed, our results here and in Ref. [4] will together allow us to verify that these two models, despite their differences, yield similar results. We shall therefore regard both models as demonstrating that vacuum energy can be successfully introduced into the overall stasis framework.

B. Stasis analysis for general w

As discussed above, we shall begin our analysis of a possible vacuum-energy/matter stasis in the same way as we did in Sec. II, specifically by assuming a flat Friedmann-Robertson-Walker (FRW) universe containing a tower of scalar fields ϕ_ℓ with masses m_ℓ, where the indices $\ell = 0, 1, 2, \ldots, N-1$ are assigned in order of increasing mass. At any time t, the fields for which $3H(t) > 2m_\ell$ will be assumed to be overdamped with a fixed equation-of-state parameter w which we can imagine is close to (but greater than) -1. By contrast, the fields for which $3H(t) < 2m_\ell$ will be assumed to be underdamped, with a fixed equation-of-state parameter $w = 0$. Thus the overdamped/underdamped transition at $3H = 2m_\ell$ converts vacuum energy (or its close approximation) to matter and proceeds down the tower as time advances. We shall let ρ_Λ and ρ_M denote the total energy densities of this system attributable to vacuum and matter respectively, while ρ_ℓ will denote the energy density associated with the individual scalar field ϕ_ℓ while it is still overdamped. We shall also let Ω_Λ, Ω_M, and Ω_ℓ represent the corresponding abundances.

Our analysis begins just as for matter/radiation stasis in Sec. II. Indeed, for any energy density ρ_i (where $i = \Lambda, M, \ell$), the corresponding abundance Ω_i continues to be given by Eq. (2.1), from which Eq. (2.2) continues to follow. However, the Friedmann "acceleration" equation now takes the form

$$\frac{dH}{dt} = -H^2 - \frac{4\pi G}{3}\left(\sum_i \rho_i + 3\sum_i p_i\right)$$

$$= -H^2 - \frac{4\pi G}{3}\left[(1 + 3w)\rho_\Lambda + \rho_M\right]$$

$$= -\frac{3}{2}H^2(1 + w\Omega_\Lambda), \qquad (3.1)$$

or equivalently

$$\kappa = \frac{2}{1 + w\Omega_\Lambda} \qquad (3.2)$$

where we generally identify κ through the parametrization

$$\frac{dH}{dt} = -\frac{3}{\kappa}H^2. \qquad (3.3)$$

Substituting Eq. (3.1) into Eq. (2.2) we then obtain

$$\frac{d\Omega_i}{dt} = \frac{8\pi G}{3H^2}\frac{d\rho_i}{dt} + 3H\Omega_i(1 + w\Omega_\Lambda), \qquad (3.4)$$

yielding

$$\frac{d\Omega_\Lambda}{dt} = \frac{8\pi G}{3H^2}\frac{d\rho_\Lambda}{dt} + 3H\Omega_\Lambda(1 + w\Omega_\Lambda),$$

$$\frac{d\Omega_M}{dt} = \frac{8\pi G}{3H^2}\frac{d\rho_M}{dt} + 3H\Omega_M(1 + w\Omega_\Lambda). \qquad (3.5)$$

These are thus general relations for the time evolution of Ω_Λ and Ω_M in terms of $d\rho_\Lambda/dt$ and $d\rho_M/dt$.

Given the relations in Eq. (3.5), our final step is to insert an appropriate equation of motion for $d\rho_\Lambda/dt$ (with the understanding that $d\rho_M/dt = -d\rho_\Lambda/dt$ by conservation of energy). It is here that we introduce the idea that vacuum energy is converted to matter when the individual states ϕ_ℓ become underdamped and begin oscillating. For each field, this is presumed to occur precisely at the time t_ℓ when $3H(t_\ell) = 2m_\ell$. In this paper, we shall refer to t_ℓ as a critical "underdamping" time. Thus, whereas the equations of motion given in Eq. (2.6) corresponded to the case in which the transition from matter to radiation occurred through an exponential decay term $\rho_\ell(t) \sim e^{-\Gamma_\ell(t-t^{(0)})}$, we shall now model the corresponding vacuum-energy/matter transition term as $\rho_\ell \sim \Theta(t_\ell - t)$ where $\Theta(x)$ denotes the Heaviside Θ-function [for which $\Theta(x) = 1$ for $x \geq 0$ and $\Theta(x) = 0$ otherwise]. This enforces our expectation that ρ_ℓ is nonzero (and can thus be attributed to vacuum energy) only for $t \leq t_\ell$. Likewise, the energy density for a fluid with equation-of-state parameter w generally scales as $a^{-3(1+w)}$. The corresponding equation of motion for each individual (vacuum) energy density ρ_ℓ is therefore given by

$$\frac{d\rho_\ell}{dt} = \rho_\ell \frac{d}{dt}\Theta(t_\ell - t) - 3(1 + w)H\rho_\ell$$

$$= -\rho_\ell\delta(t_\ell - t) - 3(1 + w)H\rho_\ell, \qquad (3.6)$$

whereupon we see that the equation of motion for the total vacuum-energy density ρ_Λ in this system is given by

$$\frac{d\rho_\Lambda}{dt} = -\sum_\ell \rho_\ell\delta(t_\ell - t) - 3(1 + w)H\rho_\Lambda. \qquad (3.7)$$

Just as in Sec. II, let us now evaluate this sum by passing to a continuum limit in which we truly have a large number of ϕ_ℓ states. However, in this case it will prove more useful to imagine that it is the spectrum of *underdamping* times t_ℓ

which is nearly continuous, merging to form a continuous variable $\hat{\imath}$. We can likewise view the discrete spectrum of energy densities ρ_ℓ and abundances Ω_ℓ as continuous functions $\rho(\hat{\imath})$ and $\Omega(\hat{\imath})$ where the states are now indexed by the continuous $\hat{\imath}$-variable corresponding to their underdamping times. We can then convert the ℓ-sum over states to a $\hat{\imath}$-integral, i.e.,

$$\sum_\ell \iff \int d\hat{\imath}\, n_{\hat{\imath}}(\hat{\imath}), \tag{3.8}$$

where $n_{\hat{\imath}} \equiv |d\ell/d\hat{\imath}|$ is the density of states per unit $\hat{\imath}$. Of course, this passage from the sum to the integral involves a number of approximations whose effects are similar to those discussed in Sec. II and in Ref. [1]. In particular, our integral approximation will be especially valid for times t within the range

$$t_{N-1} \ll t \ll t_0 \tag{3.9}$$

where we are of course assuming $t^{(0)} < t_{N-1}$. In other words, we are focusing on a time interval after which a sizable number of states at the top of the tower have already transitioned from vacuum energy to matter.

Within this integral approximation, Eq. (3.7) then becomes

$$\frac{d\rho_\Lambda}{dt} = -\int d\hat{\imath}\, n_{\hat{\imath}}(\hat{\imath})\rho(\hat{\imath})\delta(\hat{\imath}-t) - 3(1+w)H\rho_\Lambda$$
$$= -n_{\hat{\imath}}(t)\rho(t) - 3(1+w)H\rho_\Lambda. \tag{3.10}$$

In a similar way we also find that

$$\frac{d\rho_M}{dt} = +n_{\hat{\imath}}(t)\rho(t) - 3H\rho_M \tag{3.11}$$

where the first term results from the conservation of energy that governs the process of converting vacuum energy to matter while the second term incorporates the gravitational redshifting that is experienced by matter under cosmological expansion. Substituting these results into Eq. (3.5) we then find

$$\frac{d\Omega_\Lambda}{dt} = -n_{\hat{\imath}}(t)\Omega(t) - 3wH\Omega_\Lambda(1 - \Omega_\Lambda) \tag{3.12}$$

with $d\Omega_M/dt = -d\Omega_\Lambda/dt$. Note that $\Omega_\Lambda(1-\Omega_\Lambda) = \Omega_\Lambda\Omega_M = \Omega_M(1-\Omega_M)$.

The differential equation for Ω_Λ in Eq. (3.12) is completely general, describing the time evolution of Ω_Λ and Ω_M. One necessary (but not sufficient) condition for stasis is that $d\Omega_\Lambda/dt = 0$. This then yields the constraint

$$n_{\hat{\imath}}(t)\Omega(t) = -3wH\Omega_\Lambda(1 - \Omega_\Lambda). \tag{3.13}$$

Of course, for stasis we wish to have situations in which Eq. (3.13) holds not only instantaneously, but also over an extended period of time. This requires not only that Eq. (3.13) hold instantaneously, but that both sides of Eq. (3.13) have the same time dependence.

However, it is straightforward to determine the time dependence of the Hubble parameter H during an assumed period of stasis during which Ω_Λ and Ω_M are fixed at stasis values $\bar{\Omega}_\Lambda$ and $\bar{\Omega}_M$, respectively. Under such conditions, we can solve Eq. (3.1) directly to find the exact solution

$$H(t) = \left[\frac{2}{3(1+w\bar{\Omega}_\Lambda)}\right]\frac{1}{t} \implies \bar{\kappa} = \frac{2}{1+w\bar{\Omega}_\Lambda}, \tag{3.14}$$

in agreement with the result in Eq. (3.2). Note that this result holds for all $\bar{\Omega}_\Lambda$, *including* $\bar{\Omega}_\Lambda = 1$, so long as $w > -1$. Indeed, for $\bar{\Omega}_\Lambda = 0$, we verify from Eq. (3.14) the standard result that $H(t) = 2/(3t)$ for a matter-dominated universe. The solution for $H(t)$ in Eq. (3.14) in turn implies that our underdamping times t_ℓ during stasis are given by

$$t_\ell = \frac{\bar{\kappa}}{2m_\ell} = \frac{1}{1+w\bar{\Omega}_\Lambda}\frac{1}{m_\ell}. \tag{3.15}$$

Likewise, this solution for $H(t)$ implies that the scale factor grows during stasis as

$$a(t) = a_*\left(\frac{t}{t_*}\right)^{\bar{\kappa}/3} = a_*\left(\frac{t}{t_*}\right)^{2/(3+3w\bar{\Omega}_\Lambda)} \tag{3.16}$$

with t_* representing an arbitrary early fiducial time during stasis, as in Sec. II, and the "$*$" subscript indicating that the relevant quantity is evaluated at $t = t_*$. It then follows from Eq. (3.6) that

$$\Omega_\ell(t) = \Omega_\ell^*\left(\frac{t}{t_*}\right)^2\left[\frac{a(t)}{a_*}\right]^{-3(1+w)}\Theta\left(\frac{\bar{\kappa}}{2m_\ell} - t\right)$$
$$= \Omega_\ell^*\left(\frac{t}{t_*}\right)^{2-(1+w)\bar{\kappa}}\Theta\left(\frac{\bar{\kappa}}{2m_\ell} - t\right) \tag{3.17}$$

where we have further assumed that the fiducial time t_* is prior to the transition of ϕ_ℓ from vacuum energy to matter at t_ℓ. This final assumption will be discussed further and justified in Sec. VI E.

Given the result in Eq. (3.14), we find that Eq. (3.13) will be satisfied for an extended period of time so long as

$$n_{\hat{\imath}}(t)\Omega(t) = \left[-w\bar{\kappa}\bar{\Omega}_\Lambda(1 - \bar{\Omega}_\Lambda)\right]\frac{1}{t}$$
$$= \left[2 - (1+w)\bar{\kappa}\right]\bar{\Omega}_\Lambda\frac{1}{t}. \tag{3.18}$$

This result, which is the vacuum-energy/matter analog of Eq. (2.10), thus becomes our condition for vacuum-energy/matter stasis within the general-w model. Of course, as

discussed in Sec. II B, this condition is ultimately equivalent to the constraint that $\sum_\ell \Omega_\ell(t) = \bar{\Omega}_\Lambda$ where $\Omega_\ell(t)$ is given in Eq. (3.17), only expressed in differential form (and in the continuum limit) in order to expose the details of how the stasis is explicitly maintained. We shall demonstrate this equivalence explicitly below.

In parallel with our analysis in Sec. II, our goal is now to demonstrate that generic models of BSM physics that give rise to such towers of scalar states ϕ_ℓ experiencing such overdamping/underdamping transitions will satisfy the stasis constraint in Eq. (3.18) as exactly as possible over an extended time interval. For this purpose, we can adopt the same generic parametrization that was discussed in Sec. II. Specifically, we shall imagine a tower of scalars ϕ_ℓ whose abundances and masses satisfy the scaling relations in Eqs. (2.12) and (2.13) respectively. We shall also assume that the initial production time $t^{(0)}$ for these scalar fields has occurred during a period in which none of the ϕ_ℓ has yet become underdamped. As a result, in complete analogy with the model in Sec. II, we are implicitly assuming that $\Omega_\Lambda = 1$ during this initial period.

Within the context of this general model, we can now evaluate the quantities which appear on the left side of our constraint equation in Eq. (3.18). By demanding that Eq. (3.18) holds, we will then obtain the conditions on our model parameters that are required for stasis. Of course, the question of whether and how these conditions may come to be satisfied for arbitrary initial conditions is a separate one which requires a different (dynamical) analysis. We shall defer such a dynamical analysis to Sec. VII.

We begin by calculating $n_{\hat{t}}(t)$. Recall that $n_{\hat{t}}(t)$ is the density of states per unit transition time $\hat{t}$, evaluated for precisely that part of the ϕ_ℓ tower for which $t_\ell = t$. From Eqs. (2.13) and (3.15) we have

$$\ell = \left[\frac{\bar{\kappa}}{2} \frac{1}{(\Delta m) t_\ell} \right]^{1/\delta} \tag{3.19}$$

where we have adopted the simplifying approximation $m_0 \ll (\Delta m)\ell^\delta$. We thus find

$$n_{\hat{t}}(t) \equiv \left| \frac{d\ell}{dt_\ell} \right|_{t_\ell=t} = \frac{1}{\delta} \left(\frac{\bar{\kappa}}{2\Delta m} \right)^{1/\delta} t^{-1-1/\delta}. \tag{3.20}$$

Likewise, $\Omega(t)$ is the abundance that is disappearing from our tally of vacuum-energy abundances at time t [i.e., the abundance $\Omega_\ell(t)$ evaluated at time t and for that value of ℓ for which $t_\ell = t$]. However, just as in Sec. II, we recognize that our model provides specific scaling relations in Eq. (2.12) for the energy densities ρ_ℓ and corresponding abundances Ω_ℓ which hold only at the production time $t^{(0)}$. In order to calculate $\Omega(t)$ within the context of our model, we therefore can no longer use Eq. (3.17), which assumed the existence of an eternal stasis. Instead, we must express our abundances at time t in terms of the corresponding

abundances at $t^{(0)}$. To do this we can follow our analysis from Sec. II. In particular, from Eqs. (3.15) and (3.17) we have

$$\begin{aligned} \Omega(t) &= \Omega_\ell(t) \Big|_{t_\ell = t} \\ &= \Omega_0^{(0)} \left(\frac{m_\ell}{m_0} \right)^\alpha h(t^{(0)}, t_*) \left(\frac{t}{t_*} \right)^{2-(1+w)\bar{\kappa}} \\ &= \Omega_0^{(0)} \left(\frac{\bar{\kappa}}{2m_0 t} \right)^\alpha h(t^{(0)}, t_*) \left(\frac{t}{t_*} \right)^{2-(1+w)\bar{\kappa}} \end{aligned} \tag{3.21}$$

where $h(t^{(0)}, t_*)$, as in Sec. II, denotes the net gravitational redshift factor that accrues between the initial production time $t^{(0)}$ and the fiducial time t_* at which our system has reached stasis. Once again, the presence of such an h-factor will be discussed in more detail and justified in Sec. VI E.

Putting the pieces together, we thus find that requiring $n_{\hat{t}}(t)\Omega(t) \sim t^{-1}$ yields the constraint

$$\eta = 2 - (1+w)\bar{\kappa}, \tag{3.22}$$

whereupon we have $n_{\hat{t}}(t)\Omega(t) = C' t^{-1}$ with

$$C' \equiv \frac{\Omega_0^{(0)}}{\delta} \left(\frac{m_0}{\Delta m} \right)^{1/\delta} \left(\frac{\bar{\kappa}}{2m_0 t_*} \right)^\eta h(t^{(0)}, t_*). \tag{3.23}$$

We thus see that within our model specified by Eqs. (2.12) and (2.13), stasis will emerge only if Eq. (3.22) is satisfied. However, just as with Eq. (2.21), we may view this not as a constraint on our original model parameters (α, δ, w) so much as a prediction for the resulting stasis value $\bar{\kappa}$. We thus see that stasis is realized for all η within the range

$$0 < \eta < -2w, \tag{3.24}$$

with the resulting stasis abundance $\bar{\Omega}_\Lambda$ given by

$$\bar{\Omega}_\Lambda = \frac{\eta + 2w}{(2 - \eta)w} \tag{3.25}$$

and $\bar{\Omega}_M = 1 - \bar{\Omega}_\Lambda$. Indeed, we see that $\bar{\Omega}_\Lambda$ is always within the range $0 < \bar{\Omega}_\Lambda < 1$.

The limit as $w \to -1$ is particularly interesting. If we were to take $w = -1$ directly, we would find from Eq. (3.25) that $\bar{\Omega}_\Lambda|_{w=-1} = 0/0$ is indeterminate. This is why we introduced w, treating $1 + w$ as a regulator. However, evaluating our stasis abundance $\bar{\Omega}_\Lambda$ for general w as in Eq. (3.25) and then taking the $w \to -1$ limit, we find that $\lim_{w \to -1} \bar{\Omega}_\Lambda = 1$. Indeed, this limiting value for $\bar{\Omega}_\Lambda$ is consistent with our expectation for $w = -1$ that Ω_Λ will never depart from its initial value if that initial value is 1, since in that case the Hubble parameter $H(t)$ remains

constant and there is no dynamics within this model. We thus obtain a sensible result even as $w \to -1$.

It is illustrative to verify that Eq. (3.22) also emerges from the "integral" form of the stasis condition in Eq. (3.18), namely the defining requirement $\sum_\ell \Omega_\ell(t) = \bar{\Omega}_\Lambda$, where the abundances $\Omega_\ell(t)$ are given in Eq. (3.17). As we shall see, the same calculational ingredients are involved in both calculations, only slightly reshuffled. In order to evaluate $\sum_\ell \Omega_\ell(t)$, we begin by noting that the Heaviside Θ-functions within Eq. (3.17) imply that at any time t there will be a maximum ℓ-value $\ell_{\max}(t)$ for which the corresponding abundances $\Omega_\ell(t)$ are still nonzero and thus contributing to the total vacuum-energy abundance Ω_Λ of the system. Indeed, for any t, no values of $\Omega_\ell(t)$ with $\ell > \ell_{\max}(t)$ can contribute to Ω_Λ. We can therefore eliminate all of the Heaviside Θ-functions from the $\Omega_\ell(t)$ expressions within the sum by introducing a time-dependent maximum value $\ell_{\max}(t)$ on the states that should be included in the sum. We therefore have

$$
\begin{aligned}
\sum_\ell \Omega_\ell(t) &= \sum_{\ell=0}^{\ell_{\max}(t)} \Omega_\ell^* \left(\frac{t}{t_*}\right)^{2-(1+w)\bar{\kappa}} \\
&= \sum_{\ell=0}^{\ell_{\max}(t)} \Omega_0^* \left(\frac{m_\ell}{m_0}\right)^\alpha \left(\frac{t}{t_*}\right)^{2-(1+w)\bar{\kappa}} \\
&\approx \int_t^\infty d\hat{t}\, n_{\hat{\imath}}(\hat{t}) \Omega_0^* \left(\frac{\bar{\kappa}}{2m_0\hat{t}}\right)^\alpha \left(\frac{t}{t_*}\right)^{2-(1+w)\bar{\kappa}} \\
&= \frac{\Omega_0^*}{\delta} \left(\frac{\bar{\kappa}}{2\Delta m}\right)^{1/\delta} \left(\frac{\bar{\kappa}}{2m_0}\right)^\alpha \left(\frac{t}{t_*}\right)^{2-(1+w)\bar{\kappa}} \\
&\quad \times \int_t^\infty d\hat{t}\, \hat{t}^{-1-\eta} \\
&= \frac{\Omega_0^*}{\delta} \left(\frac{\bar{\kappa}}{2\Delta m}\right)^{1/\delta} \left(\frac{\bar{\kappa}}{2m_0}\right)^\alpha \left(\frac{t}{t_*}\right)^{2-(1+w)\bar{\kappa}} \frac{1}{\eta} t^{-\eta},
\end{aligned}
$$
(3.26)

where we have adopted the shorthand

$$
\Omega_\ell^* \equiv \Omega_\ell(t_*) = \Omega_\ell^{(0)} h(t^{(0)}, t_*) \tag{3.27}
$$

for all ℓ (including $\ell = 0$). In the first two lines of Eq. (3.26) we have used Eqs. (2.12) and (3.15), while in passing to the third line we have utilized the same integral approximation discussed above in terms of the continuous $\hat{\imath}$-variable. Similarly, in passing to the fourth line of Eq. (3.26) we have utilized Eq. (3.20) for the density of states per unit $\hat{\imath}$, and in passing to the final line we have recognized from Eq. (3.24) that $\eta > 0$. However, demanding that the final result in Eq. (3.26) be independent of t leads to the same constraint as we obtained previously in Eq. (3.22). Thus the integral form of our stasis condition leads to the same overall scaling constraint as we obtained through the differential form.

Thus far in our analysis of vacuum-energy/matter stasis we have concentrated on the overall scaling constraint. Indeed, as discussed in Sec. II B, we must also consider the associated prefactor constraints (both relative and absolute) as well as the associated logarithm-avoidance constraint. However, it is straightforward to see that—just as for matter/radiation stasis—the relative-prefactor and logarithm-avoidance constraints are redundant with the overall scaling constraint and therefore provide no new restrictions. In particular, writing $\sum_\ell \Omega_\ell(t) = C$, we find from Eq. (3.26) that C is given by the same expression as in Eq. (3.23) except divided by η, thereby enabling us to extract the relative-prefactor relation

$$
C' = \eta C = [2 - (1+w)\bar{\kappa}]C. \tag{3.28}
$$

This is the vacuum-energy/matter analog of the relation in Eq. (2.27). We thus find that our desired prefactor relation in Eq. (3.18) will be satisfied as long as

$$
C = \bar{\Omega}_\Lambda \tag{3.29}
$$

or equivalently

$$
C' = \eta \bar{\Omega}_\Lambda = [2 - (1+w)\bar{\kappa}]\bar{\Omega}_\Lambda. \tag{3.30}
$$

Likewise, from this result we have the stasis result

$$
n_{\hat{\imath}}(t)\Omega(t) = \eta \bar{\Omega}_M \frac{1}{t}, \tag{3.31}
$$

as required by Eq. (3.18). However, these last absolute-prefactor constraints will naturally come into balance dynamically, since the attractor behavior of this solution (which we will discuss in Sec. VII) automatically adjusts $h(t^{(0)}, t_*)$ so as to ensure that $C = \bar{\Omega}_\Lambda$. We thus see that our model naturally gives rise to the correct prefactor constraints in Eq. (3.18) as well.

As discussed in Sec. II B, we must also satisfy the logarithm-avoidance constraint. Indeed, in the present case this is nothing but the constraint $\eta > 0$ that enabled us to avoid obtaining a logarithmic time dependence when passing to the final line of Eq. (3.26). However, this constraint is already subsumed into our overall scaling constraint, as we see from the allowed ranges in Eq. (3.24). Moreover, we see that Eq. (3.22) is not really a constraint on the input parameters of our model so much as a prediction for the resulting stasis value $\bar{\kappa}$ and therefore $\bar{\Omega}_\Lambda$. Thus, so long as the input parameters of our model satisfy Eq. (3.24), a stasis state will necessarily emerge.

It is also instructive to understand in a qualitative way the behavior of the energy densities ρ_ℓ during the stasis epoch as the decays of our individual ϕ_ℓ states proceed down the tower. As we have seen in Eq. (2.12), the energy densities ϕ_ℓ have initial values $\sim (m_\ell/m_0)^\alpha$ at $t = t^{(0)}$. In the
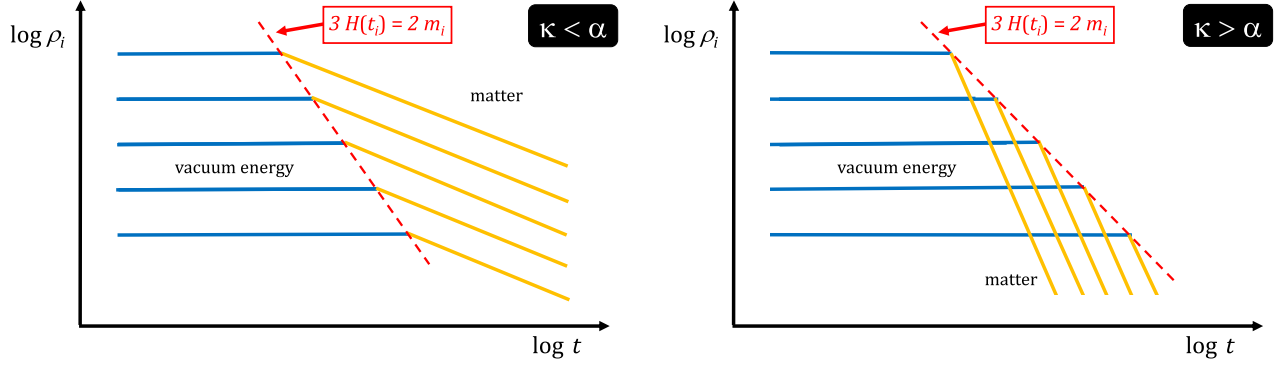
FIG. 2.   Two different scenarios illustrating possible behaviors for the individual energy densities $\rho_\ell(t)$ (blue/orange), sketched as functions of time, as our corresponding tower of states ϕ_ℓ undergoes sequential transitions from an overdamped phase to an underdamped phase at times t_ℓ for which $3H(t_\ell) = 2m_\ell$. These energy densities $\rho_\ell(t)$ are interpreted as corresponding to vacuum energy (blue) or matter (orange) when the corresponding states ϕ_ℓ are overdamped or underdamped, respectively, with the dashed line (red) indicating the moments of transition between these two regimes. For the purpose of these sketches we have assumed that states with greater energy densities have greater masses (i.e., $\alpha > 0$). We have also chosen to sketch the case in which $w \to -1$ for the vacuum energy, causing the blue lines to be almost exactly horizontal. The left and right panels show the behaviors that emerge for $\bar\kappa < \alpha$ and $\bar\kappa > \alpha$, respectively. In the latter case, the energy densities "reflect" off the red transition line, thereby giving rise to the sequential "interleaved" energy-density crossings that are the hallmark of the stasis phenomenon.

$w \to -1$ limit, these quantities then remain time independent until the time $t = t_\ell$, defined by the constraint $3H(t_\ell) = 2m_\ell$, after which they scale as $\rho_\ell(t) \sim t^{-\bar\kappa}$. Moreover, we have seen in Eq. (3.15) that $t_\ell \sim m_\ell^{-1}$, implying that $\rho_\ell \sim t_\ell^{-\alpha}$. Given these observations, rough sketches of two possible time evolutions for each $\rho_\ell(t)$ during stasis appear in Fig. 2. These energy densities are sketched in blue when they correspond to vacuum energy, and yellow when they correspond to matter. The dividing line between these two phases is indicated in red, and given our result $\rho_\ell \sim t_\ell^{-\alpha}$ we see that this line has slope $-\alpha$ on this log-log plot. For simplicity these sketches are drawn with equally spaced initial values of $\log\phi_\ell$, but this property is chosen for graphical simplicity and will play no role in our analysis.

The primary difference between the two panels of Fig. 2 concerns the value of $\bar\kappa$ that governs the logarithmic slope of each $\rho_\ell(t)$ after $t = t_\ell$. Indeed, the left panel of Fig. 2 corresponds to the case with $\bar\kappa < \alpha$, while the right panel of Fig. 2 corresponds the case with $\bar\kappa > \alpha$. However, it is immediately apparent that the change in the sign of this inequality has a profound effect on the behavior of the corresponding energy densities. For $\bar\kappa < \alpha$, the energy densities ρ_ℓ necessarily remain in the same relative order in which they began, with $\rho_{\ell'}(t) > \rho_\ell(t)$ for all t as long as $\ell' > \ell$. For $\bar\kappa > \alpha$, by contrast, the energy densities $\rho_\ell(t)$ undergo successive pairwise crossings as time evolves. Thus while the energy density associated with the top component $\ell_{\max} = N - 1$ begins as the largest, eventually the energy density associated with $\ell_{\max} - 1$ becomes the largest, then that with $\ell_{\max} - 2$, and so forth.

It is this latter behavior involving successive pairwise energy-density crossings which underlies the stasis phenomenon. This is particularly evident from the left panel of Fig. 1, which shows the analogous situation with matter/radiation stasis. Thus, just from consideration of these sorts of figures, we can immediately see that stasis requires $\bar\kappa > \alpha$. Of course, this result is entirely consistent with the full stasis condition in Eq. (3.22). Indeed, we see from Eq. (3.2) that $\bar\kappa > 2$, whereupon we see from Eq. (3.22) that $\alpha < 2$. Thus stasis necessarily requires $\alpha < \bar\kappa$, consistent with the right panel of Fig. 2 but not the left panel.

In general, these results will apply to all of the stasis situations we shall consider in this paper. In each case, we will require successive energy inversions proceeding down the ϕ_ℓ tower as time evolves. As we have seen, this requires a very particular behavior as our energy densities $\rho_\ell(t)$ approach the red lines that indicate our transitions, as in Fig. 2. Speaking qualitatively, we may regard our energy densities $\phi_\ell(t)$ as either passing *through* these red lines, as in the left panel of Fig. 2, or being *reflected* by these red lines, as in the right panel of Fig. 2. *It is the case of reflection that induces the behavior that underlies the stasis phenomenon.*

In Fig. 3 we show the emergence of vacuum-energy/matter stasis for a system in which we take $\alpha = 0.7$, $\delta = 2$, and $w = -0.8$ as reference values. As we see, this eventually results in a stasis with $\bar\kappa = 4$, consistent with Eq. (3.22), which in turn implies that $\bar\Omega_\Lambda = 5/8$ and $\bar\Omega_M = 3/8$.

IV. VACUUM-ENERGY/RADIATION STASIS

In Sec. III, we demonstrated that vacuum energy and matter can be in stasis with each other. Our analysis took place within a cosmology containing a tower of scalar fields ϕ_ℓ with masses m_ℓ which sequentially transition from an overdamped phase (during which their energies are
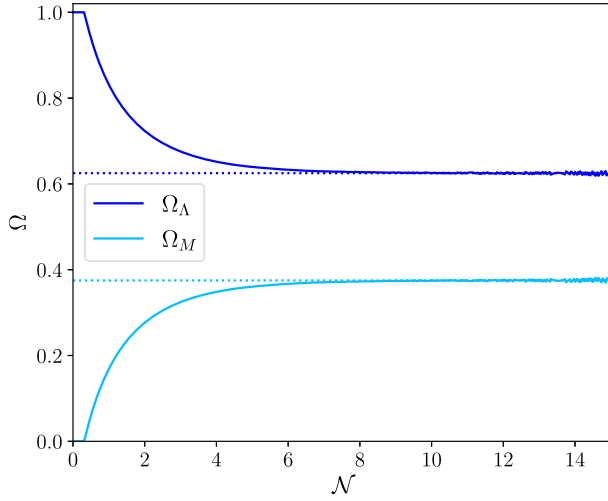
FIG. 3. Vacuum-energy/matter stasis. Here the total vacuum-energy and matter abundances, $\Omega_\Lambda(t)$ and $\Omega_M(t)$ respectively, are plotted as functions of the number $\mathcal{N}$ of e-folds since the initial production time $t^{(0)}$, taking $\alpha = 0.7$, $\delta = 2$, and $w = -0.8$ as reference values. We have also taken $H^{(0)}/m_{N-1} = 0.75$. As we see, the system eventually evolves into a stasis state with $\bar{\kappa} = 4$, $\bar{\Omega}_\Lambda = 5/8$, and $\bar{\Omega}_M = 3/8$. This stasis state ends only when the last component of the tower transitions to matter. As with matter/radiation stasis, the total number of e-folds of stasis $\mathcal{N}_s$ is determined by the total number N of states in the tower. In analogy with Eq. (2.24) for matter/radiation stasis, we expect $\mathcal{N}_s \sim \log N$. Similar stasis behavior emerges for all values of (α, δ, w) within the ranges in Eq. (3.24), with corresponding stasis abundances $\bar{\Omega}_\Lambda$ determined by Eq. (3.25) and $\bar{\Omega}_M = 1 - \bar{\Omega}_\Lambda$.

identified as vacuum energy) to an underdamped phase (during which their energies are identified as those of matter). Indeed, these transitions occur at the times t_ℓ for which $3H(t_\ell) = 2m_\ell$.

However, such ϕ_ℓ fields can also experience decays into radiation, with nonzero decay widths Γ_ℓ. Indeed, within certain regions of parameter space, it may even happen that the lifetimes $\tau_\ell \equiv 1/\Gamma_\ell$ of the components ϕ_ℓ are all smaller than the critical underdamping times t_ℓ at which these fields would have transitioned to an underdamped state. In such cases, we can then have decays directly from vacuum energy to radiation.

In general, a universe composed entirely of vacuum energy and radiation will evolve under cosmological expansion from a radiation-dominated epoch to a vacuum energy-dominated epoch. The above decays from vacuum energy back to radiation can thus provide a counterbalancing effect that could potentially lead to a stasis between vacuum energy and radiation.

A. Theoretical subtleties

In order to study this phenomenon, we must first discuss several additional theoretical subtleties that arise in

modeling the transfer of energy density from vacuum energy to radiation. The rate at which this transfer of energy density occurs depends on the properties of the vacuum-energy component.

For example, as discussed in Sec. III, one natural realization of ρ_Λ in a particle-physics context is the energy density associated with one or more overdamped scalar fields ϕ_ℓ which are displaced from their potential minima. The equation of motion for each such field is $\ddot{\phi}_\ell + (3H + \Gamma_\ell)\dot{\phi}_\ell + \partial V/\partial\phi_\ell = 0$, where V is the scalar potential and where a dot denotes a time derivative. At late times, when $3H(t) \ll 2m_\ell$ and the field is well within the underdamped regime, Γ_ℓ is often approximated as constant and identified with the proper decay width of ϕ_ℓ in Minkowski space [9,10]. However, this heuristic treatment of the dissipation rate is not appropriate while the field is in the overdamped regime [11]. Rather, Γ_ℓ must be calculated using methodologies appropriate for analyzing the non-equilibrium dynamics of a quantum field interacting with its environment, such as the closed-time path (i.e., Schwinger-Keldysh) formalism (for reviews, see, e.g., Ref. [12]) or the inference time formalism (for reviews, see, e.g., Refs. [13,14]). A number of subtleties arise in these calculations as a result of the background cosmology. For example, since there is no global timelike Killing vector in an FRW universe, particle energy is not manifestly conserved. A variety of processes which are forbidden in Minkowski space—including the decay of a field into its own quanta [15–18]—can therefore contribute to the dissipation rate. The form which Γ_ℓ takes is highly model dependent and in general depends nontrivially both on the temperature of the radiation bath—or, equivalently, on the value of ρ_γ—and on the time-varying expectation value of ϕ (for reviews and discussion, see, e.g., Refs. [19–22]).

We note that there is another natural mechanism via which the energy density associated with an overdamped scalar field can be transferred directly to a radiationlike energy component with $w = 1/3$. This mechanism is similar to the mechanism discussed in Sec. III for transferring energy density from vacuum energy to matter, which involved an overdamped/underdamped transition, but operates in scenarios in which the quadratic term for ϕ_ℓ in V is negligible or vanishing, and ϕ_ℓ is instead dominated by a higher-order polynomial $V_\ell \sim \phi_\ell^{2n}$ with $n > 1$. At early times, while $3H \gg 2(\partial^2 V/\partial\phi_\ell^2)^{1/2}$ and ϕ_ℓ is effectively stationary, the energy density ρ_ℓ associated with that field scales with a like vacuum energy. However, once $3H \approx 2(\partial^2 V/\partial\phi_\ell^2)^{1/2}$, the field ϕ_ℓ begins oscillating around its potential minimum. The effective equation-of-state parameter for ϕ_ℓ during this oscillatory phase, time averaged over many cycles of oscillation, is $w_\ell \approx (n-1)/(n+1)$ [23]. Thus, for $n = 2$—i.e., for a quartic potential—the equation-of-state parameter for such an oscillating scalar field is identical to that for radiation. As with the overdamped/underdamped transition discussed in Sec. III, we can obtain some insight

into the cosmological dynamics of scenarios involving such scalars by idealizing this transition as an instantaneous one in which ϕ_ℓ is approximated as having $w = -1$ whenever $3H > 2(\partial^2 V/\partial\phi_\ell^2)^{1/2}$ and $w = 1/3$ otherwise.

For simplicity, we shall focus in what follows on the case in which Γ_ℓ is effectively constant and independent of ρ_γ. While an analysis based on this form of Γ_ℓ does not have a straightforward motivation in terms of a top-down model, it can nevertheless serve as a convenient starting point for the analysis of specific models with more complicated, time- and temperature-dependent dissipation rates. We also note that the results obtained for this form of Γ_ℓ in the instantaneous-decay approximation turn out to be applicable, through a straightforward mapping, to the case of a scalar field ϕ_ℓ with a quartic potential whose energy density scales like that of radiation once it begins oscillating [4]. Moreover, as we shall see, the results we obtain for a constant Γ_ℓ will provide some mathematical insight into certain limiting cases of the three-component cosmological system on which we shall focus in Sec. VI.

B. Algebraic analysis

Given these understandings and assumptions, we shall now repeat the algebraic steps in the previous sections in order to investigate the possibility of achieving a two-component stasis between vacuum energy and radiation. Towards this end, our analysis will essentially be a hybrid of the analyses in Secs. II and III: we shall treat the vacuum energy according to the general-w approach of Sec. III B, assuming that each of our ϕ_ℓ fields evolves with a fixed equation-of-state parameter $w > -1$, but we shall also assume that this vacuum energy simultaneously experiences an exponential decay with lifetime $\tau_\ell \equiv \Gamma_\ell^{-1} \ll t_\ell$.

Within a cosmology consisting of only vacuum energy and radiation, the Hubble parameter evolves as

$$\frac{dH}{dt} = -\frac{1}{2}H^2\big[4 + (3w - 1)\Omega_\Lambda\big], \qquad (4.1)$$

or equivalently

$$\kappa = \frac{6}{4 + (3w - 1)\Omega_\Lambda} \qquad (4.2)$$

where κ continues to be defined through the parametrization in Eq. (3.3). Likewise, the vacuum-energy density ρ_ℓ associated with each ϕ_ℓ field evolves as

$$\frac{d\rho_\ell}{dt} = -3(1 + w)H\rho_\ell - \Gamma_\ell\rho_\ell, \qquad (4.3)$$

whereupon we find

$$\frac{d\Omega_\Lambda}{dt} = -\sum_\ell \Gamma_\ell\Omega_\ell + (1 - 3w)H\Omega_\Lambda(1 - \Omega_\Lambda). \qquad (4.4)$$

Setting $d\Omega_\Lambda/dt = 0$ and inserting the stasis Hubble parameter $H(t) = \bar{\kappa}/(3t)$ then yields the corresponding stasis condition

$$\sum_\ell \Gamma_\ell\Omega_\ell(t) = \left[\left(\frac{1}{3} - w\right)\bar{\kappa}\bar{\Omega}_\Lambda(1 - \bar{\Omega}_\Lambda)\right]\frac{1}{t}$$

$$= \big[2 - (1 + w)\bar{\kappa}\big]\bar{\Omega}_\Lambda\frac{1}{t}. \qquad (4.5)$$

This condition for vacuum-energy/radiation stasis can also be satisfied within the model of Eqs. (2.12) and (2.13). In order to determine the resulting constraints on our model parameters $(\alpha, \gamma, \delta, w)$, we can follow the steps in Sec. II. Indeed, for this purpose we adopt Sec. II rather than Sec. III as our guide because the former also involved an exponential decay from one energy component to another. Repeating the steps in Sec. II, we can convert the sum in Eq. (4.5) to an integral. Moreover, rather than introduce a continuous variable $\hat{t}$ of underdamping times as in Sec. III, we follow Sec. II and work in terms of a continuous variable τ of *decay* times τ. Assuming an eternal stasis, we then find that our parameters must satisfy the relation

$$\frac{\eta}{\gamma} = 2 - (1 + w)\bar{\kappa}. \qquad (4.6)$$

This is thus the analog of Eqs. (2.21) and (3.22). Once again, this is not a constraint on $(\alpha, \gamma, \delta, w)$ so much as a prediction for $\bar{\kappa}$. Indeed, so long as

$$0 < \frac{\eta}{\gamma} < \frac{1 - 3w}{2}, \qquad (4.7)$$

we find that the resulting value of $\bar{\Omega}_\Lambda$ during stasis is given by

$$\bar{\Omega}_\Lambda = \frac{2(2\eta + 3w\gamma - \gamma)}{(1 - 3w)(\eta - 2\gamma)}. \qquad (4.8)$$

Note that $0 < \bar{\Omega}_\Lambda < 1$ so long as Eq. (4.7) is satisfied.

Interestingly, for $w = -1$ we find that $\bar{\Omega}_\Lambda = 1$ for any η and γ. This indicates that the only "stasis" that develops in the $w = -1$ case is that with which we started, namely a universe containing nothing but vacuum energy. However, for $w > -1$, we find that a nontrivial stasis develops with $\bar{\Omega}_\Lambda < 1$.

Following the results in Sec. II, we may also compare the overall coefficients that enter into our stasis constraints. For this purpose, let us define C and C' via

$$\sum_\ell \Omega_\ell(t) = C,$$

$$\sum_\ell \Gamma_\ell\Omega_\ell(t) = C't^{-1}, \qquad (4.9)$$

where we have imposed the relation in Eq. (4.6). We can explicitly evaluate the sums on the left sides of Eq. (4.9) by converting to integrals over a continuous τ-variable, as discussed above. We then find that C and C' are related via

$$C' = \frac{\eta}{\gamma}C = [2 - (1 + w)\bar{\kappa}]C \qquad (4.10)$$

where

$$C \equiv \frac{1}{\gamma\delta}\left(\frac{m_0}{\Delta m}\right)^{1/\delta}h(t^{(0)}, t_*)\frac{\Omega_0^{(0)}}{(\Gamma_0 t_*)^{\eta/\gamma}}\Gamma\left(\frac{\eta}{\gamma}\right). \qquad (4.11)$$

These solutions for C and C' exactly match those in Sec. II. As in previous cases, the attractor behavior of the stasis solution (to be discussed in Sec. VII) then inevitably ensures that $C = \bar{\Omega}_\Lambda$. Indeed, this happens in the same manner as described in Sec. II B. The result in Eq. (4.10) then ensures that the prefactors within Eq. (4.5) match precisely. This also ensures that Eq. (2.30) holds for vacuum-energy/radiation stasis as well.

Although we have treated our decay process as a *bona fide* exponential decay, it will prove both instructive and useful to repeat this calculation within the framework of an *instantaneous-decay approximation* in which our ϕ_ℓ states decay suddenly and completely at $t = \tau_\ell = 1/\Gamma_\ell$. This is tantamount to approximating the exponential decays as sharp cutoffs by replacing

$$e^{-t/\tau_\ell} \to \Theta(\tau_\ell - t). \qquad (4.12)$$

Implementing this substitution, we find that our calculations now more closely resemble the calculations in Sec. III (wherein the underdamping times t_ℓ played the role of τ_ℓ) rather than those in Sec. II. In this case, the constraint equations for stasis in Eq. (4.5) are replaced by

$$n_\tau(t)\Omega(t) = \left[\left(\frac{1}{3} - w\right)\bar{\kappa}\bar{\Omega}_\Lambda(1 - \bar{\Omega}_\Lambda)\right]\frac{1}{t}$$
$$= [2 - (1 + w)\bar{\kappa}]\bar{\Omega}_\Lambda\frac{1}{t}. \qquad (4.13)$$

This condition for vacuum-energy/radiation stasis can also be satisfied within the model of Eqs. (2.12) and (2.13). A calculation similar to that in Eq. (3.26) tells us that $n_\tau(t)\Omega(t)$ will scale as t^{-1}, as required, only if Eq. (4.6) is satisfied. We thus see that the instantaneous-decay approximation leads to precisely the same scaling relation for the $(\alpha, \gamma, \delta, w)$ parameters as full exponential decay. Likewise, defining our C-coefficients via the relations

$$\sum_\ell \Omega_\ell(t) = C,$$
$$n_\tau(t)\Omega(t) = C't^{-1}, \qquad (4.14)$$

we again obtain the relation between C and C' given in Eq. (4.10), where now C is given by

$$C \equiv \frac{1}{\gamma\delta}\left(\frac{m_0}{\Delta m}\right)^{1/\delta}h(t^{(0)}, t_*)\frac{\Omega_0^{(0)}}{(\Gamma_0 t_*)^{\eta/\gamma}}. \qquad (4.15)$$

The attractor behavior of the stasis solution then guarantees that $C = \bar{\Omega}_\Lambda$, as before, and likewise yields Eq. (3.31).

Thus, even within the instantaneous-decay approximation, we find that stasis is achieved. This is a rather remarkable result, demonstrating that full exponential decay and the instantaneous-decay approximation are equally valid as far as stasis calculations are concerned. Indeed, both full exponential decay and the instantaneous-decay approximation lead to the identical scaling relation in Eq. (4.6) and the identical relative and absolute prefactor constraints in Eqs. (4.10). (The same is also true for the logarithmic-avoidance constraint, which now takes the form $\eta/\gamma > 0$.) Indeed, the only difference between the two formalisms for treating the decay process is in the precise absolute value of C, but this information is ultimately washed away due to the attractor nature of the stasis solution. These observations thus suggest a certain robustness to the existence of the stasis phenomenon, indicating that our conclusions regarding the emergence of stasis are largely independent of the precise details concerning how the decays of the ϕ_ℓ states are ultimately modeled.

Interestingly, we observe that the effective equation-of-state parameter for this vacuum-energy/radiation system during stasis is given by

$$\langle w \rangle = w\bar{\Omega}_\Lambda + \frac{\bar{\Omega}_\gamma}{3}. \qquad (4.16)$$

Thus, when $\bar{\Omega}_\gamma = -3w\bar{\Omega}_\Lambda$, our system has $\langle w \rangle = 0$. In other words, for the purposes of cosmological expansion, our universe behaves as if it were effectively matter-dominated despite the lack of an actual matter component. Following the arguments in Ref. [1], this means that this system can even co-exist with a "spectator" (noninteracting) additional *matter* energy component with abundance Ω_M because the introduction of such an additional spectator matter component will not disturb the stasis value $\langle w \rangle$ that has already been realized for the vacuum energy and radiation components. This then becomes an example of a system in which vacuum energy, radiation, and matter can all co-exist in a stasis configuration. Unfortunately, in such a system the matter must not have any energy-transferring interactions with either the vacuum energy or the radiation. It is for this reason that we refer to the matter as a "spectator" component of the total energy. Indeed, in such a system the matter abundance Ω_M remains fixed only because the vacuum energy and radiation in their stasis configuration with $\bar{\Omega}_\gamma = -3w\bar{\Omega}_\Lambda$ conspire to produce a universe whose expansion rate is effectively that of a
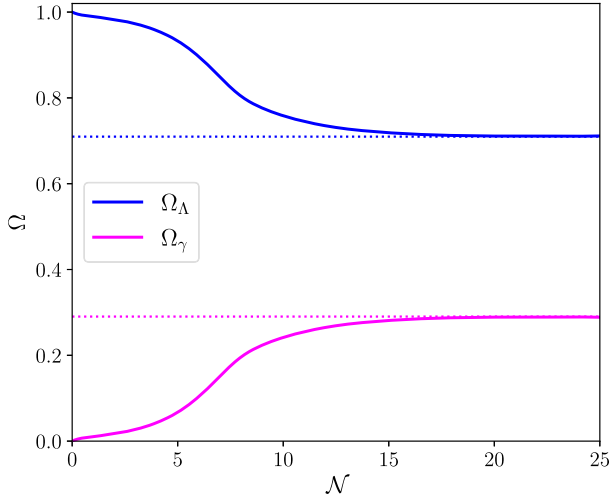
FIG. 4. Vacuum-energy/radiation stasis. Here we plot the total vacuum-energy and radiation abundances, Ω_Λ and Ω_γ respectively, as functions of time, taking $\alpha = 0.5$, $\delta = 2$, $\gamma = 1$, $w = -0.7$, and $H^{(0)}/\Gamma_{N-1} = 20$ as reference values and working with the exponential-decay formalism. As we see, these benchmark values lead to a stasis with $\bar{\kappa} = 10/3$, implying $\bar{\Omega}_\Lambda = 22/31 \approx 0.71$ and $\bar{\Omega}_\gamma = 9/31 \approx 0.29$. This stasis state ends only when the last component of the tower decays to radiation. Similar stasis behavior emerges for all values of $(\alpha, \delta, \gamma, w)$ within the range in Eq. (4.7), with corresponding stasis abundances $\bar{\Omega}_\Lambda$ determined by Eq. (4.8).

matter-dominated universe. As a result, Ω_M neither grows nor shrinks as a result of cosmological expansion, and thus remains constant without receiving energy from (or losing energy into) the other components.

In Fig. 4, we show the emergence of vacuum-energy/ radiation stasis for a system in which we take $\alpha = 0.5$, $\delta = 2$, $\gamma = 1$, and $w = -0.7$ as reference values. As we see, these lead to a stasis with $\bar{\kappa} = 10/3$, implying $\bar{\Omega}_\Lambda = 22/31$ and $\bar{\Omega}_\gamma = 9/31$. Indeed, as with the stases in Sec. II and III, this is a pairwise stasis involving only two components in which energy flows from one directly into the other, bypassing the third completely. A similar stasis would emerge for any parameters within the range in Eq. (4.7).

V. ALGEBRAIC STRUCTURE OF PAIRWISE STASES

In general, the analyses of Secs. II, III, and IV share an underlying algebraic structure which applies to any "pairwise" stasis (i.e., any stasis between two energy components). To demonstrate this, we shall maintain full generality by assuming that our two components have constant equation-of-state parameters (w_1, w_2) with corresponding abundances (Ω_1, Ω_2) such that $\Omega_1 + \Omega_2 = 1$. For concreteness we shall also assume that $w_1 < w_2$. This means that cosmological expansion will tend to convert an Ω_2-dominated universe into an Ω_1-dominated universe.

Thus stasis can be achieved only in the presence of some method of converting Ω_1 back into Ω_2. Because this conversion operates in a manner opposite to the natural effects of cosmological expansion, we shall refer to such a method of converting Ω_1 back into Ω_2 as a "pump."

Given this setup, and following our previous steps, it is straightforward to verify that our abundances $\Omega_{1,2}$ evolve according to the differential equations

$$\frac{d\Omega_1}{dt} = 3H(w_2 - w_1)\Omega_1\Omega_2 - P_{12},$$
$$\frac{d\Omega_2}{dt} = 3H(w_1 - w_2)\Omega_1\Omega_2 + P_{12}, \quad (5.1)$$

where P_{12} schematically denotes the pump term which transfers abundance from Ω_1 to Ω_2. Because we are interested in studying only the algebraic structure of the pairwise stasis, we shall leave this pump term unspecified. We verify from Eq. (5.1) that the gravitational redshifting effects indeed tend to increase Ω_1 and deplete Ω_2 if $w_2 > w_1$. We also verify, as required, that $d\Omega_2/dt = -d\Omega_1/dt$. Our condition for stasis is therefore

$$P_{12} = 3H(w_2 - w_1)\bar{\Omega}_1\bar{\Omega}_2. \quad (5.2)$$

In this system we generally have

$$\kappa = \frac{2}{1 + w_1\Omega_1 + w_2\Omega_2}. \quad (5.3)$$

Indeed this result holds regardless of whether we are in a stasis epoch. Thus our stasis condition takes the general form

$$P_{12} = \bar{\kappa}(w_2 - w_1)\bar{\Omega}_1\bar{\Omega}_2 \frac{1}{t}$$
$$= [2 - (1 + w_1)\bar{\kappa}]\bar{\Omega}_1 \frac{1}{t}. \quad (5.4)$$

This result is the (w_1, w_2) generalization of Eqs. (2.10), (3.18), and (4.5). However, we now see that this constraint is independent of the particular realization of the pump term P_{12} in terms of an underlying BSM physics model. Indeed, as we have stressed, this result reflects the general algebraic structure underlying all pairwise stases.

To proceed further we may assume that during stasis, our pumps have a general time dependence of the form

$$P_{12}(t) \sim t^{-1-p+2-(1+w_1)\bar{\kappa}} \quad (5.5)$$

where p is a general constant. Indeed, all of the pumps we have considered in this paper have this time dependence, with $p = \eta = \alpha + 1/\delta$ for the pump in Sec. III and $p = \eta/\gamma$ for the pump in Sec. II. Our pump will then have the required $1/t$ time dependence only if

$$p = 2 - (1 + w_1)\bar{\kappa}. \tag{5.6}$$

This serves as our general overall scaling constraint. This in turn implies that during stasis our pump must generally take the form

$$P_{12} = p\bar{\Omega}_1 \frac{1}{t}. \tag{5.7}$$

This is consistent with our prior results in Eqs. (2.30) and (3.31).

Given these results, the structure of the pairwise stasis solution is clear. In general we learn from Eq. (5.6) that

$$\bar{\kappa} = \frac{2 - p}{1 + w_1}. \tag{5.8}$$

We also observe from Eq. (5.3) that the abundance-weighted average $\langle w \rangle$ of w-values during stasis, i.e.,

$$\langle w \rangle \equiv w_1 \bar{\Omega}_1 + w_2 \bar{\Omega}_2, \tag{5.9}$$

is given by $\langle w \rangle = 2/\bar{\kappa} - 1$, or equivalently

$$\langle w \rangle = 2\left(\frac{1 + w_1}{2 - p}\right) - 1. \tag{5.10}$$

In conjunction with the constraint $\bar{\Omega}_1 + \bar{\Omega}_2 = 1$, Eqs. (5.9) and (5.10) then allow us to solve directly for $\bar{\Omega}_{1,2}$, yielding

$$\bar{\Omega}_1 = \frac{2(w_2 - w_1) - p(1 + w_2)}{(2 - p)(w_2 - w_1)}. \tag{5.11}$$

This of course agrees with our previous results in Eqs. (2.22), (3.25), and (4.8). We likewise have

$$\bar{\Omega}_2 = \frac{p(1 + w_1)}{(2 - p)(w_2 - w_1)}. \tag{5.12}$$

In this connection, we note that we always must have $p < 2$. More specifically, for this system we have $w_1 < \langle w \rangle < w_2$, or equivalently

$$\frac{2}{1 + w_2} < \bar{\kappa} < \frac{2}{1 + w_1}. \tag{5.13}$$

This implies via Eq. (5.6) that all values of p lead to a consistent stasis solution so long as

$$0 < p < \frac{2(w_2 - w_1)}{1 + w_2}. \tag{5.14}$$

We conclude with three important comments. First, we see from the above analysis that the details of the pump are relevant *only for determining the abundance-weighted "center" of our system in w-space*, as in Eq. (5.10).

By contrast, once this w-average $\langle w \rangle$ is determined, the two stasis abundances $\bar{\Omega}_{1,2}$ are situated relative to this average in a pump-independent way, as in Eq. (5.9). Indeed, we shall more fully exploit this way of thinking in Sec. VI F when discussing triple stasis.

Second, we note that the solution for $\langle w \rangle$ in Eq. (5.10) can also be written in a form that more manifestly respects the $1 \leftrightarrow 2$ symmetry between our two components. This can be done by extracting $\bar{\kappa}$ from the first line of Eq. (5.4) [in conjunction with Eq. (5.7)] rather than from Eq. (5.6). We thereby obtain the stasis solution

$$\langle w \rangle = \frac{4(w_2 - w_1)\bar{\Omega}_1\bar{\Omega}_2}{(1 + \bar{\Omega}_1 - \bar{\Omega}_2)p} - 1. \tag{5.15}$$

This, in conjunction with the constraint in Eq. (5.9), also permits an evaluation of the stasis abundances $\bar{\Omega}_{1,2}$.

Finally, we note that in this section we have limited our discussion to the algebraic structure of pairwise stases—namely the required relations between pumps and cosmological expansion. However, the critical remaining issue is to realize such pumps in terms of actual underlying BSM particle-physics models. For example, in Secs. II, III, and IV we worked within the context of models involving large towers of states and demonstrated that we could realize the pumps needed for stasis in terms of natural particle-physics processes such as particle decays and/or underdamping transitions. It is this success that we consider to be the primary achievement of our previous analyses.

VI. TRIPLE STASIS

In our previous paper [1] (and as reviewed in Sec. II), we demonstrated that matter can exist in stasis with radiation. Likewise, in Secs. III and IV, we further demonstrated that vacuum energy can exist in stasis with matter or with radiation, respectively. Each of these configurations represents a pairwise stasis between two different types of energy components. Given this, the obvious next question is to determine whether it is possible to have a *triple stasis* in which vacuum energy, matter, and radiation all co-exist in stasis with each other.

At the end of Sec. IV, we noted that this can occur in a universe in which the matter energy component is merely a noninteracting "spectator." However, the question we now wish to investigate concerns whether we can have a true triple stasis in which all three energy components are interacting nontrivially with each other.

Of course, in a universe that contains all three energy components, cosmological expansion inevitably shifts the identity of the dominant component along the chain

$$\gamma \to M \to \Lambda, \tag{6.1}$$

i.e., in the direction of decreasing w. In other words, a mixed-component universe that starts in a radiation-dominated configuration will eventually tend to become matter dominated and then vacuum dominated, simply as a result of cosmological expansion. However, we are now seeking to determine if this entire process can be simultaneously counterbalanced by

$$\text{underdamping transition: } \Lambda \to M,$$
$$\text{decay: } M \to \gamma. \qquad (6.2)$$

Indeed, as we have discussed in Sec. V, each of these effects essentially serves as a "pump" which counterbalances the natural tendencies induced by cosmological expansion by transferring energy back up towards components with larger values of w. While we already know that this counterbalancing can occur successfully for each step individually, the question is to determine whether (and to what extent) both counterbalancings can co-exist within the same overall cosmology.

We emphasize that this is, *a priori*, a highly nontrivial question. Even though a given energy component A might come into stasis with another energy component B in an A/B universe, and even though A might also come into stasis with C in an A/C universe, and even though B might come into stasis with C in a B/C universe, it does not necessarily follow that A, B, and C can all simultaneously come into stasis in an $A/B/C$ universe. This is because each of our previous energy-transfer processes (underdamping and decay) would now need to operate in a universe which also contains a *third* energy component. This third component affects the Hubble parameter and thus the overall expansion rates whose effects would need to cancel for a triple stasis.

Phrased slightly differently, a true triple stasis can arise only if both processes (underdamping and decay) can occur simultaneously *while embedded within a common cosmology*. Indeed, triple stasis requires that these processes be capable of co-existing with each other within the same cosmological setting, and this co-existence requirement may (and ultimately will) place new mathematical constraints on each.

To study this, we shall proceed in several steps. We shall begin, as in Sec. V, by studying the general algebraic structure of triple stasis in a model-independent way, deriving constraints that any simultaneous pumping transitions must satisfy in order to achieve triple stasis. We shall then explore the different possible configurations that a triple stasis may exhibit in terms of our underlying particle-physics model involving large towers of states with particle decays and underdamping transitions. After this, we shall perform a general analysis of triple stasis and derive the overall scaling equations that must be satisfied in order for triple stasis to exist. In so doing, we shall discover an additional constraint which must be satisfied in order for

the overdamping and decay transitions to co-exist within the same cosmology.

With these results in hand, we shall then proceed to consider the corresponding prefactor constraints. Unlike the situations that arose in previous sections for pairwise stases, we shall now find that our prefactor constraints are no longer redundant with our scaling constraints. Instead, we shall see that they actually supply additional information. Finally, we shall pull all the pieces together in a graphical, intuitive way which demonstrates how triple stasis ultimately operates.

As might be imagined, this section is in some sense the central core of this paper. We shall therefore attempt to provide as many different perspectives on our results as possible—general and specific, algebraic and intuitive. All of these perspectives will be useful in subsequent sections when we extend the results of this section in order to consider the attractor nature of all of our stases, when we develop a phase-space understanding of the stasis phenomenon as a whole, and when we extend our analysis to consider various close variants of stasis.

A. Algebraic structure of triple stasis

To analyze the algebraic structure of stasis, we shall repeat our previous steps, only now within a completely general cosmology simultaneously comprising all three components (vacuum energy, matter, and radiation), all treated dynamically. Following the previous analyses, we find in all generality that

$$\kappa \equiv \frac{6}{2 + (1 + 3w)\Omega_\Lambda + \Omega_M + 2\Omega_\gamma} \qquad (6.3)$$

where κ, as always, is related to the rate of change of the Hubble parameter via Eq. (3.3). We then have

$$\frac{d\Omega_i}{dt} = \frac{8\pi G}{3H^2}\frac{d\rho_i}{dt} + \frac{6}{\kappa}H\Omega_i. \qquad (6.4)$$

We now must insert the equations of motion $d\rho_i/dt$ for our system. In general, our system will have equations of motion with the algebraic structure

$$\frac{d\rho_\Lambda}{dt} = -P_{\Lambda M}^{(\rho)} - P_{\Lambda\gamma}^{(\rho)} - 3(1 + w)H\rho_\Lambda,$$
$$\frac{d\rho_M}{dt} = +P_{\Lambda M}^{(\rho)} - P_{M\gamma}^{(\rho)} - 3H\rho_M,$$
$$\frac{d\rho_\gamma}{dt} = +P_{\Lambda\gamma}^{(\rho)} + P_{M\gamma}^{(\rho)} - 4H\rho_\gamma, \qquad (6.5)$$

where $P_{ij}^{(\rho)}$ denotes the "pump" term that describes the conversion of energy density ρ from type i to type j, and where the signs preceding these terms indicate whether this pump is acting as a sink ($-$) or source ($+$). Inserting this into Eq. (6.4) we obtain

$$\frac{d\Omega_\Lambda}{dt} = -P_{\Lambda M} - P_{\Lambda\gamma} + \frac{6}{\kappa}H\Omega_\Lambda - 3(1+w)H\Omega_\Lambda,$$

$$\frac{d\Omega_M}{dt} = P_{\Lambda M} - P_{M\gamma} + \frac{6}{\kappa}H\Omega_M - 3H\Omega_M,$$

$$\frac{d\Omega_\gamma}{dt} = P_{\Lambda\gamma} + P_{M\gamma} + \frac{6}{\kappa}H\Omega_\gamma - 4H\Omega_\gamma, \tag{6.6}$$

where

$$P_{ij}(t) \equiv \frac{8\pi G}{3H(t)^2}P_{ij}^{(\rho)}(t). \tag{6.7}$$

Thus $P_{ij}(t)$ denotes a pump for *abundances*, while $P_{ij}^{(\rho)}(t)$ denotes the corresponding pump for *energy densities*. As a self-consistency check, we observe that $d\Omega_\Lambda/dt + d\Omega_M/dt + d\Omega_\gamma/dt$ indeed vanishes.

Let us now investigate the conditions under which our system can be in an (eternal) stasis epoch. During such a period, we must certainly have $d\Omega_\Lambda/dt = d\Omega_M/dt = d\Omega_\gamma/dt = 0$. This gives rise to the conditions

$$P_{\Lambda M} + P_{\Lambda\gamma} = \frac{6}{\bar\kappa}H\bar\Omega_\Lambda - 3(1+w)H\bar\Omega_\Lambda,$$

$$-P_{\Lambda M} + P_{M\gamma} = \frac{6}{\bar\kappa}H\bar\Omega_M - 3H\bar\Omega_M,$$

$$-P_{\Lambda\gamma} - P_{M\gamma} = \frac{6}{\bar\kappa}H\bar\Omega_\gamma - 4H\bar\Omega_\gamma, \tag{6.8}$$

where the pump terms P_{ij} are to be evaluated during a period of stasis. Likewise, from Eqs. (3.3) and (6.3) we can solve for the Hubble parameter H during stasis, obtaining

$$H(t) = \frac{\bar\kappa}{3t}. \tag{6.9}$$

Inserting this into Eq. (6.8) we obtain

$$P_{\Lambda M} + P_{\Lambda\gamma} = \left[2 - (1+w)\bar\kappa\right]\bar\Omega_\Lambda\frac{1}{t}$$

$$-P_{\Lambda M} + P_{M\gamma} = \left[2 - \bar\kappa\right]\bar\Omega_M\frac{1}{t}$$

$$-P_{\Lambda\gamma} - P_{M\gamma} = \left[2 - \frac{4\bar\kappa}{3}\right]\bar\Omega_\gamma\frac{1}{t}. \tag{6.10}$$

These, then, are the most general conditions for a triple stasis involving vacuum energy, matter, and radiation. (Similar conditions can likewise be derived for any three energy components, or even for more than three components.) Indeed, any pump terms P_{ij} satisfying these equations as functions of time will lead to an extended (eternal) stasis epoch. With $\bar\kappa$ given in Eq. (6.3) and with $\bar\Omega_\Lambda + \bar\Omega_M + \bar\Omega_\gamma = 1$ we immediately verify that the sum of these equations vanishes, implying that only two of these equations are truly independent of each other, as expected.

We also note that $2 - 4\bar\kappa/3 < 0$ for all $(\bar\Omega_\Lambda, \bar\Omega_M, \bar\Omega_\gamma)$ within the ranges $0 \le \Omega_i \le 1$ with $\sum_i\Omega_i = 1$. Thus while both sides of the first equation in Eq. (6.10) are necessarily positive, both sides of the third equation are necessarily negative. By contrast, the sign of both sides of the second equation ultimately depends on whether the pumping action produces a net flow of energy into or out of matter. Of course, during stasis, the sign of this net flow will be exactly as needed in order to compensate for the effects of cosmological expansion, the latter also having either a positive or negative sign depending on the particular values of $(\bar\Omega_\Lambda, \bar\Omega_M, \bar\Omega_\gamma)$.

We have already remarked that Eq. (5.4) describes the algebraic structure of pairwise stases. From this perspective, Eq. (6.10) is the triple-stasis analog of Eq. (5.4) and likewise describes the algebraic structure of triple stasis, once again in terms of general pumps but focused on vacuum energy, matter, and radiation.

B. Surveying the possible configurations

Our job is now to construct a particle-physics model of stasis in which the P_{ij} pump terms are consistent with these equations. To do this, let us return to our model consisting of a tower of zero-mode scalar fields ϕ_ℓ, with $\ell = 0, 1, ..., N-1$. However we shall now take into account not only the underdamping transition of Sec. III but also the possibility of particle decay, as discussed in Secs. II and IV. In general, a given field ϕ_ℓ of mass m_ℓ and decay width Γ_ℓ will experience an underdamping transition at the time t_ℓ for which $3H(t_\ell) = 2m_\ell$, while this same field will also decay with lifetime $\tau_\ell = 1/\Gamma_\ell$. For simplicity we shall assume that $t_\ell < \tau_\ell$ for all ℓ—an assumption which will be discussed in more detail below—and we shall adopt the "instantaneous decay" approximation in Eq. (4.12) in which a given state ϕ_ℓ is presumed to decay instantaneously and fully at $t = \tau_\ell$. As discussed below Eq. (4.12), this instantaneous-decay assumption will not be critical for any of our important results. However, this assumption allows the decay transition to more closely resemble the underdamping transition, with each treated as occurring instantaneously and completely at a specified time. Later in this section we shall also consider the case with full exponential decay and verify that our basic results remain intact.

In general, these fields ϕ_ℓ will have time-dependent energy densities $\rho_\ell(t)$. As in previous sections, we shall interpret this energy density as vacuum energy for times $t < t_\ell$, but as matter if $t_\ell < t < \tau_\ell$ and as radiation if $t > \tau_\ell$. We shall let $\rho_{\rm tot}^{(\Lambda)}(t)$, $\rho_{\rm tot}^{(M)}(t)$, and $\rho_{\rm tot}^{(\gamma)}(t)$ represent the corresponding total energy densities of each type at any given time t, and let $\Omega_\Lambda(t)$, $\Omega_M(t)$, and $\Omega_\gamma(t)$ represent the corresponding total abundances.

Within a period of stasis, the underdamping time t_ℓ associated with underdamping transitions is given by the condition $3H(t_\ell) = 2m_\ell$, or equivalently $t_\ell = \bar\kappa/(2m_\ell)$

where we have used Eq. (6.9). This provides a relation between t_ℓ and the corresponding mass m_ℓ. Likewise, from Eq. (2.12) we see that the lifetimes τ_ℓ are given by

$$\tau_\ell = \frac{1}{\Gamma_\ell} = \frac{1}{\Gamma_0}\left(\frac{m_\ell}{m_0}\right)^{-\gamma}. \tag{6.11}$$

This provides a relation between τ_ℓ and the mass m_ℓ. It therefore follows that when $\gamma \neq 1$ there is a critical mass for which $t_\ell = \tau_\ell$. Indeed, letting the subscript "X" denote this critical point, we find

$$t_X^{\gamma-1} = \xi^{-\gamma}\Gamma_0^{1-\gamma}, \qquad m_X^{\gamma-1} = \xi m_0^{\gamma-1}, \tag{6.12}$$

where ξ is defined in Eq. (2.14). Of course, for $\gamma = 1$, there is no single point X at which $t_X = \tau_X$.

It also follows from Eqs. (3.15) and (6.11) that

$$\frac{\tau_\ell}{t_\ell} = \xi(\Gamma_0\tau_\ell)^{1-1/\gamma}. \tag{6.13}$$

This result holds for all values of γ. However, for $\gamma \neq 1$ we find that $\xi = (\Gamma_0 t_X)^{1/\gamma-1}$, whereupon we have $\tau_\ell/t_\ell = (\tau_\ell/t_X)^{1-1/\gamma}$.

In complete analogy with the sketch in the right panel of Fig. 2, we may now sketch the anticipated behavior of the energy densities ρ_ℓ in this system as a function of time during a potential period of triple stasis. As we shall demonstrate, there are a number of distinct possibilities for how these energy densities might behave. We shall therefore begin by discussing these different possibilities.

For convenience, following the discussion in Sec. III, we shall continue to assume for the purpose of such energy-density sketches that $w \approx -1$, so that $\rho_\ell(t)$ is approximately constant for all $t < t_\ell$. Of course, the critical new feature for triple stasis is the existence of two independent transitions, the first between vacuum energy and matter occurring at the critical underdamping time t_ℓ for which $3H(t_\ell) = 2m_\ell$, and the second between matter into radiation occurring at the decay time $\tau_\ell = 1/\Gamma_\ell$. At any time t_ℓ, the original energy density $\rho_\ell^{(0)}$ which experiences the underdamping transition from vacuum energy to matter scales as

$$\rho_\ell^{(0)} \sim m_\ell^\alpha \sim t_\ell^{-\alpha}. \tag{6.14}$$

On a log-log plot of energy density versus time, this underdamping "$3H = 2m$" transition line would thus appear with slope $-\alpha$, precisely as in the right panel of Fig. 2. Likewise, at any time τ_ℓ, the original energy density $\rho_\ell^{(0)}$ which decays from matter to radiation scales as

$$\rho_\ell^{(0)} \sim m_\ell^\alpha \sim \tau_\ell^{-\alpha/\gamma}. \tag{6.15}$$

On a log-log plot of energy density versus time, this decay transition "$t = 1/\Gamma$" line would thus appear with slope $-\alpha/\gamma$.

In principle, these two transition lines govern the behavior of the system. However, for the purposes of our energy-density sketches it will prove useful to introduce a third transition line. This line is motivated by the observation that each energy density ρ_ℓ no longer has its initial value $\rho_\ell^{(0)}$ at the time when the corresponding ϕ_ℓ field decays because of the existence of the earlier under-damping transition at $t = t_\ell$ which converted the corresponding ρ_ℓ energy density from vacuum energy to matter. As a result, by the time $t = \tau_\ell$ is reached, this energy density has now fallen to $\rho_\ell \sim \rho_\ell^{(0)}(\tau_\ell/t_\ell)^{-\bar{\kappa}}$ because it has spent the time interval between t_ℓ and τ_ℓ behaving as matter rather than vacuum energy. We thus have

$$\rho_\ell(\tau_\ell) \sim m_\ell^\alpha\left(\frac{\tau_\ell}{t_\ell}\right)^{-\bar{\kappa}} \sim \tau_\ell^{-\alpha/\gamma-\bar{\kappa}(\gamma-1)/\gamma}. \tag{6.16}$$

On a log-log plot of energy density versus time, this "effective decay" transition line would thus appear with slope $-\alpha/\gamma - \bar{\kappa}(\gamma - 1)/\gamma$. Because this line corresponds to the actual values of the energy densities ρ_ℓ at the times when the corresponding states ϕ_ℓ are decaying, it is this third line which in some sense represents the true decay transition, relating the energy density at the decay time to the time at which the decay transition occurs. By contrast, the "$\tau = 1/\Gamma$" line discussed above corresponds to the decay line that would have been relevant *if no prior transition to matter had occurred*.

Putting these observations together, we see that on a log-log plot of energy density versus time, we now expect to have *three* transition lines with different slopes:

$$3H = 2m \text{ line: slope} = -\alpha,$$
$$\tau = 1/\Gamma \text{ line: slope} = -\alpha/\gamma,$$
$$\text{effective decay line: slope} = -\alpha/\gamma - \bar{\kappa}(\gamma - 1)/\gamma. \tag{6.17}$$

Of course, for $\gamma \neq 1$, all three of these lines intersect at the critical point X described in Eq. (6.12). By contrast, for $\gamma = 1$, these lines are all parallel.

There is one final point that we must also consider before sketching the possible behaviors of the energy densities during triple stasis. This is the fact that the magnitudes of our energy densities ρ_ℓ should continue to experience successive pairwise crossings as time evolves, just as we observed in the right panel of Fig. 2, so that the identity of the ϕ_ℓ component with the largest energy density is continually changing as our transitions proceed down the tower, just as each energy density changes from vacuum energy to matter to radiation. As we discussed in relation to the right panel of Fig. 2, it is this behavior involving successive energy-density crossings which underlies the pairwise stasis phenomenon, and we expect the same to be true for triple stasis as well. In Sec. III, this crossing interleaved behavior was the result of the energy densities

$\rho_\ell(t)$ "reflecting" off the transition line; indeed, this property is ultimately what distinguished the behavior sketched in the right panel of Fig. 2 from that sketched in the left panel, the latter of which does not lead to stasis. Towards this end, we shall similarly expect a reflecting inter-leaved behavior for triple stasis. However, we now have *two* transition lines relative to which such reflections could potentially occur. As a result, we can consider situations in which our energy densities reflect off the first transition line, but we can alternatively consider situations in which our energy densities pass through the first transition line and reflect off the second line instead.

Putting all of these ingredients together, we see that there are in principle *six* different classes of possible behaviors for the energy densities during triple stasis. These six resulting possible behaviors correspond to taking $\gamma > 1$, $\gamma < 1$, or $\gamma = 1$, and then in each case considering either reflection off the $3H = 2m$ transition line or reflection off the effective decay line. These six resulting possible behaviors are sketched in Figs. 5–7. Given that the slopes of the yellow (matter) and green (radiation) $\rho_\ell(t)$ lines are respectively given by $-\bar{\kappa}$ and $-4\bar{\kappa}/3$, we see that the condition for reflecting off the $3H = 2m$ transition line is simply $\bar{\kappa} > \alpha$. By contrast, the condition for *not* reflecting off this line but instead reflecting off the effective decay line is given by $\phi\alpha < \bar{\kappa} < \alpha$ where $\phi \equiv (1 + \gamma/3)^{-1}$.

As evident from Figs. 5–7, the behavior of our system is highly sensitive to whether $\gamma > 1$ (as in Fig. 5), $\gamma < 1$ (as in Fig. 6), or $\gamma = 1$ (as in Fig. 7). For $\gamma > 1$, we find that $\tau_\ell > t_\ell$ for all $m_\ell < m_X$. Thus the portion of the tower with $m < m_X$ corresponds to a region in which we can expect the underdamping transition to *precede* the eventual decay, consistent with our original assumptions. Indeed, as time evolves, the states in this region each experience a transition from vacuum energy to matter and then ultimately from matter to radiation. Thus, within this region, we might imagine a triple stasis emerging if $m_0 \ll m_{N-1} < m_X$. By contrast, for $\gamma < 1$, we find that $\tau_\ell > t_\ell$ only for $m_\ell > m_X$. It is therefore within the portion of the tower with $m > m_X$ that we might imagine a triple stasis emerging. This is especially true if $m_{N-1} \gg m_X$, so that a triple stasis has time to develop within this region. As the transitions proceed down from m_{N-1} and approach m_X, the "matter" phase experienced by the corresponding states prior to decay has shorter and shorter duration until it disappears entirely at $m = m_X$, thereby extinguishing this part of the triple stasis. Finally, for $\gamma = 1$, no critical point X exists. We then find that $\tau_\ell/t_\ell = 2m_0/(\bar{\kappa}\Gamma_0) = \xi$ for *all* masses m_ℓ. Thus in this case our *entire* tower could potentially support a triple stasis if $\tau_\ell/t_\ell > 1$ (i.e., if $\xi > 1$), but could never support a triple stasis otherwise.

Thus, to summarize, in our model of triple stasis we shall restrict our attention to those portions of our tower—and those times t—that satisfy the conditions

$$\begin{cases} m < m_X, t > t_X & \text{for } \gamma > 1, \\ m > m_X, t < t_X & \text{for } \gamma < 1, \qquad (6.18) \\ \xi > 1, \text{any } (m, t) & \text{for } \gamma = 1. \end{cases}$$

Of course, we stress that the sharp inequalities within each of the different cases in Eq. (6.18) exist only because we have assumed the instantaneous-decay approximation.

The regions of our ϕ_ℓ towers given in Eq. (6.18) are precisely those for which $t_\ell < \tau_\ell$, thereby allowing a matter phase to emerge for each ℓ. Thus, within the regions outlined in Eq. (6.18), we are assured that our tower simultaneously gives rise to vacuum energy, matter, and radiation. Likewise, within the times indicated in Eq. (6.18), there are two independent transitions occurring simultaneously: the damping transition from vacuum energy to matter, and the decay transition from matter to radiation. Taking vertical time slices through the relevant portions of Figs. 5 through 7, we then obtain the situation illustrated in Fig. 8. At any moment, the states within the lowest portion of the tower have not yet experienced any transitions and can thus be interpreted as contributing to vacuum energy, while the states within an intermediate middle portion can be interpreted as matter and the states within the upper portion have already decayed to radiation. Although the underdamping and decay transitions at any fixed time are occurring at different locations within the tower—the former occurring for lighter states and the latter occurring for heavier states—they are each independently making their way down the tower. For $\gamma > 1$, the decay transition makes its way down the tower more slowly than the underdamping transition, implying that as time evolves an increasingly large portion of the tower behaves as matter. By contrast, for $\gamma < 1$ the reverse is true: the decay transition makes its way down the tower more *rapidly* than the underdamping transition, and ultimately catches up to it when $m_\ell = m_X$ (which signals the boundary of our region of interest as far as triple stasis is concerned). Finally, for $\gamma = 1$, these transitions make their way down the tower at exactly the same rate.

In the rest of this section we shall be interested in situations in which both transitions are still occurring within the relevant portions of our tower, far from any "edge" effects either at the top or bottom of the regions of interest indicated within Eq. (6.18). This in turn implies that we shall focus our attention on situations in which our states ϕ_ℓ, $\ell = 0, 1, ..., N - 1$, have a maximum mass m_{N-1} satisfying

$$\begin{cases} m_X > m_{N-1} \gg 0 & \text{for } \gamma > 1, \\ m_{N-1} \gg m_X & \text{for } \gamma < 1, \qquad (6.19) \\ m_{N-1} \gg 0 & \text{for } \gamma = 1. \end{cases}$$

Finally, before concluding this discussion, let us briefly add further context to our assumption that $t_\ell < \tau_\ell$ for all ℓ. In making this assumption, we are explicitly disregarding
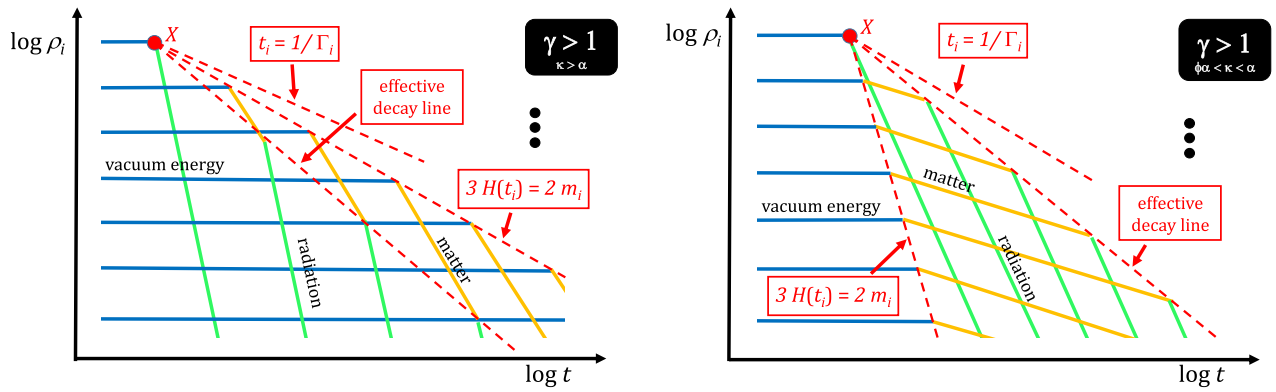
FIG. 5.   Left panel: the individual energy densities $\rho_\ell(t)$ for the states ϕ_ℓ with $m_\ell < m_X$, sketched as functions of time during a stasis epoch with $\gamma > 1$ and $\bar{\kappa} > \alpha$. Each state undergoes a transition from an overdamped phase (blue) to an underdamped phase (yellow) at a time t_ℓ for which $3H(t_\ell) = 2m_\ell$ before subsequently decaying to radiation (green) at the time $\tau_\ell \equiv 1/\Gamma_\ell$. The dashed lines (red) indicate the moments of transition between these different behaviors and have slopes given in Eq. (6.17). For the purposes of this sketch we have assumed that states with greater energy densities have greater masses (i.e., that $\alpha > 0$). We have also assumed that $H(t) \sim 1/t$ with a fixed constant of proportionality, as appropriate during stasis, and we have taken $w \approx -1$ so that our vacuum-energy lines are essentially horizontal. We see by considering vertical time slices through this figure that the identity of the state with the greatest energy density is time dependent, with lighter and lighter states carrying increasing shares of the total energy density as time evolves. Right panel: same as left panel, but now sketched for $\bar{\kappa}$ within the range $\phi\alpha < \bar{\kappa} < \alpha$ where $\phi \equiv (1 + \gamma/3)^{-1}$.
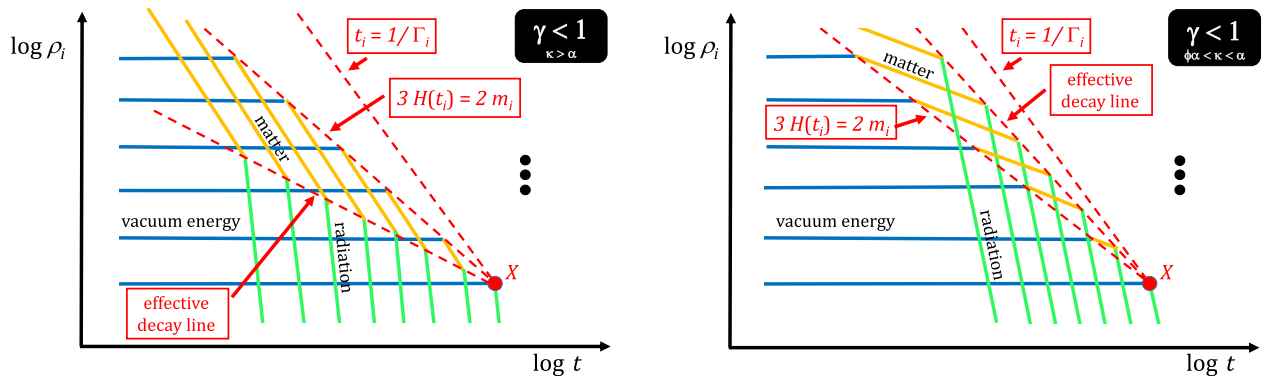

FIG. 6.   Left panel: same as Fig. 5, but now sketched for $\gamma < 1$. Here it is the *heavier* portion of the tower with $m > m_X$ for which the states experience transitions from overdamped to underdamped behavior before decaying to radiation. Right panel: same as left panel, but for $\bar{\kappa}$ within the range $\phi\alpha < \bar{\kappa} < \alpha$ where $\phi \equiv (1 + \gamma/3)^{-1}$.
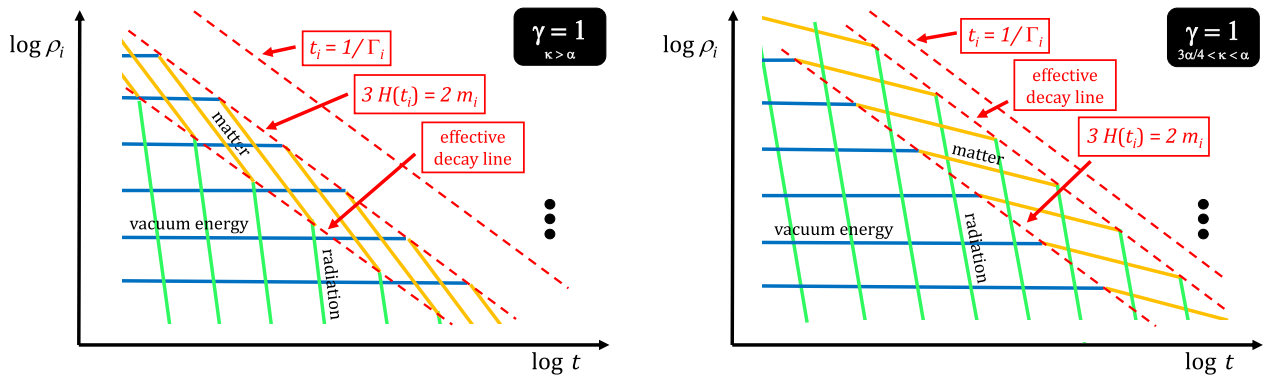

FIG. 7.   Left panel: same as Figs. 5 and 6, but now sketched for $\gamma = 1$. As long as $\xi > 1$, each component across the *entire* tower experiences a transition from overdamped to underdamped behavior before decaying to radiation. Right panel: same as left panel, but now sketched for $\bar{\kappa}$ within the range $3\alpha/4 < \bar{\kappa} < \alpha$.
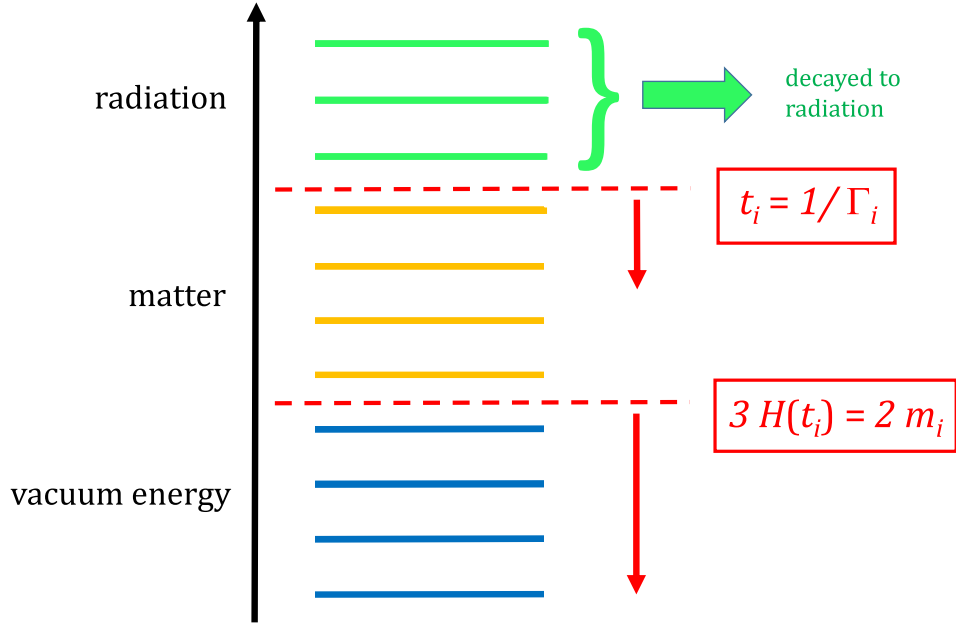
FIG. 8. Triple stasis in action: the structure of the tower ϕ_ℓ during a potential triple-stasis epoch. The individual states are shown in order of increasing ℓ, just as they are at the initial time in Figs. 5 through 7, with colors determined by considering appropriate vertical time slices through these figures as time evolves. At any moment two separate transitions are occurring at different locations within the tower: an underdamping transition from vacuum energy (blue) to matter (yellow) occurring at a lower location within the tower, and a decay transition from matter (yellow) to radiation (green) simultaneously occurring at a higher location. As time evolves, both transitions work their way down the tower, with the color of a given state changing from blue to yellow and then from yellow to green as each of the two transitions sweeps past it. For $\gamma > 1$ the decay transition proceeds down the tower more slowly than the underdamping transition, thereby allowing the matter region of the tower to continually increase in size. By contrast, for $\gamma < 1$ the decay transition proceeds more quickly down the tower than the underdamping transition, ultimately catching up with it at $m = m_X$. For $\gamma = 1$ both transitions move down the tower at the same rate. All of this occurs within an expanding universe, thereby potentially supporting a triple-stasis epoch.

the possibility that $t_\ell > \tau_\ell$—i.e., that the vacuum energy can decay directly to radiation even within the instantaneous-decay approximation. Of course, as discussed at the beginning of Sec. IV, it is indeed possible for vacuum energy to decay or dissipate directly to radiation (or to a component that functions cosmologically as radiation, with $w = 1/3$). However, for our current purposes, such transitions are of less interest because they would completely bypass the matter phase which is needed in order to have a true triple stasis. Moreover, the point X described in Eq. (6.12) signifies the critical location within the ϕ_ℓ tower which separates $t_\ell < \tau_\ell$ behavior from $t_\ell > \tau_\ell$ behavior. Thus, by choosing to focus our attention on only one side of X but not the other, we are implicitly enforcing the restriction that $t_\ell < \tau_\ell$ so that an intermediate matter phase appears.

These observations hold only within the instantaneous-decay approximation. By contrast, a treatment involving a full exponential decay (replete with exponential tails in both directions) would continue to allow vacuum energy to be converted directly to our $w = 1/3$ component even when $t_\ell < \tau_\ell$. Indeed, this possibility can occasionally be quite significant, and becomes extremely remote only when $\tau_\ell \gg t_\ell$. From Eq. (6.13), we see that the latter situation

arises only if $\xi \gg 1$. Thus, while it is certainly a mathematically self-consistent choice to adopt the instantaneous-decay approximation and restrict our attention to ϕ_ℓ towers for which $t_\ell < \tau_\ell$ for all ℓ, we expect such a treatment to match the results of a fully physical exponential decay only when $\xi \gg 1$. This issue will be discussed in more detail later in this section and in Sec. VIII.

Given this understanding, we shall proceed by adopting the instantaneous-decay approximation and assuming that $t_\ell < \tau_\ell$ for all ℓ. We shall do this with the understanding that such a model represents what we may consider to be a faithful representation of the full exponential decay within the $\xi \gg 1$ regime. With this model in hand, our goal is then to determine whether the resulting system can host a true triple stasis in which the total abundances Ω_Λ, Ω_M, and Ω_γ each remain fixed despite cosmological expansion.

C. Overall scaling constraints

Within this system, our first step is to evaluate the pump terms in Eq. (6.10) during a period of stasis. This in turn requires that we determine $d\rho_{\text{tot}}^{(i)}/dt$ for $i = \Lambda, M, \gamma$ within this model, since the pump terms P_{ij} are defined through their appearance in Eq. (6.5). In order to derive these

equations, we shall proceed in stages. First, within each of the ranges specified above in Eqs. (6.18) and (6.19) we can approximate the corresponding energy-density contributions from each ϕ_ℓ component during (eternal) stasis as

$$
\rho_\ell^{(\Lambda)}(t) = \rho_\ell^* \left(\frac{t}{t_*}\right)^{-(1+w)\bar{\kappa}} \Theta(t_\ell - t),
$$

$$
\rho_\ell^{(M)}(t) = \rho_\ell^* \left(\frac{t_\ell}{t_*}\right)^{-(1+w)\bar{\kappa}} \left(\frac{t}{t_\ell}\right)^{-\bar{\kappa}} \Theta(t - t_\ell)\Theta(\tau_\ell - t),
$$

$$
\rho_\ell^{(\gamma)}(t) = \rho_\ell^* \left(\frac{t_\ell}{t_*}\right)^{-(1+w)\bar{\kappa}} \left(\frac{\tau_\ell}{t_\ell}\right)^{-\bar{\kappa}} \left(\frac{t}{\tau_\ell}\right)^{-4\bar{\kappa}/3} \Theta(t - \tau_\ell),
$$

$$(6.20)$$

where t_* is a fiducial early time within our eternal stasis prior to t_ℓ. Indeed, these are the relations whose $w \to -1$ limits are sketched in Figs. 5 through 7, but we shall keep w arbitrary for our algebraic analysis. The Heaviside functions within these equations capture the manner in which the original energy density ρ_ℓ of each ϕ_ℓ field is transferred between the vacuum-energy, matter, and radiation components at times t_ℓ and τ_ℓ as the universe expands.

Of course, strictly speaking, our assumption that $t_* < t_\ell$ for all ℓ is inconsistent with our assumption that our stasis is eternal. Indeed, Eq. (6.20) may be viewed as the triple-stasis analog of Eq. (2.11), for which similar issues arose. However, just as in Sec. II, we shall temporarily proceed with this assumption since it will not affect our eventual stasis constraints, deferring a formal justification of our adoption of this assumption to Sec. VI E.

Given the energy densities in Eq. (6.20), we immediately find

$$
\frac{d\rho_\ell^{(\Lambda)}}{dt} = -\rho_\ell^* \left(\frac{t_\ell}{t_*}\right)^{-(1+w)\bar{\kappa}} \delta(t - t_\ell) - 3(1+w)H\rho_\ell^{(\Lambda)},
$$

$$
\frac{d\rho_\ell^{(M)}}{dt} = \rho_\ell^* \left(\frac{t_\ell}{t_*}\right)^{-(1+w)\bar{\kappa}} \delta(t - t_\ell)
$$
$$
\quad - \rho_\ell^* \left(\frac{t_\ell}{t_*}\right)^{-(1+w)\bar{\kappa}} \left(\frac{\tau_\ell}{t_\ell}\right)^{-\bar{\kappa}} \delta(t - \tau_\ell) - 3H\rho_\ell^{(M)},
$$

$$
\frac{d\rho_\ell^{(\gamma)}}{dt} = \rho_\ell^* \left(\frac{t_\ell}{t_*}\right)^{-(1+w)\bar{\kappa}} \left(\frac{\tau_\ell}{t_\ell}\right)^{-\bar{\kappa}} \delta(t - \tau_\ell) - 4H\rho_\ell^{(\gamma)}. \quad (6.21)
$$

In order to calculate the total energy densities $\rho_i = \sum_\ell \rho_\ell^{(i)}$, we now wish to sum these equations over all of the ϕ_ℓ states in our theory. To do this, we shall pass to the continuum limit in which we express our ℓ-parameter in terms of the corresponding underdamping time t_ℓ (as in Sec. III) or lifetime τ_ℓ (as in Sec. II) and then treat t_ℓ or τ_ℓ as a continuous parameter $\hat{t}$ or τ respectively. In other words, we shall replace

$$
\sum_\ell \to \int d\hat{t}\, n_{\hat{t}}(\hat{t}) \quad \text{or} \quad \sum_\ell \to \int d\tau\, n_\tau(\tau), \quad (6.22)
$$

where $n_{\hat{t}}(\hat{t})$ and $n_\tau(\tau)$ are respectively the densities of states per unit $\hat{t}$ and τ, evaluated at the locations within our tower for which the underdamping time or lifetime is given by $\hat{t}$ or τ, respectively. Indeed, for each term within Eq. (6.21), we shall choose the first option within Eq. (6.22) if the relevant term in Eq. (6.21) contains a δ-function involving t_ℓ, and the second option if the relevant term contains a δ-function involving τ_ℓ.

We shall likewise consider the energy densities $\rho_\ell(t)$ to be labeled not by the discrete variable ℓ but by the continuous variables $\hat{t}$ or τ. However, each of these energy densities itself evolves as a function of time. Thus for each energy density we actually have two kinds of time variables in play, one telling us *which* energy density we are talking about (i.e., corresponding to *which* ϕ_ℓ within the tower) and the other telling us *when* during the evolution of the universe that energy density should be evaluated. Towards this end, for absolute clarity, we shall let $\rho_{\hat{t}}(t_1; t_2)$ denote the energy density—evaluated at time t_2—of that particular ϕ-field which *becomes underdamped* precisely at t_1, and likewise let $\rho_\tau(t_1; t_2)$ denote the energy density—evaluated at time t_2—of that particular ϕ-field which *decays* at t_1. We can then replace

$$
\rho_\ell(t) \to \rho_{\hat{t}}(t_\ell; t) \quad \text{or} \quad \rho_\ell(t) \to \rho_\tau(\tau_\ell; t). \quad (6.23)
$$

Of course, the fiducial energy density ρ_ℓ^* now becomes either $\rho_{\hat{t}}(t_\ell; t_*)$ or $\rho_\tau(\tau_\ell; t_*)$, depending on the chosen integration variable.

Given these substitutions, it becomes relatively straightforward to evaluate the ℓ-summations of the terms appearing in Eq. (6.21). For example, we find

$$
\sum_\ell \rho_\ell^* \left(\frac{t_\ell}{t_*}\right)^{-(1+w)\bar{\kappa}} \delta(t - t_\ell)
$$
$$
\to \int d\hat{t}\, n_{\hat{t}}(\hat{t}) \rho_{\hat{t}}(\hat{t}; t_*) \left(\frac{\hat{t}}{t_*}\right)^{-(1+w)\bar{\kappa}} \delta(t - \hat{t})
$$
$$
= n_{\hat{t}}(t) \rho_{\hat{t}}(t; t_*) \left(\frac{t}{t_*}\right)^{-(1+w)\bar{\kappa}}. \quad (6.24)
$$

In a similar vein, we also have

$$
\sum_\ell \rho_\ell^* \left(\frac{t_\ell}{t_*}\right)^{-(1+w)\bar{\kappa}} \left(\frac{\tau_\ell}{t_\ell}\right)^{-\bar{\kappa}} \delta(t - \tau_\ell)
$$
$$
= \sum_\ell \rho_\ell^* (\xi \Gamma_0 t_*)^{w\bar{\kappa}} \left(\frac{\tau_\ell}{t_*}\right)^{-\bar{\kappa}} (\Gamma_0 \tau_\ell)^{-w\bar{\kappa}/\gamma} \delta(t - \tau_\ell)
$$
$$
\to \int d\tau\, n_\tau(\tau) \rho_\tau(\tau; t_*) (\xi \Gamma_0 t_*)^{w\bar{\kappa}} \left(\frac{\tau}{t_*}\right)^{-\bar{\kappa}}
$$
$$
\quad \times (\Gamma_0 \tau)^{-w\bar{\kappa}/\gamma} \delta(t - \tau)
$$
$$
= (\xi \Gamma_0 t_*)^{w\bar{\kappa}} \left(\frac{t}{t_*}\right)^{-\bar{\kappa}} (\Gamma_0 t)^{-w\bar{\kappa}/\gamma} n_\tau(t) \rho_\tau(t; t_*) \quad (6.25)
$$

where in passing to the second line we have used Eq. (6.13).

We thus find that Eq. (6.21) takes the anticipated form in Eq. (6.5), where can now identify the pump terms for this model:

$$P_{\Lambda M}^{(\rho)} = \left(\frac{t}{t_*}\right)^{-(1+w)\bar{\kappa}} n_{\hat{t}}(t)\rho_{\hat{t}}(t; t_*),$$

$$P_{\Lambda \gamma}^{(\rho)} = 0,$$

$$P_{M\gamma}^{(\rho)} = (\xi\Gamma_0 t_*)^{w\bar{\kappa}} \left(\frac{t}{t_*}\right)^{-\bar{\kappa}} (\Gamma_0 t)^{-w\bar{\kappa}/\gamma} n_{\tau}(t)\rho_{\tau}(t; t_*). \quad (6.26)$$

As discussed at the end of Sec. VI B, the vanishing of the $P_{\Lambda\gamma}^{(\rho)}$ pump is a consequence of our adoption of the instantaneous-decay approximation and our assumption that $t_\ell < \tau_\ell$ for all ℓ (or equivalently that we are working within the $\xi \gg 1$ limit of a treatment based on taking a adopting a full exponential decay). These results in turn yield

$$P_{\Lambda M} = \left(\frac{t}{t_*}\right)^{-(1+w)\bar{\kappa}} n_{\hat{t}}(t)\Omega_{\hat{t}}(t; t_*),$$

$$P_{\Lambda\gamma} = 0,$$

$$P_{M\gamma} = (\xi\Gamma_0 t_*)^{w\bar{\kappa}} \left(\frac{t}{t_*}\right)^{-\bar{\kappa}} (\Gamma_0 t)^{-w\bar{\kappa}/\gamma} n_{\tau}(t)\Omega_{\tau}(t; t_*), \quad (6.27)$$

where $\Omega_{\hat{t},\tau}(t_1; t_2) \equiv \frac{8\pi G}{3H(t_2)^2}\rho_{\hat{t},\tau}(t_1; t_2).$

Of course, these results make intuitive sense. Indeed, within a period of stasis we see that

$$\left(\frac{t}{t_*}\right)^{-(1+w)\bar{\kappa}} \Omega_{\hat{t}}(t; t_*) = \Omega_{\hat{t}}(t; t), \quad (6.28)$$

and this is nothing but the abundance of the field which is becoming underdamped precisely at the time t, evaluated at the moment of the underdamping transition. Indeed, the disappearance of t_* within Eq. (6.28) is consistent with our original adoption of t_* as a mere fiducial time within our eternal stasis. Likewise, we find

$$(\xi\Gamma_0 t_*)^{w\bar{\kappa}} \left(\frac{t}{t_*}\right)^{-\bar{\kappa}} (\Gamma_0 t)^{-w\bar{\kappa}/\gamma}\Omega_{\tau}(t; t_*) = \Omega_{\tau}(t; t), \quad (6.29)$$

and this is nothing but the abundance of the field which is decaying precisely at the time t, evaluated at the moment of decay. We can thus write our pumping terms in the final forms

$$P_{\Lambda M} = n_{\hat{t}}(t)\Omega_{\hat{t}}^{(\Lambda)}(t; t),$$

$$P_{\Lambda\gamma} = 0,$$

$$P_{M\gamma} = n_{\tau}(t)\Omega_{\tau}^{(M)}(t; t), \quad (6.30)$$

where we have added the superscripts (Λ) and (M) as a reminder that the associated abundances can be interpreted as corresponding to vacuum energy and matter, respectively, at times $t = \hat{t}$ and $t = \tau$. Indeed, these pumping terms describe the rates at which abundances are being transferred between our different energy components at the moments they pass across the underdamping and decay thresholds, respectively.

We now proceed to evaluate these pumping terms within the framework of the model introduced in Sec. II. In this way we shall be able to determine the conditions under which these pumps might simultaneously satisfy the triple-stasis constraints in Eq. (6.10). Recall that $n_{\hat{t}}(t)$ is the density of states per unit underdamping time $\hat{t}$, evaluated for that portion of the tower which is becoming underdamped at time t, while $n_{\tau}(t)$ is the density of states per unit decay time τ evaluated for that portion of the tower that is decaying at time t. A straightforward calculation then yields

$$n_{\hat{t}}(t) \equiv \left|\frac{d\ell}{d\hat{t}}\right|_{\hat{t}=t} = \frac{1}{\delta}\left(\frac{\bar{\kappa}}{2\Delta mt}\right)^{1/\delta}\frac{1}{t},$$

$$n_{\tau}(t) \equiv \left|\frac{d\ell}{d\tau}\right|_{\tau=t} = \frac{1}{\gamma\delta}\left(\frac{m_0}{\Delta m}\right)^{1/\delta}(\Gamma_0 t)^{-1/(\gamma\delta)}\frac{1}{t}, \quad (6.31)$$

where we have again taken $m_0 \ll (\Delta m)\ell^\delta$. Similarly, we can evaluate the abundances in Eq. (6.30), obtaining

$$\Omega_{\hat{t}}^{(\Lambda)}(t; t) = \Omega_0^*\left(\frac{\bar{\kappa}}{2m_0 t}\right)^\alpha \left(\frac{t}{t_*}\right)^{2-(1+w)\bar{\kappa}},$$

$$\Omega_{\tau}^{(M)}(t; t) = \Omega_0^*\left(\frac{m_\ell}{m_0}\right)^\alpha \left(\frac{t_\ell}{t_*}\right)^{2-(1+w)\bar{\kappa}} \left(\frac{t}{t_\ell}\right)^{2-\bar{\kappa}}$$

$$= \Omega_0^*(\xi\Gamma_0 t_*)^{w\bar{\kappa}}\left(\frac{t}{t_*}\right)^{2-\bar{\kappa}}(\Gamma_0 t)^{-\alpha/\gamma-w\bar{\kappa}/\gamma}. \quad (6.32)$$

Given these results, we see that

$$P_{\Lambda M} = \frac{\Omega_0^*}{\delta t}\left(\frac{m_0}{\Delta m}\right)^{1/\delta}(\xi\Gamma_0 t_*)^{-\eta}\left(\frac{t}{t_*}\right)^{2-\bar{\kappa}-(\eta+w\bar{\kappa})},$$

$$P_{M\gamma} = \frac{\Omega_0^*}{\gamma\delta t}\left(\frac{m_0}{\Delta m}\right)^{1/\delta}(\Gamma_0 t_*)^{-\eta/\gamma}$$

$$\times \left[\xi(\Gamma_0 t_*)^{1-1/\gamma}\right]^{w\bar{\kappa}}\left(\frac{t}{t_*}\right)^{2-\bar{\kappa}-(\eta+w\bar{\kappa})/\gamma}. \quad (6.33)$$

Thus, the scaling for our first pump $P_{\Lambda M}$ will be consistent with the scaling t^{-1} required for triple stasis only if

$$\eta = 2 - (1+w)\bar{\kappa}. \quad (6.34)$$

This is precisely the constraint that we already obtained for the single pairwise (Λ, M) stasis in Sec. III. Likewise, demanding that our second pump $P_{M\gamma}$ scale as t^{-1} yields the constraint

$$\eta = 2\gamma - (\gamma + w)\bar{\kappa}. \qquad (6.35)$$

Subtracting Eqs. (6.34) and (6.35) then yields the constraint

$$(2 - \bar{\kappa})\left(1 - \frac{1}{\gamma}\right) = 0. \qquad (6.36)$$

Indeed, this last constraint ensures that our two pumps $P_{\Lambda M}$ and $P_{M\gamma}$ are compatible with each other within the same background cosmology.

The result in Eq. (6.36) indicates that there are two mutually disjoint "branches" of our theory that are potentially capable of yielding triple stasis: one has $\gamma = 1$ and any value of $\bar{\kappa}$, while the other has $\bar{\kappa} = 2$ and any value of γ. Such branches have a common intersection point with $\gamma = 1$ and $\bar{\kappa} = 2$. However, for reasons to become clear, it will prove useful to define these two branches to be mutually exclusive by assigning the $(\gamma, \bar{\kappa}) = (1, 2)$ point to be a member of the first of these branches but not the second. We thus define Branches A and B to consist of potential stasis solutions satisfying not only Eq. (6.34) but also the additional constraints

$$\text{Branch A}: \gamma = 1, \text{any } \bar{\kappa},$$
$$\text{Branch B}: \bar{\kappa} = 2, \text{any } \gamma \neq 1. \qquad (6.37)$$

The $(\gamma, \bar{\kappa})$ parameter-space domains corresponding to these additional constraints are sketched in Fig. 9. We shall soon find that these two branches have very different behaviors.

At this stage, we have learned that any possible triple-stasis solutions are limited to Branch A or Branch B. Moreover, given that we have already satisfied the constraint in Eq. (6.36) by limiting our attention to Branch A or Branch B, Eq. (6.34) becomes the only additional relation that we have thus far governing such potential triple stases.
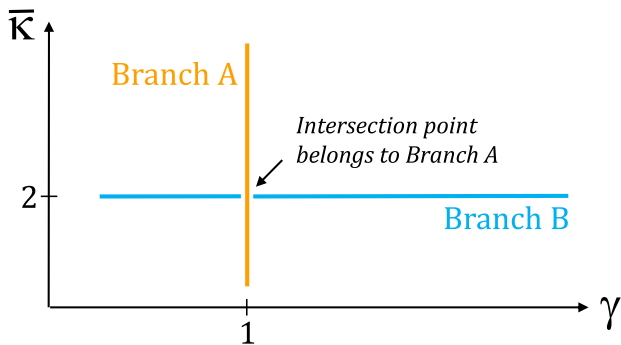

FIG. 9. Two branches of solutions to Eqs. (6.36). These branches are defined as in Eq. (6.37) with the convention that the point with $(\gamma, \bar{\kappa}) = (1, 2)$ is considered to be part of Branch A but not Branch B. With this convention the two branches are mutually exclusive.

However, this relation is no different from that in Sec. III, with any choice of input parameters (α, δ, w) leading to a unique value of $\bar{\kappa}$. Of course, if we also choose $\gamma = 1$ we find ourselves on the Branch A line. By contrast, leaving γ arbitrary, we find that only those choices of (α, δ, w) that lead to $\bar{\kappa} = 2$ correspond to Branch B.

In either case, however, we see that $\bar{\kappa}$ is uniquely determined from our choice of the initial parameters (α, δ, w). In the previous pairwise cases which involved only two stasis abundances, such predictions for $\bar{\kappa}$ (along with the usual normalization constraint $\sum_i \bar{\Omega}_i = 1$) were sufficient to permit us to uniquely determine the corresponding stasis abundances. However, for *triple* stasis, the specification of $\bar{\kappa}$ only restricts us to a *line* of solutions for the stasis abundances $\bar{\Omega}_i$. Thus, at first glance, it would no longer appear possible to obtain firm predictions for the stasis abundances.

D. Prefactor constraints, log-avoidance constraints, and the emergence of triple stasis

Fortunately, we have two further classes of constraints at our disposal: these are the log-avoidance constraints as well as the prefactor constraints. These general types of constraints were discussed in some detail in Sec. II B. In the case of the pairwise stases in Secs. II, III, and IV, we found that these prefactor constraints were redundant with our scaling constraints. Indeed, this redundancy is what allowed stasis to be a self-consistent phenomenon in such pairwise situations. *However, for triple stasis, we shall find that these prefactor constraints are no longer redundant with our scaling constraints and therefore contain further information.* Indeed, we shall find that this further information will play two roles. First, it will provide an additional condition for stasis, one which further restricts the potential solutions that we have thus far obtained. In particular, this additional information will allow us to distinguish between Branches A and B and thereby demonstrate that only one of these branches gives rise to a full triple stasis. However, this additional information will also allow us to determine the stasis abundances $\bar{\Omega}_{\Lambda, M, \gamma}$ uniquely.

In order to derive these results, we follow previous sections and shift from the differential to the integral form of our calculations and directly evaluate the abundances $\bar{\Omega}_{\Lambda, M, \gamma}$ during stasis. In order to expose the common algebraic structure of these calculations, we shall evaluate these abundances in parallel. Our calculation begins, as before, with Eq. (6.20). Even though this equation gives expressions for the energy densities $\rho_\ell(t)$, the corresponding abundances $\Omega_\ell(t)$ take precisely the same forms except multiplied by $(t/t^{(0)})^2$. The Heaviside Θ-function structure within Eq. (6.20) tells us that at any time t we can interpret our abundance as corresponding to vacuum energy, matter, or radiation according to

$$\Lambda: t < t_\ell,$$
$$M: t_\ell < t < \tau_\ell,$$
$$\gamma: t > \tau_\ell. \tag{6.38}$$

At any time t, this in turn implies that the lower parts of our ϕ_ℓ tower are generally still vacuum energy while the middle parts of our tower have already transitioned to matter and the upper parts have already decayed to radiation. Indeed, this configuration is consistent with Fig. 8.

Our goal, of course, is to sum over the contributions from each relevant part of the tower in order to obtain our total abundances $\bar{\Omega}_{\Lambda,M,\gamma}$. In order to perform these sums in a parallel fashion, we shall express each state at level ℓ in terms of its decay lifetime τ_ℓ and then treat these decay lifetimes as forming a continuous parameter τ. We can thus rewrite

$$m_\ell/m_0 \to (\Gamma_0\tau)^{-1/\gamma},$$
$$t_\ell \to (\Gamma_0\tau)^{1/\gamma}/(\xi\Gamma_0), \tag{6.39}$$

where in the last line we have made use of Eq. (6.13). Finally, at any moment t, we can calculate the critical τ-values that demarcate the boundaries between the regions of the ϕ_ℓ tower corresponding to vacuum energy, matter, and radiation. Indeed, the boundary between vacuum energy and matter occurs where $t = t_\ell$, while that between matter and radiation occurs where $t = \tau_\ell$. We thus have

$$\Lambda: (\xi\Gamma_0 t)^\gamma\tau_0 < \tau < \tau_0,$$
$$M: t < \tau < (\xi\Gamma_0 t)^\gamma\tau_0,$$
$$\gamma: \tau_{N-1} < \tau < t, \tag{6.40}$$

where $\tau_0 \equiv 1/\Gamma_0$. Note that strictly speaking, our range of τ-values stretches from τ_{N-1} (the smallest value, corresponding to the top state ϕ_{N-1} within the tower) all the way to τ_0 (the largest value, corresponding to the bottom state ϕ_0 within the tower). In previous sections, we have noted that we are ultimately interested in times t for which $\tau_{N-1} \ll t \ll \tau_0$, so that we are far from any "edge" effects. We therefore made the approximations $\tau_{N-1} \approx 0$ and $\tau_0 \approx \infty$. However, in order to be absolutely rigorous, we have retained these precise values within our integration limits for $\bar{\Omega}_\Lambda$ and $\bar{\Omega}_\gamma$ in Eq. (6.40).

Given these ingredients, our calculation of the total abundances $\bar{\Omega}_{\Lambda,M,\gamma}$ is relatively straightforward. Just as in previous sections, we shall no longer assume an eternal stasis, but instead recognize that stasis will only begin at times $t \gg t^{(0)}$ where $t^{(0)}$ is the production time for our ϕ_ℓ states. We shall also now seek to evaluate these abundances in terms of their values $\Omega_{\Lambda,M,\gamma}^{(0)}$ at $t^{(0)}$ rather than at a fiducial time t_* during an eternal stasis. Towards this end, we shall

again introduce an h-function $h(t^{(0)}, t_*)$ which describes the evolution of the abundances due to gravitational redshifting between $t^{(0)}$ and t_*. We shall further assume that our abundances all share this common factor even though there are now *three* abundances in play, rather than only two. At first glance, the presence of three abundances would seem to allow room for a second h-factor, even while demanding that the sum of the abundances remain at 1. However, as we shall demonstrate in Sec. VI E, our assumption of a common h-function across all three abundances is indeed appropriate for our stasis calculations. We shall therefore proceed with only one h-function, deferring further discussion of this issue to Sec. VI E.

In the continuum limit with τ chosen as our continuous variable, each of these abundances can be ultimately expressed in the form

$$\bar{\Omega}_i = \int d\tau\, n_\tau(\tau)\Omega_\tau^{(i)}(\tau; t) \tag{6.41}$$

for $i = \Lambda, M, \gamma$. Here $n_\tau(\tau)$ is the density of states per unit τ, while $\bar{\Omega}_i(\tau; t)$ represents the contribution to the abundance $\bar{\Omega}_i$, evaluated at time t, from the field which decays at time τ. Of course, in each case the integral will be delimited according to Eq. (6.40).

The density of states $n_\tau(\tau)$ is given in Eq. (6.31). Likewise, the abundances $\Omega_\tau^{(i)}(\tau; t)$ follow readily from the energy densities in Eq. (6.20) upon making the substitutions listed in Eqs. (6.13) and (6.39):

$$\Omega_\tau^{(\Lambda)}(\tau; t) = \Omega_\tau(\tau; t^{(0)})h(t^{(0)}, t_*)\left(\frac{t}{t_*}\right)^{2-(1+w)\bar{\kappa}}$$
$$\times \Theta\left(\frac{(\Gamma_0\tau)^{1/\gamma}}{\xi\Gamma_0} - t\right),$$

$$\Omega_\tau^{(M)}(\tau; t) = \Omega_\tau(\tau; t^{(0)})h(t^{(0)}, t_*)\left(\frac{t}{t_*}\right)^{2-\bar{\kappa}}$$
$$\times \left[\frac{(\Gamma_0\tau)^{1/\gamma}}{\xi\Gamma_0 t_*}\right]^{-w\bar{\kappa}}\Theta\left(t - \frac{(\Gamma_0\tau)^{1/\gamma}}{\xi\Gamma_0}\right)\Theta(\tau - t),$$

$$\Omega_\tau^{(\gamma)}(\tau; t) = \Omega_\tau(\tau; t^{(0)})h(t^{(0)}, t_*)\left(\frac{t}{t_*}\right)^{2-\bar{\kappa}}$$
$$\times \left[\frac{(\Gamma_0\tau)^{1/\gamma}}{\xi\Gamma_0 t_*}\right]^{-w\bar{\kappa}}\left(\frac{t}{\tau}\right)^{-\bar{\kappa}/3}\Theta(t - \tau). \tag{6.42}$$

However, we know that $\Omega_\tau(\tau; t^{(0)}) = \Omega_0^{(0)}(\Gamma_0\tau)^{-\alpha/\gamma}$. [This is the continuum limit of the relation $\Omega_\ell^{(0)} = \Omega_0^{(0)}(m_\ell/m_0)^\alpha$.] It therefore follows that we can write all three stasis abundances in the compact form

$$\bar{\Omega}_\Lambda = A(t) \int_{\tau_0(\xi\Gamma_0 t)^\gamma}^{\tau_0} d\tau (\Gamma_0 \tau)^{-1-\eta/\gamma},$$

$$\bar{\Omega}_M = A(t)(\xi\Gamma_0 t)^{w\bar{\kappa}}$$
$$\times \int_t^{\tau_0(\xi\Gamma_0 t)^\gamma} d\tau (\Gamma_0 \tau)^{-1-(\eta+w\bar{\kappa})/\gamma},$$

$$\bar{\Omega}_\gamma = A(t)(\xi\Gamma_0 t)^{w\bar{\kappa}}(\Gamma_0 t)^{-\bar{\kappa}/3}$$
$$\times \int_{\tau_{N-1}}^t d\tau (\Gamma_0 \tau)^{-1-(\eta+w\bar{\kappa})/\gamma+\bar{\kappa}/3}, \quad (6.43)$$

where each integral is delimited according to Eq. (6.40) and where the common t-dependent prefactor in each expression is

$$A(t) \equiv \frac{\Omega_0^{(0)} \Gamma_0}{\gamma\delta} \left(\frac{m_0}{\Delta m}\right)^{1/\delta} h(t^{(0)}, t_*) \left(\frac{t}{t_*}\right)^{2-(1+w)\bar{\kappa}}. \quad (6.44)$$

Our first interest is in the t-dependence of each expression within Eq. (6.43). This in turn depends in part on the exponent of τ in the corresponding integrand. Since we are evaluating these total abundances during an epoch of triple stasis—i.e., at a time both well after the heaviest ϕ-field decays and well before the lightest ϕ-field begins to oscillate—it follows that $\tau_{N-1} \ll t \ll \hat{t}_0 = \tau_0/\xi$. Thus, to a very good approximation, we find that $\bar{\Omega}_\Lambda$ has the t-scaling behavior

$$\bar{\Omega}_\Lambda \sim \begin{cases} t^{2-(1+w)\bar{\kappa}} & \eta < 0, \\ t^{2-(1+w)\bar{\kappa}} \log{(\xi\Gamma_0 t)} & \eta = 0, \\ t^{2-(1+w)\bar{\kappa}-\eta} & \eta > 0. \end{cases} \quad (6.45)$$

Likewise, we find that $\bar{\Omega}_M$ has the t-scaling behavior

$$\bar{\Omega}_M \sim \begin{cases} t^{2-\bar{\kappa}} \left[t^{-(\eta+w\bar{\kappa})/\gamma} - \frac{\tau_0^{-(\eta+w\bar{\kappa})/\gamma}}{(\xi\Gamma_0 t)^{\eta+w\bar{\kappa}}} \right] & \eta+w\bar{\kappa} \neq 0, \\ t^{2-\bar{\kappa}} \log{\left[\xi(\Gamma_0 t)^{1-1/\gamma} \right]} & \eta+w\bar{\kappa} = 0. \end{cases} \quad (6.46)$$

Finally, we find that $\bar{\Omega}_\gamma$ scales with time according to

$$\bar{\Omega}_\gamma \sim \begin{cases} t^{2-\bar{\kappa}-(\eta+w\bar{\kappa})/\gamma} & \eta+w\bar{\kappa} < \bar{\kappa}\gamma/3, \\ t^{2-4\bar{\kappa}/3} \log{\left(\frac{t}{\tau_{N-1}}\right)} & \eta+w\bar{\kappa} = \bar{\kappa}\gamma/3, \\ t^{2-4\bar{\kappa}/3} & \eta+w\bar{\kappa} > \bar{\kappa}\gamma/3. \end{cases} \quad (6.47)$$

Given these scaling behaviors, we now seek to determine the conditions under which all three of these abundances will be independent of time. It will prove simplest to begin by considering $\bar{\Omega}_M$. Close inspection of our results for $\bar{\Omega}_M$ in Eq. (6.46) indicates that $\bar{\Omega}_M$ will be a constant only if

$$\eta = 2 - (1+w)\bar{\kappa} \quad \text{and} \quad \gamma = 1. \quad (6.48)$$

Indeed, the upper line of Eq. (6.46) will be a constant only if we additionally impose the requirement that $\bar{\kappa} \neq 2$ (so that the relevant condition for that case applies), but the lower line applies if $\bar{\kappa} = 2$ and also yields a constant so long as $\gamma = 1$. We thus find that any value of $\bar{\kappa}$ is allowed in Eq. (6.48).

With Eq. (6.48) in hand, let us now consider our results for $\bar{\Omega}_\gamma$ in Eq. (6.47). From Eq. (6.47), we learn that the logarithmic case can never yield a constant, while the lower case within Eq. (6.47) is fundamentally inconsistent with Eq. (6.48). By contrast, the upper case within Eq. (6.47) yields a constant so long as

$$\bar{\kappa} > 3/2. \quad (6.49)$$

However, this relation is not a surprise: *any* system consisting of a nontrivial mixture of vacuum energy, matter, and radiation must have $\bar{\kappa} > 3/2$ simply because radiation alone has $\kappa = 3/2$ while matter and vacuum energy necessarily have κ-values that are larger than $3/2$. Indeed, this constraint is always satisfied (essentially by construction). It therefore does not represent an additional constraint that needs to be imposed on our system, and we need not consider it further.

Finally, we must demand that $\bar{\Omega}_\Lambda$ also be a constant. From our results for $\bar{\Omega}_\Lambda$ in Eq. (6.45) we immediately observe that the middle line can never yield a constant (thanks to the logarithm), while the top line is fundamentally inconsistent with the first relation in Eq. (6.48) since the power of t is consistent with Eq. (6.48) only if $\eta = 0$, while the relevant condition for that case requires $\eta < 0$. Indeed, the only case within Eq. (6.45) for which $\bar{\Omega}_\Lambda$ can be a constant is that on the final line, whereupon we obtain another condition for constant abundances, namely

$$\eta > 0. \quad (6.50)$$

However, this relation is entirely subsumed within the first relation in Eq. (6.48). To see this, we recognize that a universe consisting only of vacuum energy within the general-w model would have $\kappa = 2/(1+w)$, while matter-or radiation-dominated universes would necessarily have smaller κ-values, namely $\kappa = 2$ or $\kappa = 3/2$ respectively. Thus, by construction, triple stasis can only give rise to universes satisfying $\bar{\kappa} < 2/(1+w)$, whereupon the first relation in Eq. (6.48) immediately yields Eq. (6.50). Thus Eq. (6.50)—like Eq. (6.49)—does not provide an additional constraint on our system and can henceforth be disregarded.

We thus conclude that the conditions for triple stasis are simply those listed in Eqs. (6.48). Indeed, because our analysis has followed the integral form of our constraints and has therefore involved evaluating the abundances $\bar{\Omega}_{\Lambda,M,\gamma}$ directly, these are the *complete set of constraints needed for triple stasis*. From this observation we learn several important things:

(i) The scaling relation in Eq. (6.34) that emerged from the differential form of our constraints now appears within the integral form as well, as the first constraint within Eq. (6.48).

(ii) The additional constraint that we now have within Eq. (6.48), namely $\gamma = 1$, can be identified as a *log-avoidance constraint*. We shall discuss this additional constraint below.

(iii) Finally, we have not yet examined our prefactor constraints. However, we already see that any such prefactor constraints cannot possibly be needed as preconditions for stasis, since stasis has already been assured through the above constraints alone. Indeed, as we shall see, our prefactor constraints will serve another purpose entirely, ultimately allowing us to solve for the abundances $\bar{\Omega}_{\Lambda,M,\gamma}$ during stasis.

In Sec. VI C, we found that the requirements of triple stasis—as obtained through the differential form of our constraints—led uniquely to two "branches" of potential solutions. These branches were indicated in Eq. (6.37) and sketched in Fig. 9. However, comparing with our current constraints obtained via the integral form of our stasis relations, we now see that Branch B violates the $\gamma = 1$ constraint and thus does not lead to triple stasis. It is easy to see what is going wrong within Branch B. Recall that Branch B is defined by the overall scaling constraint in Eq. (6.34) along with the extra conditions $\bar{\kappa} = 2$ and $\gamma \neq 1$. Under these circumstances, we find from Eqs. (6.45) and (6.47) that both $\bar{\Omega}_\Lambda$ and $\bar{\Omega}_\gamma$ nominally continue to remain constant. However we find from Eq. (6.46) that $\bar{\Omega}_M$ now accrues a nominally logarithmic time dependence. It is for this reason that we may regard $\gamma = 1$ as a logarithm-avoidance constraint. Indeed, this nominal logarithmic time dependence for $\bar{\Omega}_M$ emerges for all points along Branch B (with the understanding that the case with $\bar{\kappa} = 2$ and $\gamma = 1$ belongs to Branch A). *Thus, we conclude that Branch B fails to yield a true triple stasis.*

In this context, one important comment is in order—one which explains the word "nominally" which we have used above. Even though we occasionally obtain what look like logarithmic time dependences within Eqs. (6.45), (6.46), and (6.47), this does not imply that our corresponding abundances actually exhibit time dependences which are precisely logarithmic. This is because the derivation leading to these equations assumed the existence of an eternal stasis. Indeed, this was the underpinning of Eq. (6.20) with which we started our calculations. For example, within Eq. (6.20) we implicitly assumed that our FRW scale factor a evolves as a fixed power of time, yet such behavior emerges only if the corresponding κ is a constant. Thus the results in Eqs. (6.45), (6.46), and (6.47) are absolutely trustworthy only in situations in which all three abundances are constants.

By contrast, in order to determine the true time dependence of our abundances in situations in which these abundances vary with time, we would ultimately need a more general derivation in which such initial stasis assumptions are not made. This has the potential to deform our results away from those obtained from Eqs. (6.45), (6.46), and (6.47) above. Indeed, the fastest way to see that deformations are needed in such cases is to recognize from the above analysis that Branch B appears to lead to only one abundance (specifically $\bar{\Omega}_M$) which has a nonzero time dependence, yet this cannot be consistent with our overall normalization constraint $\sum_i \bar{\Omega}_i = 1$. Thus even $\bar{\Omega}_\Lambda$ and $\bar{\Omega}_\gamma$ must accrue a suppressed time dependence as well. However, even if the actual time dependences that emerge within such an analysis are not precisely logarithmic, they will continue to be nonvanishing. Thus our conclusion that Branch B does not lead to stasis remains unchanged. The resulting time dependences are nevertheless likely to be highly suppressed compared with our usual ΛCDM expectations.

These observations are relevant for understanding the properties of Branch B. Because Branch B involves abundances which are not truly static, it may therefore seem that Branch B is uninteresting. However, although Branch B does not lead to stasis, it does lead to a new phenomenon: abundances which evolve unexpectedly slowly as functions of time. Indeed, although Branch B fails to satisfy the $\gamma = 1$ constraint in Eq. (6.48), it does satisfy our overall scaling constraint and thus gives rise to abundances exhibiting extremely suppressed time evolutions. This in and of itself is also an interesting new feature which does not emerge in the standard ΛCDM cosmologies but which may nevertheless have important phenomenological implications. We shall refer to this phenomenon involving abundances with extremely suppressed time dependences as a *quasi-stasis*. We shall return to this issue in Sec. IX.

By contrast, Branch A satisfies all of our stasis constraints, even when $\bar{\kappa} = 2$, by virtue of the fact that $\gamma = 1$ along the full length of Branch A. Thus Branch A exhibits a full triple stasis, thereby verifying that triple stasis is possible! Even though the case with $\bar{\kappa} = 2$ corresponds to the logarithmic case within Eq. (6.46), the fact that $\gamma = 1$ assures us that the argument of the logarithm is itself time independent. Thus the stasis behavior is preserved even in this case.

Now that we have determined the conditions for (eternal) stasis in Eq. (6.48), we can proceed to evaluate the corresponding stasis abundances $\bar{\Omega}_\Lambda$, $\bar{\Omega}_M$, and $\bar{\Omega}_\gamma$. Indeed, from the bottom line of Eq. (6.45), both lines of Eq. (6.46), and the top line of Eq. (6.47) we find

$$\bar{\Omega}_\Lambda = \frac{\Omega_0^{(0)}}{\delta\eta}\left(\frac{m_0}{\Delta m}\right)^{1/\delta} h(t^{(0)}, t_*)(\xi\Gamma_0 t_*)^{-\eta},$$

$$\bar{\Omega}_M = \frac{\Omega_0^{(0)}}{\delta}\left(\frac{m_0}{\Delta m}\right)^{1/\delta} h(t^{(0)}, t_*)\xi^{w\bar{\kappa}}(\Gamma_0 t_*)^{-\eta}X^{-1},$$

$$\bar{\Omega}_\gamma = \frac{\Omega_0^{(0)}}{(4\bar{\kappa}/3 - 2)\delta}\left(\frac{m_0}{\Delta m}\right)^{1/\delta} h(t^{(0)}, t_*)\xi^{w\bar{\kappa}}(\Gamma_0 t_*)^{-\eta}, \quad (6.51)$$

where the quantity X within $\bar{\Omega}_M$ is given by

$$X \equiv \begin{cases} \frac{2-\bar{\kappa}}{1-\xi^{\bar{\kappa}-2}}, & \bar{\kappa} \neq 2, \\ (\log \xi)^{-1}, & \bar{\kappa} = 2. \end{cases} \quad (6.52)$$

Note that L'Hôpital's Rule guarantees that X is continuous across $\eta + w\bar{\kappa} = 0$.

Likewise, from Eq. (6.33), we find that our pumps during stasis take the form

$$P_{\Lambda M} = \frac{\Omega_0^{(0)}}{\delta} \left(\frac{m_0}{\Delta m} \right)^{1/\delta} h(t^{(0)}, t_*)(\xi\Gamma_0 t_*)^{-\eta} \frac{1}{t},$$

$$P_{M\gamma} = \frac{\Omega_0^{(0)}}{\delta} \left(\frac{m_0}{\Delta m} \right)^{1/\delta} h(t^{(0)}, t_*)\xi^{w\bar{\kappa}}(\Gamma_0 t_*)^{-\eta} \frac{1}{t}. \quad (6.53)$$

For $\eta + w\bar{\kappa} = 0$ (i.e., for $\bar{\kappa} = 2$), we thus immediately observe that

$$P_{\Lambda M} = P_{M\gamma}. \quad (6.54)$$

This case will be discussed extensively below. However in all other cases we find that our pumps are unequal.

It is now straightforward to derive the relative prefactor constraints for triple stasis. Following the same path as in previous sections (but bypassing the C-and C'-coefficients since our only interest is in the *relative* prefactor constraints), we can simply write our pumps in Eq. (6.53) directly in terms of our abundances in Eq. (6.51):

$$P_{\Lambda M} = \eta\bar{\Omega}_\Lambda \frac{1}{t},$$

$$P_{M\gamma} = X\bar{\Omega}_M \frac{1}{t} = \left(\frac{4\bar{\kappa}}{3} - 2 \right) \bar{\Omega}_\gamma \frac{1}{t}, \quad (6.55)$$

where the second expression for $P_{M\Lambda}$ follows from the relation

$$X\bar{\Omega}_M = \left(\frac{4\bar{\kappa}}{3} - 2 \right) \bar{\Omega}_\gamma \quad (6.56)$$

which emerges from a direct comparison between the final two lines in Eq. (6.51). Happily, the results in Eq. (6.55) immediately satisfy the first and third pump constraints in Eq. (6.10), providing further evidence that our model successfully yields stasis. Indeed, these are the constraints governing the independent flows of energy density out of Ω_Λ and into Ω_γ, respectively. However, just as in previous sections, we learn nothing new from these two relative prefactor constraints.

There is, however, another prefactor constraint—one which is nontrivial. This is the *middle* constraint in Eq. (6.10) which links the two pumps $P_{\Lambda M}$ and $P_{M\gamma}$ to each other and thereby ensures that they are compatible with each other within a single cosmology in which the sum of all three abundances is restricted to remain at 1. [Alternatively, as discussed below Eq. (6.10), this constraint is not new if we impose the relation in Eq. (6.3), which likewise ensures that our cosmology simultaneously includes all three energy components.] Comparing our results in Eq. (6.55) with the middle equation in Eq. (6.10) we obtain the additional constraint

$$\eta\bar{\Omega}_\Lambda = (X + \bar{\kappa} - 2)\bar{\Omega}_M. \quad (6.57)$$

Taking this constraint together with Eq. (6.56) and the constraint that $\sum_i \bar{\Omega}_i = 1$, we then find that our relative prefactor constraints can be satisfied only if our stasis abundances are given by

$$\bar{\Omega}_i = r_i \Big/ \sum_j r_j \quad (6.58)$$

where

$$r_\Lambda = (4\bar{\kappa} - 6)(X + \bar{\kappa} - 2),$$

$$r_M = (4\bar{\kappa} - 6)\eta,$$

$$r_\gamma = 3\eta X. \quad (6.59)$$

Of course, we know from Eq. (6.34) that

$$\bar{\kappa} = \frac{2 - \eta}{1 + w}. \quad (6.60)$$

With Eq. (6.60) inserted into Eq. (6.59), we therefore find that our final stasis abundances in Eq. (6.58) can be written directly in terms of the input variables $(\alpha, \gamma, \delta, w)$. Indeed, only for these values of our three abundances is the middle pump equation in Eq. (6.33) consistent with the other two [or equivalently is the value of $\bar{\kappa}$ in these constraint equations consistent with its original definition in Eq. (6.3)].

The above analysis, which employed the instantaneous-decay approximation, may be refined in a straightforward manner in order to account for the full exponential nature of the ϕ_ℓ decays. After making the replacements $\Theta(\tau - t) \rightarrow e^{-t/\tau}$ and $\Theta(t - \tau) \rightarrow 1 - e^{-t/\tau}$ in Eqs. (6.20) and (6.42), we find that Eq. (6.55) still holds, but with the expression for X in Eq. (6.52) replaced by

$$X \equiv \frac{\Gamma(3 - \bar{\kappa}, \xi^{-1})}{\Gamma(2 - \bar{\kappa}, \xi^{-1})}. \quad (6.61)$$

Here $\Gamma(a, z)$ denotes the upper incomplete gamma function, with the usual domain of the argument a extended to include all nonpositive real values:

$$\Gamma(a, z) \equiv \int_z^\infty dy \, y^{a-1} e^{-y}. \quad (6.62)$$

It therefore follows that the stasis abundances $\bar{\Omega}_i$ have the same forms as in Eqs. (6.58) and (6.59), but with X defined in Eq. (6.61).

We emphasize once again that the model of triple stasis that we have presented in this section represents a complete and self-consistent picture of the underlying dynamics only when certain conditions are satisfied. In particular, since we are neglecting the direct transfer of energy density from vacuum energy to radiation, this model is valid only within the regime wherein this transfer of energy density has a negligible effect on the cosmological dynamics. Thus, in what follows, we shall restrict our attention to regions of our parameter space wherein the ratio τ_ℓ / t_ℓ is sufficiently large for all ϕ_ℓ that only a negligible fraction of the comoving number density of each particle species would have decayed at times $t < t_\ell$. In other words, we shall require that

$$1 - e^{-\Gamma_\ell t_\ell} < \epsilon_{\text{dec}}, \qquad (6.63)$$

for all ϕ_ℓ, where ϵ_{dec} is an arbitrary small number. However, since triple stasis requires that $\gamma = 1$, Eq. (6.13) implies that $\Gamma_\ell t_\ell = \xi^{-1}$ for all ϕ_ℓ. Thus, the condition in Eq. (6.63) is tantamount to imposing an lower bound on ξ of the form

$$\xi > \xi_{\text{min}} \equiv \frac{-1}{\log(1 - \epsilon_{\text{dec}})}. \qquad (6.64)$$

In what follows, we shall take $\epsilon_{\text{dec}} = 0.05$, which yields $\xi_{\text{min}} \approx 19.5$. That said, we note that since no energy density is transferred to radiation by the decay of each ϕ_ℓ at times $t < \tau_\ell$ in the instantaneous-decay approximation, our

analysis is formally valid in this approximation for all $\xi > 1$.

In Fig. 10, we illustrate the emergence of triple stasis along Branch A. In each panel of Fig. 10, we plot the three abundances Ω_Λ, Ω_M, and Ω_γ as functions of the number of e-folds since the original production time within the framework of a full exponential decay. These three cases correspond to sections of Branch A with $\bar{\kappa} > 2$, $\bar{\kappa} = 2$, and $\bar{\kappa} < 2$ respectively. In all cases we find that a triple stasis is reached, with the stasis abundances precisely matching the predictions in Eqs. (6.58) and (6.59) with X given in Eq. (6.61). This then provides numerical confirmation of the existence of triple stasis. We also note that it takes longer to reach triple stasis as $\bar{\kappa}$ is decreased.

In Fig. 11, we illustrate how the expressions for the stasis abundances $\bar{\Omega}_\Lambda$, $\bar{\Omega}_M$, and $\bar{\Omega}_\gamma$ in Eqs. (6.58) and (6.59) depend on our model parameters η, w, and ξ. In the panels appearing along the top row of the figure, we plot these abundances as functions of η for three different values of w, with ξ fixed. We note that since ξ depends on $\bar{\kappa}$, and hence on η, the ratio m_0/Γ_0 also varies with η in each panel such that ξ remains constant within each panel. The results shown in the left, middle, and right panels of this row correspond to the choices $w = -0.9$, $w = -0.7$, and $w = -0.35$, respectively, and in all three panels we have taken $\xi = 20$—a value which exceeds ξ_{min} for our chosen value of ϵ_{dec}. The solid curves in each panel indicate the values of $\bar{\Omega}_\Lambda$ (blue), $\bar{\Omega}_M$ (cyan), and $\bar{\Omega}_\gamma$ (magenta) obtained using the form for X in Eq. (6.61) corresponding to full exponential decay, while the dashed curves indicate the corresponding abundances obtained using the form for X in Eq. (6.52) corresponding to the instantaneous-decay approximation. The gray region on the right side of each of these panels is excluded by the constraint
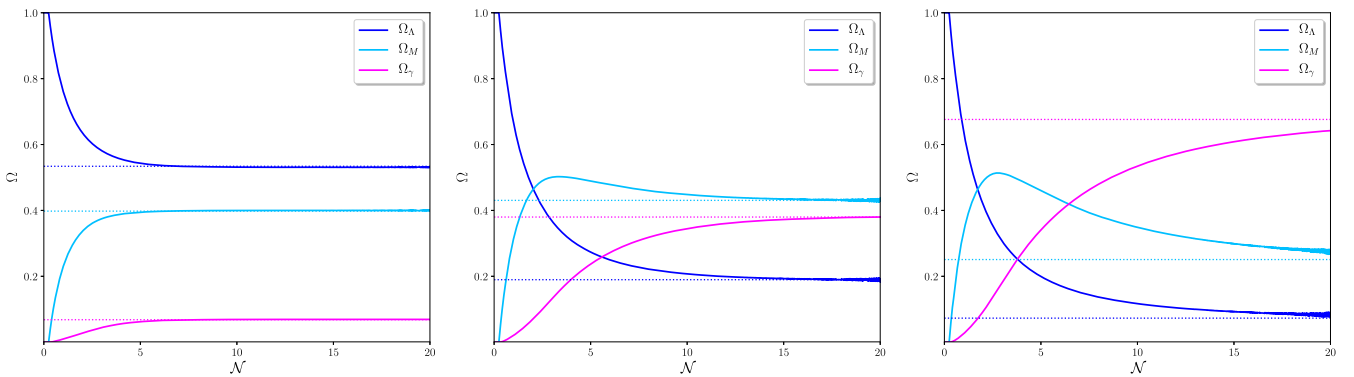

FIG. 10. An illustration of triple stasis. The abundances Ω_Λ (solid dark blue curves), Ω_M (solid cyan curves), and Ω_γ (solid magenta curves) are plotted as functions of the number $\mathcal{N}$ of e-folds of cosmic expansion since the production time $t^{(0)}$. In each case these abundances approach and then remain fixed at the corresponding stasis values (dotted lines) predicted in Eqs. (6.58) and (6.59), with X given in Eq. (6.61). These curves are calculated for reference values $\alpha = 2/3$ (left panel), 1 (middle panel), and 1.1 (right panel), holding $\delta = 3$, $\gamma = 1$, and $w = -2/3$ fixed across all panels. The full exponential nature of the decay process was taken into account in modeling the transition of energy density from matter to radiation. These choices lead to stasis values $\bar{\kappa} = 3$, 2, and 1.7, respectively, and we have adjusted Γ_0/m_0 in each case in order to hold $\xi = 20$ fixed for all panels. These figures confirm that we can achieve triple stasis for $\bar{\kappa} > 2$, $\bar{\kappa} = 2$, and $\bar{\kappa} < 2$, respectively, and that it takes less time to achieve triple stasis as $\bar{\kappa}$ increases.
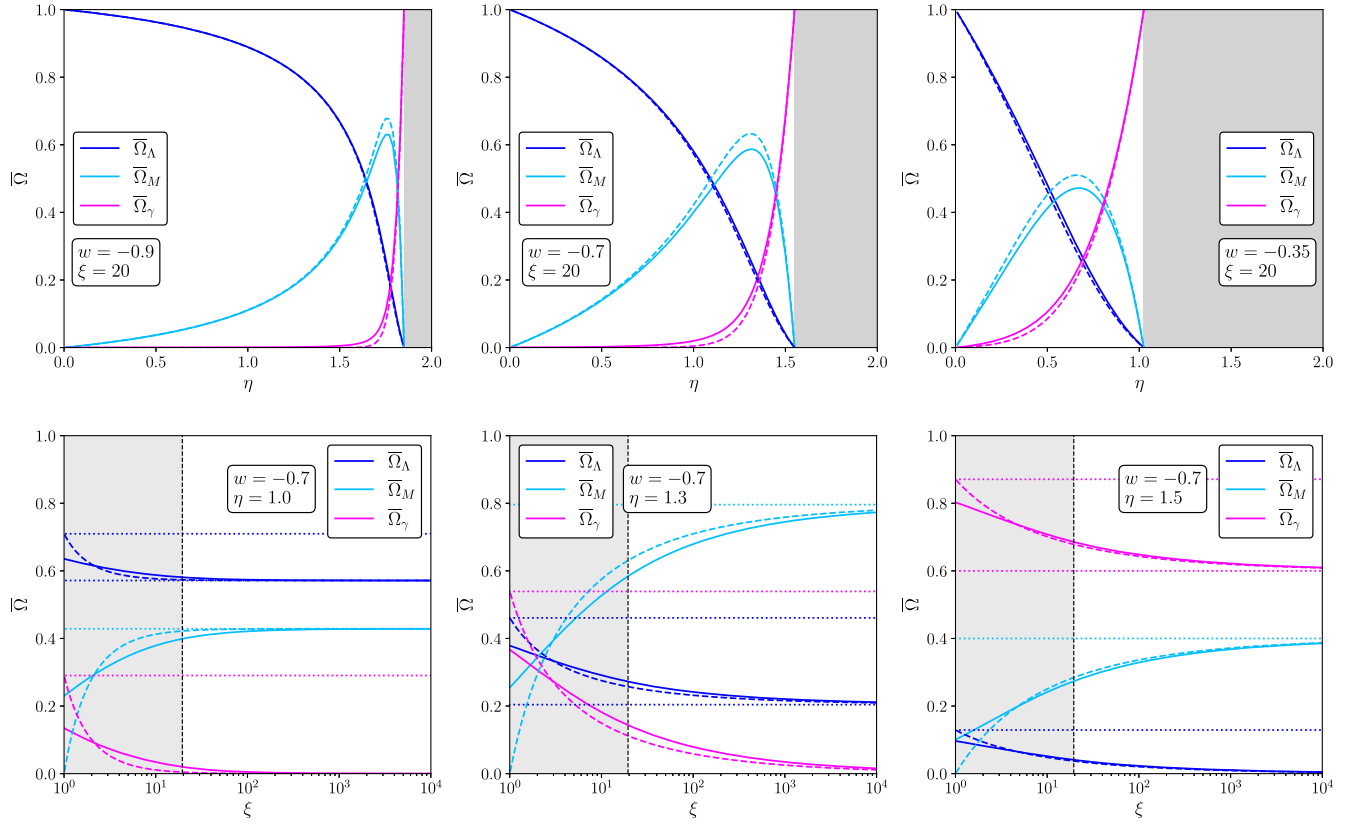
FIG. 11.   Top panels: the stasis abundances $\bar{\Omega}_\Lambda$ (blue), $\bar{\Omega}_M$ (cyan), and $\bar{\Omega}_\gamma$ (magenta), plotted as functions of η for different values of w with ξ held fixed. The solid curves are calculated assuming full exponential decay, while the dashed curves are calculated within the instantaneous-decay approximation. The gray region on the right side of each panel is excluded by the constraint $0 < \eta \leq (1 - 3w)/2$, which follows from the constraint $\bar{\kappa} > 3/2$ in Eq. (6.49). Bottom panels: the stasis abundances $\bar{\Omega}_\Lambda$ (blue), $\bar{\Omega}_M$ (cyan), and $\bar{\Omega}_\gamma$ (magenta), plotted as functions of ξ for different values of η with w held fixed. The gray regions on the left sides of these panels correspond to $\xi < \xi_{\min}$ and are thus outside our regime of validity. In the instantaneous-decay approximation, we see that $\bar{\Omega}_M \to 0$ as $\xi \to 0$ irrespective of the value of η, whereupon our triple stasis reduces to a pairwise stasis involving vacuum energy and radiation. By contrast, the behavior of the abundances as $\xi \to \infty$ limit depends on the relationship between η and w. For $\eta < 2w$, as illustrated in the left and middle panels, $\bar{\Omega}_\gamma \to 0$ and the triple stasis reduces to a pairwise stasis involving vacuum energy and matter. By contrast, for $\eta > 2w$, as illustrated in the right panel, $\bar{\Omega}_\Lambda \to 0$ and the triple stasis reduces to a pairwise stasis involving matter and radiation.

$0 < \eta \leq (1 - 3w)/2$, which follows from the constraint $\bar{\kappa} > 3/2$ in Eq. (6.49).

From these panels we observe that the universe during stasis is effectively vacuum-energy dominated in the $\eta \to 0$ limit, with $\bar{\Omega}_\Lambda \to 1$ and $\bar{\Omega}_M, \bar{\Omega}_\gamma \to 0$. Indeed, this holds true regardless of the value of w. However, as η increases, we see that $\bar{\Omega}_\gamma$ rises monotonically and reaches unity at the point at which η reaches its maximum value, while $\bar{\Omega}_\Lambda$ falls monotonically to zero over the same interval. By contrast, $\bar{\Omega}_M$ initially increases with η, reaching a maximum (the value of which depends nontrivially on η, w, and ξ), and then falling to zero as η increases toward its maximum value. Thus, in each case, we see that our triple stasis as a function of η *interpolates* between a fully vacuum-energy dominated universe and a radiation-dominated one.

In the panels along the bottom row of Fig. 11, we instead plot $\bar{\Omega}_\Lambda$, $\bar{\Omega}_M$, and $\bar{\Omega}_\gamma$ as functions of ξ for different values of η, with w held fixed. The results in the left, middle, and

right panels of this row correspond to the choices $\eta = 1.0$, $\eta = 1.3$, and $\eta = 1.5$, respectively, and for all three panels we have taken $w = -0.7$. The gray region on the left side of each of these three panels indicates the region wherein $\xi < \xi_{\min}$, which lies outside our regime of validity.

We observe from these panels that the behavior of the abundances in the $\xi \to \infty$ limit depends on the relationship between η and w. For $\eta < 2w$, as illustrated in the left and middle panels, $\bar{\Omega}_\gamma \to 0$ and the triple stasis reduces to a pairwise stasis involving vacuum energy and matter alone in both the exponential-decay treatment and the instantaneous-decay approximation. By contrast, for $\eta > 2w$, as illustrated in the right panel, $\bar{\Omega}_\Lambda \to 0$ and the triple stasis reduces to a pairwise stasis involving matter and radiation alone in both the exponential-decay model and the instantaneous-decay approximation. In the opposite limit, as ξ becomes small, the exponential-decay treatment becomes increasingly unreliable, since the direct transfer

of vacuum-energy to radiation, which we are neglecting, becomes important when $\xi < \xi_{\min}$. However, the instantaneous-decay approximation is formally valid for all $\xi < 1$. In this approximation, $\bar{\Omega}_M \to 0$ in the $\xi \to 1$ limit irrespective of the relationship between η and w. Thus, in this limit, the triple stasis reduces to a pairwise stasis involving vacuum energy and radiation.

It is also instructive to "look under the hood" and examine how these triple stasis configurations are realized in terms of the behaviors of the abundances $\Omega_\ell(t)$ of the individual constituents within the towers. In Fig. 12, we have chosen a triple stasis corresponding to the input parameters $(\alpha, \gamma, \delta, w) = (1, 1, 5, -0.7)$ and plotted the total abundances Ω_Λ (thick dark-blue solid line), Ω_M (thick cyan solid line), and Ω_γ (thick magenta solid line) as functions of the number $\mathcal{N}$ of e-folds since the initial

production time. We have also plotted the individual abundances $\Omega_\ell(t)$ corresponding to the uppermost states within the tower that give rise to this stasis over the time interval shown. These latter abundances are shown as thin lines as they transition between vacuum energy (blue), then matter (cyan), and ultimately radiation (magenta). The underdamping transition between the vacuum-energy and matter phases occurs along the upper dashed black line, while the instantaneous-decay transition between the matter and radiation phases occurs along the lower dashed black line.

This figure can be viewed as an explicit numerical realization of the left panel of Fig. 7 except that it is plotted for individual *abundances* $\Omega_\ell(t)$ rather than individual *energy densities* $\rho_\ell(t)$. Indeed, for each line this change from energy density to abundance introduces an
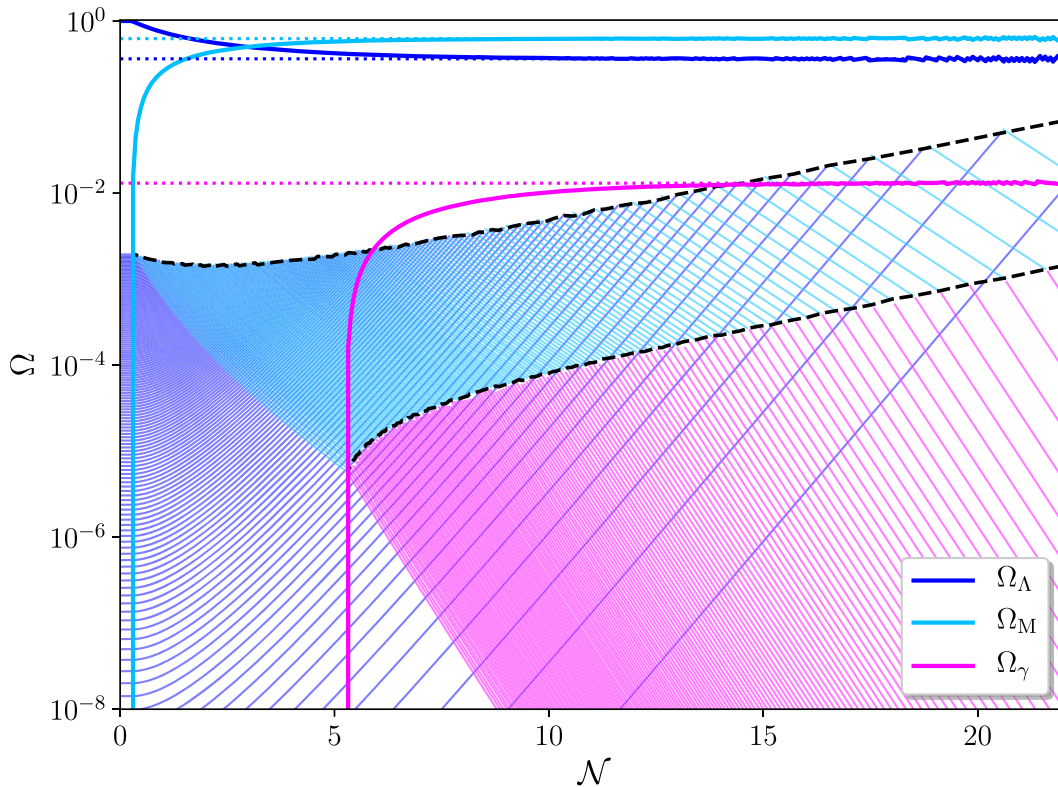

FIG. 12.   Triple stasis "under the hood," illustrating how the individual abundances $\Omega_\ell(t)$ conspire to bring our system into—and then sustain—triple stasis. Working within the framework of the instantaneous-decay approximation and choosing $(\alpha, \gamma, \delta, w) = (1, 1, 5, -0.7)$ in order to highlight critical features, we plot the three total abundances Ω_Λ (thick dark-blue solid line), Ω_M (thick cyan solid line), and Ω_γ (thick magenta solid line) as functions of the number $\mathcal{N}$ of e-folds since the initial production time. We also plot the individual abundances $\Omega_\ell(t)$ (thin lines) as they evolve in time, starting as vacuum energy (dark blue) before transitioning to matter (cyan) and eventually to radiation (magenta). For the sake of graphical clarity we have only shown every 20th individual abundance $\Omega_\ell(t)$, starting from the top of the tower, and adjusted Γ_0/m_0 such that $\xi = 300$. The underdamping transition between the vacuum-energy and matter phases occurs along the upper dashed black line, while the instantaneous-decay transition between the matter and radiation phases occurs along the lower dashed black line. This figure can be viewed as an explicit numerical realization of Fig. 7 except that it is plotted for individual abundances $\Omega_\ell(t)$ rather than individual energy densities $\rho_\ell(t)$ and also includes the initial transient behavior of our system as it evolves from the production time $t^{(0)}$ into stasis. The red transition lines in Fig. 7 correspond to the dashed black lines here, asymptotically becoming parallel once stasis is reached. This figure can also be viewed as a triple-stasis analog of the left panel of Fig. 1.

extra overall factor of H^2 (which scales as t^2 during stasis), thereby tilting all slopes upward relative to those shown in Fig. 7. However, this figure also includes the initial transient behavior of our system as it evolves from the production time $t^{(0)}$ into stasis. The red transition lines in Fig. 7 correspond to the dashed black lines here, asymptotically becoming parallel once stasis is reached. This figure can also be viewed as a triple-stasis analog of the left panel of Fig. 1.

As we see from Fig. 12, each abundance begins immediately after production with a horizontal slope, as appropriate for a highly vacuum-energy-dominated universe. However, these curves all begin to curve upwards as increasing amounts of matter are produced near the top of the tower, thereby affecting the Hubble parameter for the overall cosmology. However, this behavior is part of the overall transition to stasis. Indeed, we see that within several e-folds our abundances begin to exhibit the "cross-hatched" behavior that is the hallmark of stasis, with the identity of the most abundant state continually shifting down the tower as time evolves. The fact that these abundances "reflect" off the underdamping transition line rather than the effective decay line (not shown) allows us to identify this figure as the analog of the left panel, rather than the right panel, within Fig. 7. This is consistent with the fact that Fig. 7 was evaluated numerically for parameters corresponding to $\bar{\kappa} = 8/3$, whereupon we see that indeed $\bar{\kappa} > \alpha$.

E. More about h-factors

At long last, we are now in a position to circle back and address one of the assumptions with which we started in Sec. VI C, namely our assumption discussed below Eq. (6.20) that $t_* < t_\ell$ for all ℓ, where t_* is a fiducial time during stasis. Strictly speaking, such an assumption cannot hold throughout our tower: since t_ℓ gets smaller and smaller as we proceed up the tower, we must inevitably reach a point at which t_ℓ becomes less than t_*. The states above this point therefore violate our assumption. Yet this assumption has been made at many points throughout this paper—not only below Eq. (6.20), but also in Sec. III [see below Eq. (3.17)] and implicitly in Secs. II and IV. Although this issue has been relevant in each of these earlier cases, it is within the case of triple stasis that this issue becomes the most critical. It is for this reason that we have deferred this discussion until now.

There is another related concern that might also seem to cast doubt on our previous analyses. If we were to go back to Eq. (6.20) and describe the time evolution of the individual constituent energy densities $\rho_\ell^{(\Lambda,M,\gamma)}$ since the initial *production* time $t^{(0)}$—as needed in order to make contact with the scaling relations in Eq. (2.12) that define our BSM model—we might attempt to follow our results from previous sections such as those in Eq. (2.15) and write these energy densities in terms of an appropriate $h(t^{(0)}, t_*)$

function which describes the net (*a priori* unknown) gravitational redshifting that occurs between $t^{(0)}$ and t_*. However, as we proceed toward the heavier states in the tower, both t_ℓ and τ_ℓ become increasingly small. As a result, it is possible to reach a point at which the relative ordering between t_* and t_ℓ, and potentially even between t_* and τ_ℓ, will change. However, if either t_ℓ or τ_ℓ becomes smaller than t_*, then the corresponding field will already begin to behave as matter or radiation before reaching stasis. This means that the time evolution of such a field will be *different* than it would have been for fields with t_ℓ larger than t_*, since the latter fields will behave as vacuum energy all the way until reaching stasis. It is therefore possible that a single undetermined h-function may not be sufficient to describe all the states in our tower prior to reaching stasis.

This argument can also be phrased in terms of the *total* abundances $\Omega_{\Lambda,M,\gamma}$. Within our pairwise stasis analyses only one h-function was needed because there was only one independent total abundance whose behavior we needed to describe between $t^{(0)}$ and t_*. Indeed, the second abundance was not an independent degree of freedom because the sum of our two abundances was fixed at 1. However, for a triple stasis, we now have *three* total abundances which must sum to 1, implying that there could be *two* independent h-functions describing our total abundances.

The presence of multiple h-functions is exceedingly dangerous for the analysis we have been performing. In this paper we have been deriving not only overall scaling constraints and log-avoidance constraints, but also relative prefactor constraints. For example, in the case of triple stasis, such relative prefactor constraints are none other than the relations in Eq. (6.55) which express our pumps directly in terms of our abundances, thereby bypassing all of the leading coefficients that are common to the pumps and the abundances. When there is only a single h-function, it cancels from both sides of these *relative* prefactor constraints. This unknown h-function will therefore not affect the nature of such constraints. However, with multiple h-functions, it is possible that different h-functions will appear on each side of our relative prefactor constraints. Such h-functions would no longer cancel, thereby bringing our previous results into doubt.

These are all serious concerns. However, we will now demonstrate that none of these worries are ultimately realized. In particular, we will explain why we can indeed assume that $t_* < t_\ell$ in our analysis, and why only a single h-function is relevant for calculations of stasis quantities such as the stasis abundances $\bar{\Omega}_i$. It therefore follows that all of our previous results remain valid.

To understand why only a single h-function is relevant—and likewise to understand why we may assume $t_* < t_\ell$ in our analysis—let us go back to Eq. (6.20) and attempt to write our different energy densities $\rho_\ell(t)$ in terms of the initial energy densities $\rho_\ell^{(\Lambda,M,\gamma)}(t)$ at the production time

$t = t^{(0)}$. We know, of course, that $t_\ell < \tau_\ell$, and likewise we know that vacuum energy, matter, and radiation respectively correspond to $t < t_\ell$, $t_\ell < t < \tau_\ell$, and $t > \tau_\ell$. We also seek to be describing these energy densities during stasis, and therefore we know $t > t_*$. However, since different parts of the tower will have different relative orderings of t_*, t_ℓ, and τ_ℓ, we will make no assumption regarding this ordering. We then find that there are only six different potential orderings of the relevant timescales in our model:

$$
\begin{aligned}
\Lambda: &\quad t^{(0)} < t_* < t < t_\ell < \tau_\ell, \\
M1: &\quad t^{(0)} < t_* < t_\ell < t < \tau_\ell, \\
M2: &\quad t^{(0)} < t_\ell < t_* < t < \tau_\ell, \\
\gamma1: &\quad t^{(0)} < t_* < t_\ell < \tau_\ell < t, \\
\gamma2: &\quad t^{(0)} < t_\ell < t_* < \tau_\ell < t, \\
\gamma3: &\quad t^{(0)} < t_\ell < \tau_\ell < t_* < t. \quad (6.65)
\end{aligned}
$$

Given these orderings, we can then write down the corresponding energy densities ρ_ℓ at time t in terms of their values $\rho_\ell^{(0)}$ at $t^{(0)}$. Each takes the general form

$$
\rho_\ell(t) = \rho_\ell^{(0)} \cdot G_\ell(t) \cdot \text{Heaviside} \quad (6.66)
$$

where "Heaviside" denotes the specific Θ-function combinations in Eq. (6.20) for vacuum energy, matter, and radiation, and where $G_\ell(t)$ are the net gravitational redshift factors given by

$$
G_\ell^{(\Lambda)}(t) = h_\Lambda(t^{(0)}, t_*)\left(\frac{t}{t_*}\right)^{-(1+w)\bar\kappa},
$$

$$
G_\ell^{(M1)}(t) = h_\Lambda(t^{(0)}, t_*)\left(\frac{t_\ell}{t_*}\right)^{-(1+w)\bar\kappa}\left(\frac{t}{t_\ell}\right)^{-\bar\kappa},
$$

$$
G_\ell^{(M2)}(t) = h_\Lambda(t^{(0)}, t_\ell)h_M(t_\ell, t_*)\left(\frac{t}{t_*}\right)^{-\bar\kappa},
$$

$$
G_\ell^{(\gamma1)}(t) = h_\Lambda(t^{(0)}, t_*)\left(\frac{t_\ell}{t_*}\right)^{-(1+w)\bar\kappa}\left(\frac{\tau_\ell}{t_\ell}\right)^{-\bar\kappa}\left(\frac{t}{\tau_\ell}\right)^{-4\bar\kappa/3},
$$

$$
G_\ell^{(\gamma2)}(t) = h_\Lambda(t^{(0)}, t_\ell)h_M(t_\ell, t_*)\left(\frac{\tau_\ell}{t_*}\right)^{-\bar\kappa}\left(\frac{t}{\tau_\ell}\right)^{-4\bar\kappa/3},
$$

$$
G_\ell^{(\gamma3)}(t) = h_\Lambda(t^{(0)}, t_\ell)h_M(t_\ell, \tau_\ell)h_\gamma(\tau_\ell, t_*)\left(\frac{t}{t_*}\right)^{-4\bar\kappa/3}.
$$

$$(6.67)$$

Here h_Λ, h_M, and h_γ represent the unknown but distinct gravitational redshift factors that are accrued by vacuum energy, matter, and radiation prior to stasis (i.e., prior to t_*). It is the appearance of all three redshift factors in these expressions which is our primary concern. In general, all three redshift factors will propagate throughout our

subsequent calculations, potentially leading to the difficulties discussed above.

It is important to note that all of these difficulties arise only for cases in which $t_\ell > t_*$. If it were possible to impose the constraint that $t_* < t_\ell$, then cases $M2$, $\gamma2$, and $\gamma3$ in Eq. (6.65) would be eliminated, and multiple h-factors would no longer arise—even in situations in which vacuum energy, matter, and radiation are all present. Moreover, the only remaining redshift factor would be $h_\Lambda(t^{(0)}, t_*)$, and this is entirely ℓ-independent. It would therefore be possible to form a coherent ℓ-sum, thereby yielding a single h-factor for total abundances such as Ω_Λ, Ω_M, and Ω_γ.

The issue, then, boils down to a simple question: what justifies the assumption that $t_* < t_\ell$? We have already seen that there can exist states at the top of the tower for which this assumption is not true. What, then, would justify disregarding these states in our analysis?

To analyze this issue, let us return to Fig. 12 and consider the behavior of the individual abundances at some time t deep within stasis. For example, such a time t is indicated as the right-most vertical orange/red dashed line in Fig. 13. At the time t, it is clear that only the states with significant abundances can possibly be important players in continuing to produce the stasis phenomenon. By contrast, states whose abundances at time t have fallen below some chosen cutoff value can no longer play a significant role in supporting the stasis at time t. We have indicated such a cutoff as corresponding to the horizontal orange/red line in Fig. 13, and states whose abundances at time t have fallen
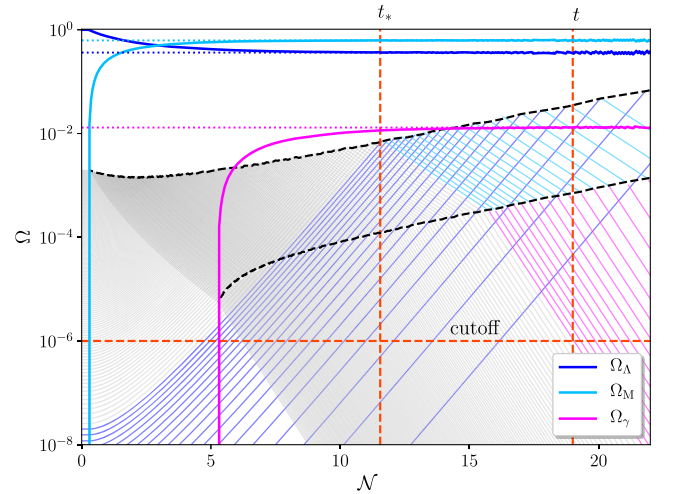

FIG. 13. A version of Fig. 12 illustrating that at any sufficiently late time t during triple stasis it is possible to choose an earlier fiducial time t_*—also during triple stasis—such that all states ϕ_ℓ with significant abundances Ω_ℓ at time t are still overdamped at t_*. Thus, when studying the properties of stasis at any sufficiently late time t during triple stasis, it is a legitimate approximation to assume that all relevant states ϕ_ℓ have $t_\ell > t_*$, with all other states from Fig. 12 disregarded and hence shown in gray.

below this cutoff have been colored in gray. Such states simply do not matter for the purposes of analyzing the stasis phenomenon at time t. However, tracing the remaining (colored) states backwards in Fig. 13, we see that there is a lower limit to the times t_ℓ at which such states all became underdamped. Thus, so long as this lower limit is still within the stasis epoch, we can identify this lower limit as t_*. We thus have a situation in which $t_* < t_\ell$ for all of the states which will ultimately play a role in supporting stasis at time t—i.e., the states whose abundances exceed a critical cutoff value at time t. Indeed, the deeper into the stasis epoch we go (i.e., the larger t becomes), the larger the corresponding fiducial time t_* can be for which we may safely assume $t_* < t_\ell$ for all relevant states.

This argument can also be understood in the forward direction, starting with our entire tower at the production time. As we have discussed above, it is generally the heavier states within the tower which are most in danger of becoming underdamped (or potentially even decaying) prior to our system entering stasis, thereby violating our assumption that $t_* < t_\ell$. However, for sufficiently late times t during stasis, we need no longer consider the contributions from such heavier states, since their abundances at time t will have dropped below a critical relevance cutoff. In other words, such states can be viewed as "turning gray" within the conventions of Fig. 13, with increasingly many states becoming gray as the time t evolves. We can then safely ignore the contributions from such states when discussing analyzing stasis at time t. Since stasis persists over many e-folds, we are free to choose t sufficiently large so that t_*—which is smaller than all of the relevant t_ℓ—is itself within stasis. We can then freely assume that $t_* < t_\ell$ for all relevant ℓ.

We have already noted at numerous points in this paper that one critical property of stasis is that the identity of the most-abundant state at any given time t itself progresses down the tower as t increases. Each state "gets its day" supporting the stasis before yielding its dominant role to the next state in the tower and subsequently diminishing into irrelevance as time proceeds. In this sense, old age does indeed each generation waste. But this is how the stasis state continues to be supported, extended across a cold pastoral landscape of many e-folds, with the abundances $\bar{\Omega}_{\Lambda,M,\gamma}$ remaining fixed as if carved in marble.

Of course, as evident in Figs. 12 and 13, the heaviest states in the tower play a critical role in shaping the initial *transient* behavior that occurs between $t^{(0)}$ and t_*. These states thus play an important in role in guiding the system towards stasis. However, as we have seen, these states cease to play a role within the stasis itself. The same interpretation may be given to the different h-functions in Eq. (6.67). Clearly they are relevant for describing the initial transient behavior of our system. However, the further into stasis our system gets, the smaller the influence of the initial behavior encapsulated within h_γ and then h_M. Ultimately we reach a time t beyond

which only the single h-function h_Λ remains to play a role. Thus only h_Λ is ultimately needed for describing the stasis state, as discussed above. Indeed, taking $t_* < t_\ell$ and the ability to eliminate h_M and h_γ from our stasis calculations go hand in hand.

We thus conclude that it is legitimate to assume $t_* < t_\ell$ for all relevant ℓ, whereupon we may disregard all but the single h-function $h_\Lambda(t^{(0)}, t_*)$. Moreover, this single h-function will cancel from all relative prefactor constraints. We thus conclude that all of the triple-stasis results we have derived thus far remain valid.

Having discussed the h-factors that are relevant for individual abundances Ω_ℓ, let us turn to the h-factors that are relevant for the *total* abundances Ω_Λ, Ω_M, and Ω_γ during stasis. However, as we have seen, the fact that we can now restrict our contributing states to those satisfying $t_* < t_\ell$ during stasis means that our individual abundances during stasis depend only on $h_\Lambda(t^{(0)}, t_*)$, and this quantity is ℓ-independent. This factor can therefore be pulled out of any ℓ-sum, whereupon we see that the corresponding *total* abundances during stasis will also share this same h-factor. We thus see that the $h(t^{(0)}, t_*)$ function that has appeared throughout this section for our abundances and pumps during stasis is nothing but $h_\Lambda(t^{(0)}, t_*)$.

That said, it is also interesting to consider the manner in which our total abundances transition from their initial values at $t^{(0)}$ towards their ultimate stasis values. Of course, throughout this paper we have described the *net* effects of this prestasis process on our total abundances through a single h-factor which we have denoted $h(t^{(0)}, t_*)$. By extending from $t^{(0)}$ all the way to t_*, this factor in principle encapsulates the all of this initial transient behavior. However, we have not examined the actual time dependence associated with this transient behavior—i.e., the time dependence of our abundances $\Omega_{\Lambda,M,\gamma}(t)$ *as they evolve* towards their stasis values. Indeed, this evolution is of interest since it corresponds to the initial curvatures in the plots of the total abundances in Figs. 1, 3, 4, 10, and 12.

Ultimately, this behavior can also be written in terms of the h_Λ, h_M, and h_γ functions we have discussed above. For this analysis we shall content ourselves with understanding the basic algebraic structural elements associated with this behavior. Once again evaluating $\Omega_{\Lambda,M,\gamma}(t)$ as functions of t—but now *without* the assumption of stasis—we obtain

$$\Omega_\Lambda(t) = \int d\tau\, n_\tau(\tau) \Omega_0^{(0)} (\Gamma_0 \tau)^{-1/\gamma} h_\Lambda(t^{(0)}, t),$$

$$\Omega_M(t) = \int d\tau\, n_\tau(\tau) \Omega_0^{(0)} (\Gamma_0 \tau)^{-1/\gamma} h_\Lambda\big(t^{(0)}, f(\tau)\big) h_M(f(\tau), t),$$

$$\begin{aligned}
\Omega_\gamma(t) = \int d\tau\, n_\tau(\tau) \Omega_0^{(0)} (\Gamma_0 \tau)^{-1/\gamma} h_\Lambda\big(t^{(0)}, f(\tau)\big) \\
\times h_M(f(\tau), \tau) h_\gamma(\tau, t). \quad (6.68)
\end{aligned}$$

where these τ-integrals have limits that follow the general structure

$$\Lambda\colon \int_{f^{-1}(t)}^{\tau_0}, \quad M\colon \int_{t}^{f^{-1}(t)}, \quad \gamma\colon \int_{\tau_{N-1}}^{t}. \quad (6.69)$$

In these equations, $f(\tau)$ denotes the underdamping time [i.e., the time $\hat{t}$ at which $3H(\hat{t}) = 2m$] for that part of the tower which decays at time τ, while $f^{-1}(t)$ denotes the inverse of this function. If we were in a stasis configuration, we would have $H(t) = \bar{\kappa}/(3t)$, whereupon we would identify

$$f(\tau) = \frac{(\Gamma_0\tau)^{1/\gamma}}{\xi\Gamma_0} \iff f^{-1}(t) = \frac{(\xi\Gamma_0 t)^{\gamma}}{\Gamma_0}. \quad (6.70)$$

The limits in Eq. (6.69) would then be nothing other than those in Eq. (6.40). However, since we are not assuming stasis for this calculation, we can no longer assert that $H(t) = \bar{\kappa}/(3t)$. Thus the identifications in Eq. (6.70) will no longer hold. The function $f(\tau)$ will nevertheless depend on the values of the abundances $\Omega_\Lambda(t)$ themselves, thereby creating a highly nonlinear system of equations.

The overall algebraic structure indicated in Eqs. (6.68) and (6.69) is valid for all times t. Indeed, given this general structure, we thus see that it is the integrals of products of our $h_{\Lambda,M,\gamma}$ functions which are responsible for producing the initial curvatures for the total abundances plotted in our figures.

One feature which is worthy of note from this structure is that the h_Λ, h_M, and h_γ functions are not independent of each other. Instead, they must be related in such a way that $\Omega_\Lambda(t) + \Omega_M(t) + \Omega_\gamma(t) = 1$ for all t. Of course, the overall value of this sum of abundances is determined by the choice of $\Omega_0^{(0)}$ at the initial time. However, what is remarkable is that once this value is set, this sum of abundances remains fixed as a function of t.

In order to see how this feat is ultimately accomplished, we note that the variable t appears within Eq. (6.68) in only two sets of locations. The first set of locations consists of those within the limits of integration that determine the boundaries between the integration domains for Ω_Λ and Ω_M, and between Ω_M and Ω_γ, as indicated in Eq. (6.69). By contrast, the second set of locations consists of those within the final h-factors that appear within the integrands for each of the three total abundances in Eq. (6.68). The appearance of t within the first set of locations tells us that t determines the *partition* of the total τ-range $\tau_{N-1} \leq \tau \leq \tau_0$ into the individual ranges corresponding to Λ, M, and γ. Indeed, as t increases, the range of τ corresponding to Λ decreases, while that corresponding to γ increases. This is consistent with Fig. 8. Thus, different portions of the τ-range pass directly from one type of energy component to another. However, this passing of abundance between the individual components $\Omega_i(t)$ does not affect the *total* abundance

$\sum_i \Omega_i(t)$. By contrast, it is the appearance of t within the second set of locations—i.e., within the different *integrands* within Eq. (6.68), each with its own unique time dependence—that can potentially affect the value of $\sum_i \Omega_i$. Indeed, since the time t appears within h_Λ function for $\Omega_\Lambda(t)$, within the h_M function for $\Omega_M(t)$, and within the h_γ function for $\Omega_\gamma(t)$, the cancellation of these time dependences for the sum $\sum_i \Omega_i(t)$ implies a relation between these three h-functions.

These assertions can be made mathematically explicit by considering the time derivatives of the total abundances in Eq. (6.68). Considering $d\Omega_\gamma(t)/dt$ first, we find

$$\begin{aligned} \frac{d\Omega_\gamma(t)}{dt} &= n_\tau(t)\Omega_0^{(0)}(\Gamma_0 t)^{-1/\gamma} h_\Lambda\big(t^{(0)}, f(t)\big) \\ &\quad \times h_M(f(t), t) h_\gamma(t, t) \\ &\quad + \int_{\tau_{N-1}}^{t} d\tau\, n_\tau(\tau)\Omega_0^{(0)}(\Gamma_0\tau)^{-1/\gamma} h_\Lambda\big(t^{(0)}, f(\tau)\big) \\ &\quad \times h_M(f(\tau), \tau) \frac{d}{dt} h_\gamma(\tau, t), \end{aligned} \quad (6.71)$$

where the first term [top two lines of Eq. (6.71)] comes from differentiating the factor of t within the integration limit, while the second term [remaining three lines of Eq. (6.71)] comes from differentiating the factor of t in the integrand. Note that $h_\gamma(t, t) = 1$ in the second line of Eq. (6.71). As a result, h_γ completely disappears from the first term of Eq. (6.71)—a feature which allows us to identify the remaining h-factor structure as appropriate for a matter abundance rather than a radiation abundance. Indeed, taken together, this first term is nothing but $n_\tau(t)\Omega_\tau^{(M)}(t; t)$, and this product in turn is nothing but our pump $P_{M\gamma}$ in Eq. (6.30). Equation (6.71) thus takes the relatively simple form

$$\frac{d\Omega_\gamma(t)}{dt} = P_{M\gamma}(t) + \int_{\tau_{N-1}}^{t} d\tau\, n_\tau(\tau) \frac{d}{dt}\Omega_\tau^{(\gamma)}(\tau; t). \quad (6.72)$$

This result of course makes perfect intuitive sense, asserting that the total rate of change for the total radiation abundance Ω_γ has two contributions: one from the abundance being pumped into radiation through ϕ_ℓ decays, and the second from the natural Hubble scaling associated with this abundance itself. *We stress that this result holds in complete generality, and does not assume a stasis of any sort.* We also remark that it is not surprising that one of our pumps has made an appearance in this calculation. Eq. (6.68) essentially represents the integral form for our analysis, while taking the time derivative has thrown us into the differential form in which our pumps make an appearance. As we see, this remains true even if we are not in a stasis epoch.

Proceeding similarly for $d\Omega_\Lambda(t)/dt$, we find

$$
\begin{aligned}
\frac{d\Omega_\Lambda(t)}{dt} = &-\frac{df^{-1}(t)}{dt} n_\tau(f^{-1}(t))\Omega_0^{(0)} \\
&\times [\Gamma_0 f^{-1}(t)]^{-1/\gamma} h_\Lambda(t^{(0)}, t) \\
&+ \int_{f^{-1}(t)}^{\tau_0} d\tau n_\tau(\tau)\Omega_0^{(0)}(\Gamma_0\tau)^{-1/\gamma} \\
&\times \frac{d}{dt} h_\Lambda(t^{(0)}, t).
\end{aligned}
\tag{6.73}
$$

However, as discussed below Eq. (6.69), $f(\tau)$ is essentially $\hat{t}$ (the continuous variable associated with underdamping times rather than decay times). We can then identify

$$
\frac{df^{-1}(t)}{dt} n_\tau = n_{\hat{t}}
\tag{6.74}
$$

whereupon we see that the first term in Eq. (6.73) is nothing but the product of two factors:
  (i) the density of states per unit $\hat{t}$ evaluated for the part of the tower with τ-value $f^{-1}(t)$; and
  (ii) the vacuum-energy abundance evaluated at the time t for the part of the tower with τ-value $f^{-1}(t)$.
However, the first of these factors is nothing but the density of states per unit $\hat{t}$ for that part of the tower with $\hat{t}$-value t, previously denoted $n_{\hat{t}}(t)$. Likewise, the second factor is nothing but the vacuum-energy abundance evaluated at the time t for that part of the tower with $\hat{t}$-value t, previously denoted $\Omega_{\hat{t}}^{(\Lambda)}(t; t)$. Upon comparison with Eq. (6.30), we then see that the product of these two factors is nothing but the pump $P_{\Lambda M}(t)$. We thus have

$$
\frac{d\Omega_\Lambda(t)}{dt} = -P_{\Lambda M}(t) + \int_{f^{-1}(t)}^{\tau_0} d\tau n_\tau(\tau)\frac{d}{dt}\Omega_\tau^{(\Lambda)}(\tau; t).
\tag{6.75}
$$

Likewise, for $d\Omega_M(t)/dt$, we have

$$
\frac{d\Omega_M(t)}{dt} = P_{\Lambda M}(t) - P_{M\gamma}(t) + \int_{t}^{f^{-1}(t)} d\tau n_\tau(\tau)\frac{d}{dt}\Omega_\tau^{(M)}(\tau; t).
\tag{6.76}
$$

Collecting our results in Eqs. (6.72), (6.75), and (6.76), we thus find

$$
\begin{aligned}
\sum_i \frac{d\Omega_i(t)}{dt} = &\int_{f^{-1}(t)}^{\tau_0} d\tau n_\tau(\tau)\frac{d}{dt}\Omega_\tau^{(\Lambda)}(\tau; t) \\
&+ \int_{t}^{f^{-1}(t)} d\tau n_\tau(\tau)\frac{d}{dt}\Omega_\tau^{(M)}(\tau; t) \\
&+ \int_{\tau_{N-1}}^{t} d\tau n_\tau(\tau)\frac{d}{dt}\Omega_\tau^{(\gamma)}(\tau; t).
\end{aligned}
\tag{6.77}
$$

Interestingly, all of the pump terms have cancelled within this sum. As anticipated above, this reflects the fact that the pump terms describe the *redistributions* of energy density between the different energy components *within* our system, but do not affect the total energy density of the system itself. Only the Hubble redshifting effects can do that.

The statement that $\sum_i \Omega_i(t)$ is a constant then boils down to the constraint that $\sum_i d\Omega_i(t)/dt = 0$. We thus find that the three terms on the right side of Eq. (6.77) must cancel directly amongst themselves, i.e.,

$$
\begin{aligned}
0 = &\int_{f^{-1}(t)}^{\tau_0} d\tau n_\tau(\tau)\frac{d}{dt}\Omega_\tau^{(\Lambda)}(\tau; t) \\
&+ \int_{t}^{f^{-1}(t)} d\tau n_\tau(\tau)\frac{d}{dt}\Omega_\tau^{(M)}(\tau; t) \\
&+ \int_{\tau_{N-1}}^{t} d\tau n_\tau(\tau)\frac{d}{dt}\Omega_\tau^{(\gamma)}(\tau; t).
\end{aligned}
\tag{6.78}
$$

This is then a constraint on the three h-functions which appear within these three integrands and which help to determine the time derivatives therein. As noted above, these h-functions also help to determine the value of $f^{-1}(\tau)$ which appears within the limits associated with two of these integrals. This is therefore a complicated system of equations which does not have an obvious analytical solution. These results are nevertheless the underpinnings of the initial curvatures in the plots of the total abundances in Figs. 1, 3, 4, 10, and 12.

The terms in Eq. (6.78) all reflect the time dependences that come from cosmological redshifting effects. Their cancellation when summed across all three abundances implies that while one abundance has a positive time derivative under gravitational redshifting, another must have a negative time derivative. Indeed, this feature is readily apparent within the figures previously cited. That said, we stress that *the cancellation of gravitational redshifting factors across all abundances has nothing whatsoever to do with stasis*. Indeed, while Eq. (6.78) implies a cancellation between redshift factors across different abundances, stasis is a cancellation between the redshift factor *and the corresponding pump* within *each* abundance individually. Indeed, this is what is required in order to have each derivative $d\Omega_\Lambda/dt$, $d\Omega_M/dt$, and $d\Omega_\gamma/dt$ vanish independently.

As we have stressed, the results in Eqs. (6.72), (6.75), and (6.76) are completely general and make no assumption of stasis. However, it is easy to see what becomes of these results if we make the further assumption that we are within a stasis epoch. Within a stasis epoch, we know that the vacuum-energy, matter, and radiation abundances have gravitational redshift factors that scale as

$$h_\Lambda(t_*, t) \sim \left(\frac{t}{t_*}\right)^{2-(1+w)\bar{\kappa}},$$

$$h_M(t_*, t) \sim \left(\frac{t}{t_*}\right)^{2-\bar{\kappa}},$$

$$h_\Lambda(t_*, t) \sim \left(\frac{t}{t_*}\right)^{2-4\bar{\kappa}/3}, \tag{6.79}$$

where t_*, as always, is any time within stasis prior to t. Since these h-functions are the only places that carry an explicit t-dependence within the abundances $\Omega_\tau^{(\Lambda, M, \gamma)}(\tau; t)$ that appear within the integrands of the τ-integrals on the right sides of Eqs. (6.72), (6.75), and (6.76), we immediately find upon taking the t-derivatives of these expressions that

$$\frac{d}{dt}\Omega_\tau^{(\Lambda)}(\tau; t) = [2 - (1+w)\bar{\kappa}]\Omega_\tau^{(\Lambda)}(\tau; t)\frac{1}{t},$$

$$\frac{d}{dt}\Omega_\tau^{(M)}(\tau; t) = [2 - \bar{\kappa}]\Omega_\tau^{(M)}(\tau; t)\frac{1}{t},$$

$$\frac{d}{dt}\Omega_\tau^{(\gamma)}(\tau; t) = [2 - 4\bar{\kappa}/3]\Omega_\tau^{(\gamma)}(\tau; t)\frac{1}{t}. \tag{6.80}$$

Performing the τ-integrals in Eqs. (6.72), (6.75), and (6.76) and then setting $d\Omega_i(t)/dt = 0$ for each $i = \Lambda, M, \gamma$ then yields precisely the pump equations in Eq. (6.10) with which we started, thereby providing a critical cross-check on our results. Indeed, Eqs. (6.72), (6.75), and (6.76) may be taken as the more general underpinning behind Eq. (6.10), one which does not assume stasis but which yields Eq. (6.10) as a special case. On the other hand, our results within Eqs. (6.72), (6.75), and (6.76) assume an instantaneous decay from matter to radiation (and likewise assume that $P_{\Lambda\gamma} = 0$), while the result in Eq. (6.10) is more general and in principle also allows for the possibility of a direct energy transfer from vacuum energy to radiation.

F. Pumps, seesaws, and energy flows

Finally, in order to understand these triple-stasis solutions along Branch A more intuitively, let us consider the flows of energy density that they imply.

We shall begin by analyzing the case with $\bar{\kappa} = 2$, since this case turns out to have the greatest symmetry and simplicity. With $\bar{\kappa} = 2$, Eq. (6.34) reduces to the constraint $\eta = -2w$, which implies that $\eta < 2$. Since $\delta > 0$, this means we must have $\alpha < 2$, and thus $\alpha < \bar{\kappa}$. This then corresponds to the left panel of Fig. 7, but not the right panel.

Given the result in Eq. (6.3), we learn that the constraint $\bar{\kappa} = 2$ restricts our corresponding stasis abundances to lie along a *line* of solutions for which

$$\bar{\Omega}_\Lambda = -\frac{1}{3w}\bar{\Omega}_\gamma \tag{6.81}$$

with $\bar{\Omega}_M = 1 - \bar{\Omega}_\Lambda - \bar{\Omega}_\gamma$. Indeed, it is only the specific choices of (α, δ, w, ξ) that distinguish between the different abundance solutions along this line. For example, as $w \to -1$, a particularly symmetric distribution of abundances satisfying these constraints is $(\bar{\Omega}_\Lambda, \bar{\Omega}_M, \bar{\Omega}_\gamma) = (1/6, 1/3, 1/2)$. Indeed, this is the three-component analog of matter/radiation equality in the sense that Ω_M now carries $1/3$ of the total abundance while the other two abundances collectively carry $2/3$.

Finally, given the constraints in Eqs. (6.10), we see that our pump terms $P_{\Lambda M}$ and $P_{M\gamma}$ for $\bar{\kappa} = 2$ become equal during triple stasis and are given by

$$P_{\Lambda M} = P_{M\gamma} = -2w\bar{\Omega}_\Lambda\frac{1}{t} = \frac{2}{3}\bar{\Omega}_\gamma\frac{1}{t}. \tag{6.82}$$

It turns out that this $\bar{\kappa} = 2$ stasis solution can be visualized in a particularly useful and compelling way. The $\bar{\kappa} = 2$ constraint means that the corresponding triple-stasis universe must be effectively matter dominated, i.e., with an effective abundance-weighted equation-of-state parameter

$$\langle w \rangle \equiv \sum_{i=\Lambda, M, \gamma} w_i\Omega_i = 0 \tag{6.83}$$

where $w_\Lambda = w$, $w_M = 0$, and $w_\gamma = 1/3$. Indeed, this constraint is nothing but the result in Eq. (6.81). However, we may also view Eq. (6.83) as the condition for a "balancing" along a *w-seesaw*, as illustrated in Fig. 14, with the fulcrum position $\langle w \rangle = w_\triangle$ identified as $w_\triangle = 0$. We emphasize in this context that having $\bar{\kappa} = 2$ does not mean that all of the abundance is in the matter component—it just means that the radiation abundance must be three times (or more precisely $-3w$ times) the vacuum-energy abundance, so that the seesaw balances. Whatever abundance is left over is thus the matter abundance. Of course, this matter abundance sits immediately above the fulcrum, so any common rescaling of the vacuum-energy and radiation abundances continues to maintain the seesaw balance. This then provides a seesaw-based explanation for the existence of a line of triple-stasis solutions, all of which are balanced around the fulcrum at $w_\triangle = 0$ with the individual values of (α, δ, w, ξ) selecting between them.

In this connection, we recall from the end of Sec. IV that we previously had a case of vacuum-energy/radiation abundance which allowed for a spectator matter abundance. That universe was also required to be effectively matter-dominated. The special case in Sec. IV can thus be interpreted as a variant of the current triple-stasis phenomenon—a variant in which the two equal pumps $P_{\Lambda M}$ and $P_{M\gamma}$ are merged into a single pump $P_{\Lambda\gamma}$ which bypasses Ω_M completely, thereby rendering Ω_M a mere spectator abundance.
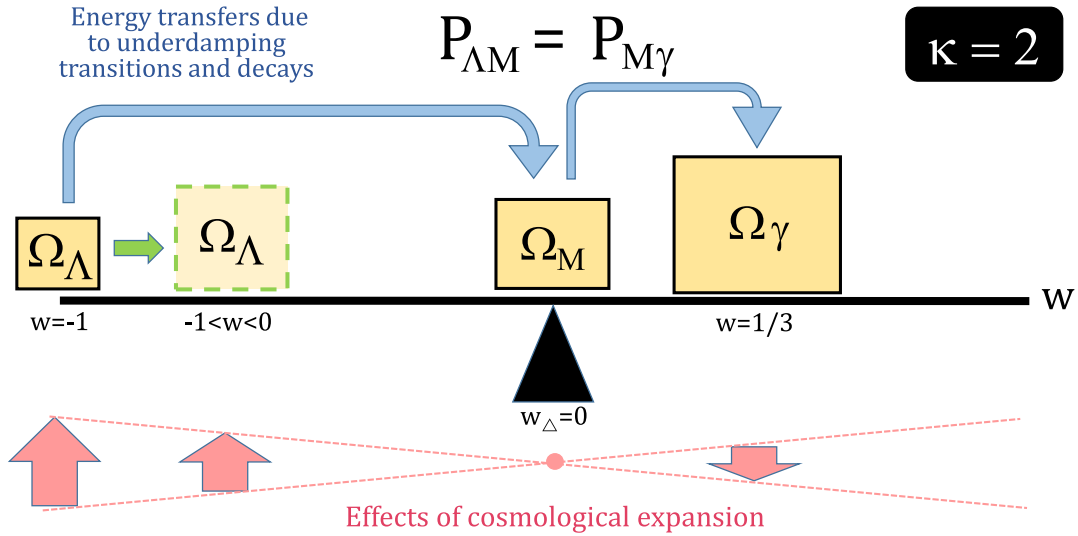
FIG. 14.   The "seesaw" structure of triple stasis with $\bar{\kappa} = 2$ along Branch A in which the abundances of the different energy components along the w-axis are balanced around a "fulcrum" located at $\langle w \rangle = w_\triangle = 0$. The location of the fulcrum corresponds to a $\bar{\kappa} = 2$ universe which is effectively matter dominated. The pumps $P_{\Lambda M}$ and $P_{M\gamma}$ (shown schematically in blue) transfer energy from vacuum energy to matter and from matter to radiation, respectively. These pumps exactly compensate for the effects of cosmological expansion wherein the effects due to gravitational redshifting (shown schematically in pink) either increase or decrease the relative abundances of these different components according to their distances from the fulcrum at $w_\triangle = 0$. Changing the value of w for the vacuum energy component (shown schematically in green) corresponds to "sliding" the position of the corresponding abundance along the w-seesaw. This abundance is then rescaled according to Eq. (6.81) in order to maintain the balancing of the w-seesaw. However, this increased abundance experiences a weakened gravitational redshifting and thus the delicate balancing inherent in triple stasis is maintained.

The manner in which this triple-stasis solution works is thus clear, and is illustrated in Fig. 14. Because the universe is matter dominated, the total matter abundance Ω_M does not feel any tendency to evolve in either direction (rise or fall) under cosmological expansion. Given this, the triple-stasis solution then operates through the following balancing act:

(i) *Vacuum-energy abundance* Ω_Λ: In a matter-dominated universe Ω_Λ wants to *rise* due to cosmological expansion (as indicated through the pink arrows in Fig. 14). However, the pump $P_{\Lambda M}$ continually drains away this excess so that Ω_Λ stays fixed.

(ii) *Radiation abundance* Ω_γ: Conversely, in a matter-dominated universe the radiation abundance Ω_γ wants to *fall* due to cosmological expansion. However, here the pump $P_{M\gamma}$ keeps sourcing a fresh supply so that Ω_γ also stays fixed.

(iii) *Matter abundance* Ω_M: Finally, it is through the central matter abundance Ω_M that the "collision" between these two pairwise pumps occurs. However, with $\bar{\kappa} = 2$ this collision is nonproblematic: the universe is effectively matter-dominated, and thus the matter abundance sits directly atop the fulcrum at $w_\triangle = 0$. In this case there is no tendency for the matter abundance to rise or fall, which is consistent with the fact that the pumps into and out of $\bar{\Omega}_M$ exactly cancel.

Note that this is a true triple stasis, with each energy component experiencing interactions with others and experiencing sources and/or sinks. Moreover, it is remarkable that this solution balances correctly and that our simple scalar model actually realizes it—especially given that one of the pumps results from the transition from an overdamped to underdamped phase while the other pump involves decay, which is a completely different underlying process! Moreover, even though this solution may seem trivially balanced, with equal pumps into and out of the "central" matter component Ω_M, we must remember that our physical *realization* of this triple stasis is actually highly nontrivial, with both pumps operating as the associated transitions make their way down the ϕ_ℓ tower (as illustrated in Fig. 8). Finally, we did not need to create a contorted model with arbitrary interactions in order to realize this stasis—literally *any* coherent state of boson zero modes (such as naturally arise in axion physics) will necessarily experience not only a transition from an overdamped to an underdamped regime but also an eventual decay. Moreover, we will naturally obtain a tower of such states if this boson is higher-dimensional, with the different ϕ_ℓ fields identified as different KK modes.

This seesaw picture also enables us to understand intuitively why this triple-stasis solution works for all $-1 < w < 0$. Towards this end, let us imagine sliding Ω_Λ along the seesaw from $w = -1$ to $w > -1$, as illustrated

in Fig. 14, while keeping $\bar{\Omega}_M$ and $\bar{\Omega}_\gamma$ fixed. Under these assumptions, we see from Eq. (6.81) that $\bar{\Omega}_\Lambda$ grows by a factor of w^{-1}:

$$\bar{\Omega}_\Lambda = 3\bar{\Omega}_\gamma \quad \rightarrow \quad \bar{\Omega}'_\Lambda = -\frac{3}{w}\bar{\Omega}_\gamma. \qquad (6.84)$$

This too is illustrated in Fig. 14. However, following Eq. (6.82) and given that $\bar{\kappa}$ remains fixed at $\bar{\kappa} = 2$ even as w shifts, we see that the total pump rate $P_{\Lambda M}$ is unchanged:

$$P_{\Lambda M} = 2\bar{\Omega}_\Lambda \frac{1}{t} \quad \rightarrow \quad P'_{\Lambda M} = -2w\bar{\Omega}'_\Lambda \frac{1}{t} = P_{\Lambda M}. \qquad (6.85)$$

Thus $P_{\Lambda M}$ remains equal to $P_{M\gamma}$. Moreover, although the shift in w causes the abundance $\bar{\Omega}_\Lambda$ to increase, it also causes the *rate of increase per unit abundance* due to cosmological expansion (as indicated by the wide pink arrows in Fig. 14) to decrease. Thus the net rate at which $\bar{\Omega}_\Lambda$ would tend to increase under cosmological expansion alone is unchanged. This too is consistent with our observation that the pump $P_{\Lambda M}$ is unchanged.

We now turn our attention to Branch A cases with $\bar{\kappa} \neq 2$. These situations correspond to Fig. 7. Indeed, one important feature of Branch A when $\bar{\kappa} \neq 2$ is that we can now in principle have stasis configurations with $3\alpha/4 < \bar{\kappa} < \alpha$, as illustrated in the right panel of Fig. 7. As an existence proof of such a possibility, let us consider the case with $w = -0.99$ and $(\bar{\Omega}_\Lambda, \bar{\Omega}_M, \bar{\Omega}_\gamma) = (0.05, 0.1, 0.85)$. This configuration corresponds to $\bar{\kappa} \approx 1.621$, whereupon we see that $2 - (1 + w)\bar{\kappa} \approx 1.984$. This in turn implies that α could potentially be as large as 1.984, thereby exceeding $\bar{\kappa}$ while nevertheless ensuring that $3\alpha/4 < \bar{\kappa}$. This configuration therefore meets the conditions needed in order to realize the stasis behavior in the right panel of Fig. 7.

Because we are no longer restricting our attention to $\bar{\kappa} = 2$, our resulting stasis need not be effectively matter dominated. This means that during stasis all three of our energy components (vacuum energy, natter, and radiation) can experience gravitational redshifts, implying that our two pumps $P_{\Lambda M}$ and $P_{M\gamma}$ will no longer generally be equal. We must nevertheless continue to have a balancing as illustrated in Fig. 14. However, the fulcrum need no longer be located at $w_\triangle = 0$.

In general, for any system with Hubble expansion coefficient $\bar{\kappa}$, it is straightforward to determine the equation-of-state parameter that a fluid must have in order that its abundance neither rise nor fall as a result of cosmological expansion. This defines the corresponding fulcrum location $w_\triangle$, and indeed one finds

$$w_\triangle \equiv \frac{2}{\bar{\kappa}} - 1. \qquad (6.86)$$

For a universe consisting of only matter, radiation, and vacuum energy (the latter with equation-of-state parameter w), we then find that Eq. (6.3) can be rewritten in the form

$$\langle w \rangle = w\bar{\Omega}_\Lambda + \bar{\Omega}_\gamma/3 = w_\triangle. \qquad (6.87)$$

This is the generalization of Eq. (6.83) with arbitrary $w_\triangle$, and tells us that our seesaw must indeed be balanced around $w_\triangle$. In particular we see that $w_\triangle \geq w$, with the inequality saturated only when $\bar{\Omega}_\Lambda = 1$ and $\bar{\Omega}_M = \bar{\Omega}_\gamma = 0$.

Given these results, the stasis constraint in Eq. (6.34) then tells us that

$$w_\triangle = \frac{2w + \eta}{2 - \eta} \qquad (6.88)$$

or, equivalently, that

$$w_\triangle + 1 = \left(\frac{2}{2 - \eta}\right)(w + 1). \qquad (6.89)$$

We thus see that η and w determine the fulcrum location $w_\triangle$ and thereby determine the line along which the corresponding abundances lie, while these same variables—with the addition of ξ—determine the precise locations along this line for the final stasis abundances. Thus while ξ is not required in order to determine the fulcrum location $w_\triangle$, it is needed for determining the absolute magnitudes of the specific abundances *around* this point.

The corresponding energy flows for $\bar{\kappa} \neq 2$ can be illustrated as in Fig. 15. In general, the results depend on whether $\bar{\kappa} < 2$ or $\bar{\kappa} > 2$. In the first case (corresponding to the upper panel in Fig. 15), we illustrate the situation for $\bar{\kappa} < 2$. In this case $w_\triangle > 0$, which implies that Ω_M will generally tend to increase under the effects of cosmological expansion. Stasis is then achieved only for $P_{\Lambda M} < P_{M\gamma}$, which is consistent with the fact that $\Omega_\Lambda/\Omega_\gamma$ must be smaller than it was in Fig. 14 in order to achieve a balanced seesaw. The lower panel of Fig. 15 illustrates the opposite situation with $\bar{\kappa} > 2$.

VII. STASIS AS A GLOBAL ATTRACTOR

In this section we study the extent to which the different forms of cosmic stasis that we have examined in the previous sections are local or global attractors. As we shall see, the stasis solutions for the pairwise (two-component) systems which we considered in Secs. II through V are all global attractors. Moreover, we shall demonstrate that the triple stasis considered in Sec. VI is a global attractor as well.

A. Pairwise stases

We first analyze the attractor behavior of the pairwise stases discussed in Secs. II, III, and IV. In each case we
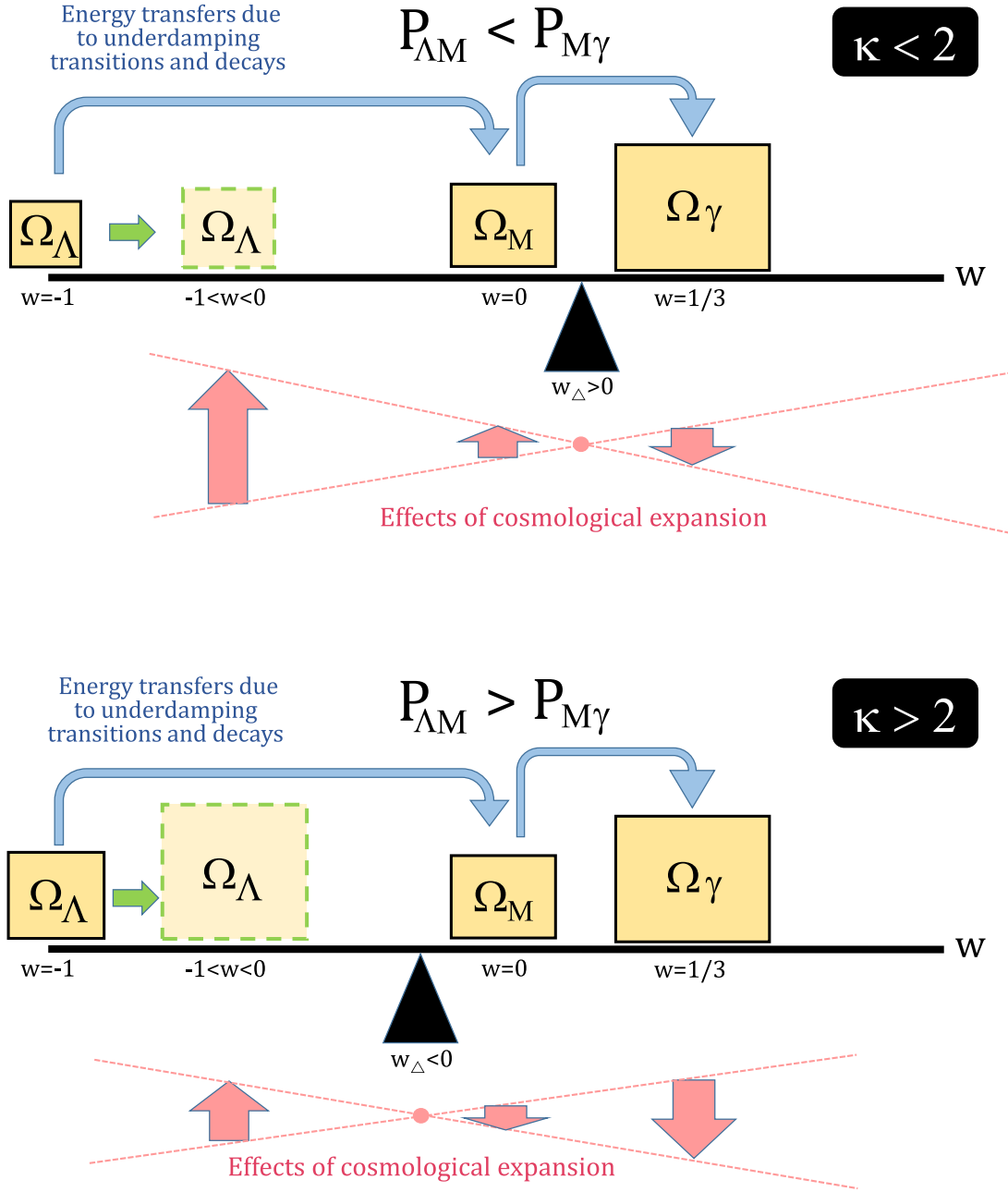
FIG. 15.   Same as Fig. 14, except for stasis solutions with $\bar{\kappa} \neq 2$. Upper panel: in this case $\bar{\kappa} < 2$, implying that $w_\triangle > 0$. This causes Ω_M to tend to increase under the effects of cosmological expansion, which implies that stasis is achieved only for $P_{\Lambda M} < P_{M\gamma}$. This inequality of the pumps is consistent with the fact that $\Omega_\Lambda / \Omega_\gamma$ must be smaller than it was in Fig. 14 in order to achieve a balanced "seesaw." Lower panel: the same situation, but for $\bar{\kappa} > 2$. In this case the signs of all inequalities are reversed, with $P_{\Lambda M} > P_{M\gamma}$ and $\Omega_\Lambda / \Omega_\gamma$ now larger than it was in Fig. 14.

shall begin by demonstrating that the corresponding stasis is a local attractor. With these results in hand, we shall then proceed to demonstrate that these attractors are all in fact global.

Broadly speaking, in particle-physics realizations of stasis which involve towers of states, the physical condition which determines the time t at which each individual such state effectively transitions from one equation of state to another can generally be classified into one of two overall categories:

(i) Class I: transitions for which this transition time is *intrinsic* to the particle in the sense that it depends on the time t in the cosmological background frame alone and is essentially independent of the expansion history. Examples of transitions within this class include the decay transitions which underpin

the matter/radiation and vacuum-energy/radiation stases discussed in Secs. II and IV, respectively. In these realizations of stasis, the intrinsic timescale for these transitions—e.g., the proper lifetime τ_ℓ of the particle ϕ_ℓ at each level—was assumed to scale across the tower as a function of mass according to a power law of the form $\tau_\ell = \tau_0(m_\ell/m_0)^{-\gamma}$. Passing to the continuum limit, we thus have

$$\tau = \tau_0\left(\frac{m}{m_0}\right)^{-\gamma}. \qquad (7.1)$$

(ii) Class II: transitions for which the transition time is *extrinsic* to the particle in the sense that the transition is triggered when the temperature, critical density, or expansion rate of the universe drops below some threshold value. For transitions within this second class, the time t at which the transition takes place *does* depend on the expansion history of the universe through the Hubble parameter $H(t)$. Examples of transitions within this class include the transition from overdamped to underdamped oscillation which underpins the vacuum-energy/matter stasis discussed in Sec. III. In this realization of stasis, the transition of the particle species of mass m_ℓ is triggered at a time t_ℓ when $3H(t_\ell) = 2m_\ell$. Phrased slightly differently, this transition for each ϕ_ℓ is triggered when the Hubble parameter $H(t)$ drops below the critical threshold scale $\hat{H}_\ell = 2m_\ell/3$, with the corresponding time t_ℓ determined *implicitly* through the condition $H(t_\ell) = \hat{H}_\ell$. For complete generality, we shall focus in what follows on the case in which $\hat{H}_\ell$ scales across the tower according to a power law of the form $\hat{H}_\ell = \hat{H}_0(m_\ell/m_0)^{\hat{\gamma}}$ where $\hat{\gamma}$ is a general scaling exponent. In the continuum limit this becomes

$$\hat{H} = \hat{H}_0\left(\frac{m}{m_0}\right)^{\hat{\gamma}}. \qquad (7.2)$$

Thus $\hat{H}$, like τ, is a continuous variable that specifies a particular part of our ϕ-tower, namely that part which has a Class II transition occurring when $H(t) = \hat{H}$. Since $H(t)$ decreases monotonically with t in a flat universe, and since we are primarily interested in situations in which $\hat{H}$ increases with m, we shall henceforth restrict our attention to the regime in which $\hat{\gamma} > 0$. Indeed, as we have seen, an overdamped/underdamped transition of the sort discussed in Sec. III obeys a scaling relation of this form with $\hat{\gamma} = 1$ and $\hat{H}_0 = 2m_0/3$.

When the universe is already deeply in stasis, the distinction between these two classes of transitions is not terribly important. Indeed, since $H \approx \bar{\kappa}/(3t)$ within

stasis, we can obtain a direct expression for the underdamping transition time t_ℓ, namely $t_\ell = \bar{\kappa}/(2m_\ell)$, as we have used throughout this paper. However, if we now wish to extend our analysis to situations in which the universe is not already in stasis, whether a transition is intrinsic or extrinsic matters. Thus, by rephrasing our transition times in terms of critical values $\hat{H}$ of the Hubble parameter, we can extend our analysis beyond stasis and allow the transition times $\hat{t}$ to be determined implicitly.

In what follows, we shall examine these two classes of transitions in turn. For each class, we shall concentrate on two-component systems with abundances $\Omega_{1,2}$ and corresponding equation-of-state parameters $w_{1,2}$ with $-1 < w_1 < w_2 < 1$, as in Sec. V. Within this general framework, we shall derive the coupled equations of motion for the Hubble parameter and for the abundance Ω_1 of the component with the smaller equation-of-state parameter w_1. We shall then demonstrate analytically that the stasis solution to these equations of motion in each case is a local attractor for all possible such combinations of w_1 and w_2. Finally, we shall demonstrate that these stasis solutions are also *global* attractors for the cases of physical interest discussed in Secs. II, III, and IV.

1. Local attractor behavior: Class I transitions

In general, for any pairwise stasis involving two components with equation-of-state parameters w_1 and w_2, where $w_1 < w_2$, the equation of motion for Ω_1 is given by Eq. (5.1). For a stasis of this sort involving Class I transitions, the pump term in this expression, evaluated in the continuum limit, takes the form $P_{12} = n_\tau(t)\Omega_\tau^{(1)}(t;t)$, with $n_\tau(t)$ given by Eq. (6.31). However, since we are not assuming stasis, the expression for $\Omega^{(1)}(t;t)$ is given by

$$\Omega_\tau^{(1)}(\tau;t) = \Omega_0^{(0)}(\Gamma_0\tau)^{-\alpha/\gamma}h_1(t^{(0)},t)\Theta(\tau-t) \qquad (7.3)$$

with $\tau = t$. We caution that while the "(1)" superscript on $\Omega_\tau^{(1)}(\tau;t)$—just like the "1" subscript on $h_1(t^{(0)},t)$—indicates the energy component with equation-of-state parameter w_1, the "(0)" superscript on $\Omega_0^{(0)}$ continues to indicate the value at the initial production time $t^{(0)}$. It therefore follows that

$$P_{12} = \frac{\Omega_0^{(0)}\Gamma_0}{\gamma\delta}\left(\frac{m_0}{\Delta m}\right)^{1/\delta}(\Gamma_0 t)^{-1-\eta/\gamma}h_1(t^{(0)},t). \qquad (7.4)$$

Moreover, the total abundance Ω_1 of the component with equation-of-state parameter w_1, evaluated in the continuum limit, is given for $t \ll \tau_0$ by

$$\Omega_1 = \int_{\tau_{N-1}}^{\tau_0} d\tau n_\tau(\tau) \Omega_\tau^{(1)}(\tau; t)$$

$$\approx \frac{\Omega_0^{(0)}}{\eta\delta} \left(\frac{m_0}{\Delta m}\right)^{1/\delta} (\Gamma_0 t)^{-\eta/\gamma} h_1(t^{(0)}, t). \qquad (7.5)$$

Comparing this expression to the expression for P_{12} in Eq. (7.4), we obtain

$$P_{12} = \frac{\eta}{\gamma} \Omega_1 \frac{1}{t}. \qquad (7.6)$$

Interestingly, this result reduces to our result in Eq. (2.30) during stasis. However, we now see that this result applies even without the assumption of stasis. We thus find that the time evolution of Ω_1 and H is described by the system of equations

$$\frac{d\Omega_1}{dt} = -p\Omega_1 \frac{1}{t} + 3H(w_2 - w_1)\Omega_1(1 - \Omega_1),$$
$$\frac{dH}{dt} = -\frac{3}{2}H^2[1 + w_2 + (w_1 - w_2)\Omega_1]. \qquad (7.7)$$

We may recast these equations in a more revealing form by parametrizing the expansion rate of the universe in terms of the quantity

$$\mathcal{H}(t) \equiv H(t)\left(\frac{3t}{\bar{\kappa}}\right) \qquad (7.8)$$

which represents the ratio of the Hubble parameter $H(t)$ at any given time t to the value which it would have at that time if the universe were in stasis. In particular, we find that

$$\frac{d\Omega_1}{d\log t} = -p\Omega_1 + \bar{\kappa}(w_2 - w_1)\mathcal{H}\Omega_1(1 - \Omega_1),$$
$$\frac{d\mathcal{H}}{d\log t} = \mathcal{H} - \frac{\bar{\kappa}}{2}\mathcal{H}^2[1 + w_2 + (w_1 - w_2)\Omega_1]. \qquad (7.9)$$

Taking $d\Omega_1/d\log t = d\mathcal{H}/d\log t = 0$, we find that indeed the only equilibrium solution for this system with non-vanishing Ω_1 is the stasis solution in which $\mathcal{H} = 1$ and in which $\Omega_1 = \bar{\Omega}_1$, with $\bar{\Omega}_1$ given by Eq. (5.11).

In order to determine whether or not this stasis solution is a local attractor, we evaluate the eigenvalues of the Jacobian matrix for the system of equations in Eq. (7.9). Using the fact that $\bar{\kappa}$ is given by Eq. (5.3) during a general pairwise stasis, we can eliminate $\bar{\kappa}$ in favor of $\bar{\Omega}_1$. These eigenvalues can then be written in the form

$$\lambda_\pm = -\frac{1}{2}\left[\frac{1 + w_2 - (w_1 - w_2)\bar{\Omega}_1}{1 + w_2 + (w_1 - w_2)\bar{\Omega}_1}\right.$$
$$\left. \mp \sqrt{1 - \frac{4(w_2 - w_1)(1 + 2w_1 - w_2)\bar{\Omega}_1}{[1 + w_2 + (w_1 - w_2)\bar{\Omega}_1]^2}}\right]. \qquad (7.10)$$

For all possible combinations of $\bar{\Omega}_1$, w_1, and w_2 within the ranges $0 < \bar{\Omega}_1 \leq 1$ and $-1 < w_1 < w_2 < 1$, both of these eigenvalues are real and negative. Thus, we conclude that for any combination of w_1 and w_2 which satisfies these conditions, the stasis solution is a local attractor.

This general result is applicable to any pairwise stasis involving a Class I pump. For example, this result implies that the stasis solution that we obtained for the matter/radiation system in Sec. II is a local attractor. Indeed, for this realization of stasis we have $w_1 = 0$ and $w_2 = 1/3$, whereupon we see that Eq. (7.10) reduces to

$$\lambda_\pm = -\frac{1}{2}\left[\frac{4 + \bar{\Omega}_M}{4 - \bar{\Omega}_M} \mp \sqrt{1 - \frac{8\bar{\Omega}_M}{(4 - \bar{\Omega}_M)^2}}\right]. \qquad (7.11)$$

Likewise, our results also imply that the stasis solution that we obtained for the vacuum-energy/radiation system in Sec. IV is a local attractor. For this realization of stasis, we have $w_1 = w$ and $w_2 = 1/3$, whereupon we see that Eq. (7.10) reduces to

$$\lambda_\pm = -\frac{1}{2}\left[\frac{4 - (3w - 1)\bar{\Omega}_\Lambda}{4 + (3w - 1)\bar{\Omega}_\Lambda} \mp \sqrt{1 - \frac{8(1 - 9w^2)\bar{\Omega}_\Lambda}{[4 + (3w - 1)\bar{\Omega}_\Lambda]^2}}\right].$$
$$(7.12)$$

2. Local attractor behavior: Class II transitions

For a pairwise stasis involving Class II transitions, as discussed above, the contribution $\Omega_\ell^{(1)}$ from each ϕ_ℓ to the overall abundance Ω_1 associated with the component with equation-of-state parameter w_1 is transferred to the component with equation-of-state parameter w_2 when H drops below a particular threshold $\hat{H}$. In the approximation that this transition occurs sharply at the time t at which $H(t) = \hat{H}$, this contribution takes the form

$$\Omega_\ell^{(1)}(t) = \Omega_\ell^{(0)} h_1(t^{(0)}, t)\Theta(H(t) - \hat{H}_\ell). \qquad (7.13)$$

For a universe involving only two components, with $\Omega_1 + \Omega_2 = 1$, the time derivative of this expression may be written in the form

$$\frac{d\Omega_\ell^{(1)}}{dt} = \Omega_\ell^{(0)} h_1(t^{(0)}, t)\delta(H - \hat{H})\frac{dH}{dt}$$
$$+ 3H\Omega_\ell^{(1)}(w_2 - w_1)(1 - \Omega_1). \qquad (7.14)$$

The rate of change of the total abundance Ω_1 is simply the direct sum of the individual contributions in Eq. (7.14). In order to evaluate this sum, we shall pass to the continuum limit in which we express ℓ in terms of the corresponding transition scale $\hat{H}_\ell$ and then treat $\hat{H}$ as a continuous parameter. In other words, we shall replace

$$\sum_{\ell} \to \int d\hat{H} n_{\hat{H}}(\hat{H}), \tag{7.15}$$

where $n_{\hat{H}}(\hat{H})$ denotes the density of states within the tower per unit $\hat{H}$, evaluated at the location within the tower for which the transition scale is $\hat{H}$. For a scaling relation between $\hat{H}$ and m of the form given in Eq. (7.2), this density of states takes the form

$$n_{\hat{H}}(\hat{H}) \equiv \left| \frac{d\ell}{d\hat{H}} \right| = \frac{1}{\hat{\gamma}\delta\hat{H}_0} \left(\frac{m_0}{\Delta m} \right)^{1/\delta} \left(\frac{\hat{H}}{\hat{H}_0} \right)^{1/(\hat{\gamma}\delta)-1}. \tag{7.16}$$

In analogy with the quantities $\Omega_\tau(\tau; t)$ and $\Omega_{\hat{t}}(\hat{t}; t)$ that we defined in Sec. VI, we shall find it convenient to define $\Omega_{\hat{H}}(\hat{H}; t)$ to represent the abundance—evaluated at time t—of that particular ϕ-field whose transition threshold is $\hat{H}$. For a scaling relation between $\hat{H}$ and m of the form given in Eq. (7.2), this abundance is given by

$$\Omega_{\hat{H}}^{(1)}(\hat{H}; t) = \Omega_0^{(0)} \left(\frac{\hat{H}}{H_0} \right)^{\alpha/\hat{\gamma}} h_1(t^{(0)}, t) \Theta(H(t) - \hat{H}). \tag{7.17}$$

The rate of change of the total abundance Ω_1, evaluated in the continuum limit, is

$$\frac{d\Omega_1}{dt} = \int_{\hat{H}_0}^{\hat{H}_{N-1}} d\hat{H} \frac{d\Omega_{\hat{H}}^{(1)}(\hat{H}; t)}{dt}, \tag{7.18}$$

which yields an expression of the general form given in Eq. (5.1). However, we see from Eq. (7.14) that the pump term P_{12} for a Class II transition is in general given by

$$P_{12} = n_{\hat{H}}(H) \Omega_{\hat{H}}^{(1)}(H; t) \frac{dH}{dt}. \tag{7.19}$$

For the particular set of transitions we are considering here, with $n_{\hat{H}}(\hat{H})$ and $\Omega_{\hat{H}}^{(1)}(\hat{H}; t)$ given by Eqs. (7.16) and (7.17), respectively, we have

$$P_{12} = \frac{3H_0 \Omega_0^{(0)}}{\kappa\hat{\gamma}\delta} \left(\frac{m_0}{\Delta m} \right)^{1/\delta} \left(\frac{H}{H_0} \right)^{1+\eta/\hat{\gamma}} h_1(t^{(0)}, t), \tag{7.20}$$

with κ given by Eq. (5.3).

The total abundance of the component with equation-of-state parameter w_1 in this case, evaluated in the continuum limit, is

$$\Omega_1 = \int_{\hat{H}_{N-1}}^{\hat{H}_0} d\hat{H} n_{\hat{H}}(\hat{H}) \Omega_{\hat{H}}^{(1)}(\hat{H}; t). \tag{7.21}$$

Explicit integration yields

$$\Omega_1 = \frac{\Omega_0^{(0)}}{\hat{\gamma}\delta} \left(\frac{m_0}{\Delta m} \right)^{1/\delta} H_0^{-\eta/\hat{\gamma}} h_1(t^{(0)}, t) \int_{\hat{H}_0}^{H(t)} d\hat{H} \hat{H}^{\eta/\hat{\gamma}-1}$$

$$\approx \frac{\Omega_0^{(0)}}{\delta\eta} \left(\frac{m_0}{\Delta m} \right)^{1/\delta} \left(\frac{H}{H_0} \right)^{\eta/\hat{\gamma}} h_1(t^{(0)}, t), \tag{7.22}$$

where in going from the first to the second line we have used the fact that $H \gg \hat{H}_0$ at times well before the energy density associated with the lightest tower state is transferred to the energy component with equation-of-state parameter w_2. Comparing this expression to the expression for P_{12} in Eq. (7.20), we observe that

$$P_{12} = \frac{\eta}{\hat{\gamma}} \Omega_1 \left(\frac{3}{\kappa} H \right). \tag{7.23}$$

For $\hat{\gamma} = 1$, we find that this result reduces to Eq. (3.31) during stasis. However, we now see that Eq. (7.23) holds even without the assumption of stasis. Moreover, comparing this result to the stasis expectation in Eq. (5.7), we observe that $p = \eta/\hat{\gamma}$ for a Class II transition of this sort with arbitrary $\hat{\gamma} > 0$.

It follows from the result in Eq. (7.23) that the time evolution of Ω_1 and $\mathcal{H}$ in this case is described by the equations

$$\frac{d\Omega_1}{d\log t} = -\frac{\bar{\kappa}}{2} p \mathcal{H}\Omega_1 [1 + w_2 + (w_1 - w_2)\Omega_1]$$
$$+ \bar{\kappa}(w_2 - w_1)\mathcal{H}\Omega_1(1 - \Omega_1),$$

$$\frac{d\mathcal{H}}{d\log t} = \mathcal{H} - \frac{\bar{\kappa}}{2} \mathcal{H}^2 [1 + w_2 + (w_1 - w_2)\Omega_1]. \tag{7.24}$$

The only equilibrium solution for this system with non-vanishing Ω_1 is the stasis solution in which $\mathcal{H} = 1$ and in which $\Omega_1 = \bar{\Omega}_1$, where $\bar{\Omega}_1$ given by Eq. (5.11) with $p = \eta/\hat{\gamma}$.

Using Eq. (3.14) in order to eliminate $\bar{\kappa}$ in favor of $\bar{\Omega}_1$, we find that the eigenvalues of the Jacobian matrix in this case are

$$\lambda_+ = \frac{2(1 + w_1)(w_1 - w_2)\bar{\Omega}_1}{[1 + w_2 + (w_1 - w_2)\bar{\Omega}_1]^2},$$
$$\lambda_- = -1. \tag{7.25}$$

For all possible combinations of $\bar{\Omega}_1$, w_1, and w_2 within the ranges $0 < \bar{\Omega}_1 \leq 1$ and $-1 < w_1 < w_2 < 1$, both of these eigenvalues are real and negative. Thus, we conclude that for any combination of w_1 and w_2 which satisfies these conditions, the stasis solution is a local attractor.

This general result is applicable to any pairwise stasis involving a Class II pump. For example, it implies that the stasis solution that we obtained for the vacuum-energy/matter system that we examined in Sec. IV is a local

attractor. Indeed, for this realization of stasis, wherein an energy component with equation-of-state parameter $w_1 = w$ transfers its energy density to an energy component with $w_2 = 0$ via a transition from overdamped to underdamped oscillation, Eq. (7.25) reduces to

$$\lambda_+ = \frac{2w(1+w)\bar{\Omega}_\Lambda}{(1+w\bar{\Omega}_\Lambda)^2},$$

$$\lambda_- = -1. \qquad (7.26)$$

3. Global attractor behavior

We have thus far demonstrated that each of our pairwise stasis solutions is a local attractor. In order to assess whether these solutions are also *global* attractors, we map the trajectories along which the system evolves in the $(\bar{\Omega}_1, \mathcal{H})$-plane for different initial combinations of $\bar{\Omega}_1$ and $\mathcal{H}$, where in each case $\bar{\Omega}_1$ once again represents the abundance of the cosmological energy component with the smaller equation-of-state parameter. In Fig. 16, the left panel shows a number of such trajectories for the matter/radiation system obtained by taking $w_1 = 0$ and $w_2 = 1/3$ in Eq. (7.9). The middle panel shows trajectories for the vacuum-energy/matter system obtained by taking $w_1 = w = -0.8$ and $w_2 = 0$ in Eq. (7.24). The right panel shows trajectories for the vacuum-energy/radiation system obtained by taking $w_1 = w = -0.8$ and $w_2 = 1/3$ in Eqs. (7.9). The point within the $(\bar{\Omega}_1, \mathcal{H})$-plane which corresponds to the stasis solution in each panel is indicated with a red dot. The value of p in each case is chosen such that $\bar{\Omega}_1 = 0.5$.

In all three panels of Fig. 16, we see that our trajectories ultimately flow toward the stasis solution. Indeed, this remains true even if we consider other values of $\bar{\Omega}_i$, other values of w (when relevant), and even regions of the $(\bar{\Omega}_1, \mathcal{H})$ plane with values of $\mathcal{H}$ beyond those shown. We therefore conclude that the stasis solution is not only a local attractor for all three kinds of pairwise stasis we have considered here, but a global attractor as well.

B. Triple stasis

We now turn to consider whether the triple-stasis solution which emerged from the three-component system in Sec. VI is likewise an attractor. The analysis in this case is significantly more complicated than it is for the two-component systems that we considered in the previous subsection—not merely because this system involves a larger number of dependent variables, but also because the coupled equations which describe the time evolution of these variables are not differential equations, but rather integrodifferential equations. As a result, we cannot determine whether the triple-stasis solution is a local attractor analytically using the methods we employed when analyzing our two-component systems.

For this reason, we instead investigate the attractor behavior of our triple-stasis system numerically by varying the initial conditions for the system at $t^{(0)}$. In Fig. 17, we illustrate the effect on the abundances of varying the ratio $H(t_{N-1})/H^{(0)}$ where t_{N-1} is the time at which the heaviest field in the ensemble becomes underdamped and begins oscillating and where $H^{(0)}$ is the Hubble parameter at the initial production time $t^{(0)}$. The abundances Ω_Λ, Ω_M, and Ω_γ are plotted in the left, middle, and right panels of the
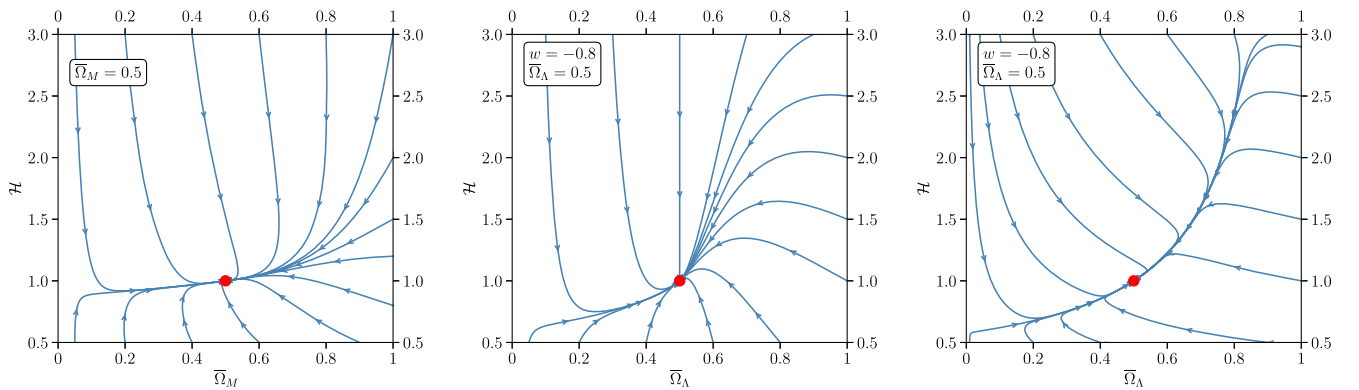

FIG. 16. Attractor behavior for $M\gamma$ stasis (left panel), ΛM stasis (middle panel), and $\Lambda\gamma$ stasis (right panel). Shown in each case are the trajectories (blue curves) within the $(\Omega_1, \mathcal{H})$-plane, where Ω_1 in each case represents the abundance of the cosmological energy component with the smaller equation-of-state parameter. These trajectories correspond respectively to the dynamical system described in Eq. (7.9) with $w_1 = 0$ and $w_2 = 1/3$, the dynamical system described in Eq. (7.24) with $w_1 = w = -0.8$ and $w_2 = 0$, and the dynamical system described in Eq. (7.9) with $w_1 = w = -0.8$ and $w_2 = 1/3$. The red dot in each case indicates the corresponding attractor stasis solution. We have chosen p in each case such that $\bar{\Omega}_1 = 0.5$, and we have used the instantaneous-decay approximation in obtaining the results shown in the left and right panels. We emphasize that while we have taken $w = -0.8$ for each pairwise stasis involving vacuum energy, similar results are obtained for other values of w.
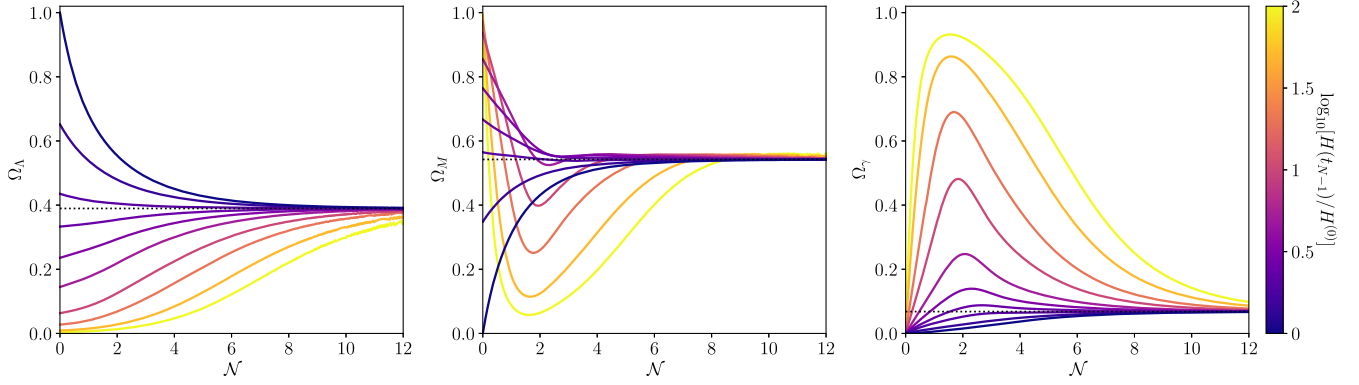
FIG. 17. The abundances of vacuum energy (left panel), matter (center panel), and radiation (right panel) in a three-component system exhibiting a triple-stasis solution, plotted as functions of the number $\mathcal{N}$ of e-folds of cosmological expansion since the initial production time $t^{(0)}$. The different curves in each panel correspond to different values of the ratio $H(t_{N-1})/H^{(0)}$, where t_{N-1} denotes the time at which the heaviest of the ϕ_ℓ fields becomes underdamped and begins oscillating. These results were calculated within the full exponential-decay framework and correspond to the parameter choices $\alpha = 0.95$, $\delta = 4$, $w = -0.7$, $\xi = 20$, and $\Delta m/m_0 = 1$. For all values of $H(t_{N-1})/H^{(0)}$, we observe that $\Omega_\Lambda(t)$, $\Omega_M(t)$, and $\Omega_\gamma(t)$ all evolve toward their stasis values. We also note that it takes longer for the universe to settle into its asymptotic stasis state for some values of $H(t_{N-1})/H^{(0)}$ than for others.

figure, respectively, as functions of the number $\mathcal{N}$ of e-folds of expansion since $t^{(0)}$. The different curves appearing in each panel correspond to different values of $H(t_{N-1})/H^{(0)}$ within the range $0.01 \leq H^{(0)}/H(t_{N-1}) \leq 1$. The dotted horizontal line in each panel indicates the stasis value given in Eq. (6.58) for the corresponding abundance. In each case we have taken $\Omega_\Lambda^{(0)} = 1$ and $\Omega_M^{(0)} = \Omega_\gamma^{(0)} = 0$.

For all values of $H(t_{N-1})/H^{(0)}$, we observe that Ω_Λ, Ω_M, and Ω_γ all evolve toward their stasis values. Thus, we may conclude that the emergence of a triple stasis is not predicated on a particular choice of $H(t_{N-1})/H^{(0)}$. We also note that it takes the universe longer to settle into its asymptotic stasis state for some values of $H(t_{N-1})/H^{(0)}$ than it does for others.

One might also ask whether the emergence of a stasis epoch depends sensitively on the initial values $\Omega_\Lambda^{(0)}$, $\Omega_M^{(0)}$, and $\Omega_\gamma^{(0)}$ of our three abundances. However, given the assumptions inherent in our model, we do not have the freedom to vary these three abundances arbitrarily. Indeed, our model comprises only the ϕ_ℓ fields and one or more effectively massless fields which behave as radiation throughout the entirety of the stasis epoch. Likewise, the individual masses and abundances of the ϕ_ℓ fields are assumed to scale across the tower according to the relations in Eqs. (2.12) and (2.13), respectively. Given these assumptions, it is not possible to adjust the relationship between $\Omega_\Lambda^{(0)}$ and $\Omega_M^{(0)}$ arbitrarily without introducing additional spectator fields which behave as either matter or vacuum energy. That said, we *do* have the freedom to adjust $\Omega_\gamma^{(0)}$ arbitrarily, provided that we compensate for this adjustment by shifting the values of both $\Omega_\Lambda^{(0)}$ and $\Omega_M^{(0)}$ such that $\Omega_\Lambda^{(0)} + \Omega_M^{(0)} + \Omega_\gamma^{(0)} = 1$ and the appropriate

relationship between $\Omega_\Lambda^{(0)}$ and $\Omega_M^{(0)}$ is maintained. Thus, in what follows, we shall continue to take $\Omega_M^{(0)} = 0$ and focus on the effect of varying $\Omega_\Lambda^{(0)}$ and $\Omega_\gamma^{(0)}$.

In Fig. 18 we illustrate the effect on the abundances that emerges upon varying $\Omega_\Lambda^{(0)}$ and $\Omega_\gamma^{(0)}$ subject to the constraints that $\Omega_\gamma^{(0)} = 1 - \Omega_\Lambda^{(0)}$ and $\Omega_M^{(0)} = 0$. As in Fig. 17, the three abundances $\Omega_\Lambda(t)$, $\Omega_M(t)$, and $\Omega_\gamma(t)$ are plotted as functions of $\mathcal{N}$ in the left, middle, and right panels, respectively. In each panel, the dotted horizontal line once again indicates the stasis value given in Eqs. (6.58) and (6.59) for the corresponding abundance.

In each case, we observe that $\Omega_\Lambda(t)$, $\Omega_M(t)$, and $\Omega_\gamma(t)$ all evolve toward their stasis values. Thus, we may further conclude that the emergence of triple stasis is not predicated on the universe being fully vacuum-energy dominated at the initial time $t^{(0)}$, much less devoid of radiation. Indeed, we see that stasis emerges *regardless* of the admixture of vacuum energy and radiation at the initial time. However, we also observe that it takes the universe longer to settle into its asymptotic stasis state for some admixtures than others.

Taken together, the empirical results shown in Figs. 17 and 18 strongly suggest that our triple-stasis solution in Sec. VI is not only a local attractor but also a global attractor, pulling our system towards the stasis state for a wide range of dynamical parameters and initial configurations.

VIII. A PHASE DIAGRAM FOR STASIS

It is interesting to synthesize the results of this paper thus far by investigating how our different forms of stasis relate to each other. Collecting our results from Secs. II, III, IV,
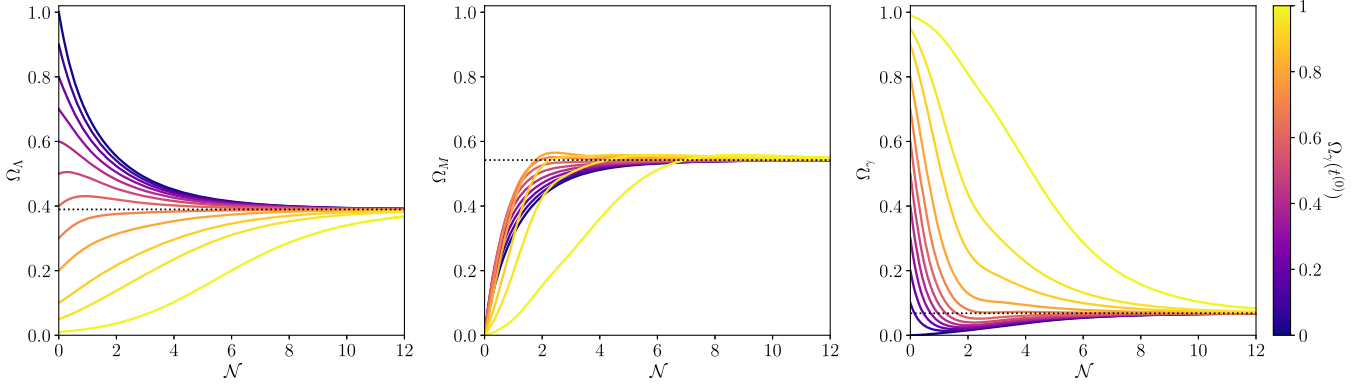
FIG. 18.   Same as Fig. 17, except that the different curves now correspond to different values for the initial vacuum-energy and radiation abundances $\Omega_\Lambda^{(0)}$ and $\Omega_\gamma^{(0)} = 1 - \Omega_\Lambda^{(0)}$, with $\Omega_M^{(0)} = 0$ held fixed. These results were calculated within the full exponential-decay framework and correspond to the parameter choices $\alpha = 0.95$, $\delta = 4$, $w = -0.7$, $\xi = 20$, $\Delta m / m_0 = 1$, and $3H^{(0)}/(2m_{N-1}) = 1$. For all values of $\Omega_\Lambda^{(0)}$ and $\Omega_\gamma^{(0)}$, we see that $\Omega_\Lambda(t)$, $\Omega_M(t)$, and $\Omega_\gamma(t)$ all ultimately evolve toward their stasis values, with the universe taking longer to settle into its asymptotic stasis state for some values of $\Omega_\Lambda^{(0)}$ and $\Omega_\gamma^{(0)}$ than for others.

and VI, we see that our different stases have the constraint equations

$$M\gamma \text{ Stasis:} \quad \frac{\eta}{\gamma} = 2 - \bar\kappa,$$

$$\Lambda M \text{ Stasis:} \quad \eta = 2 - (1 + w)\bar\kappa,$$

$$\Lambda\gamma \text{ Stasis:} \quad \frac{\eta}{\gamma} = 2 - (1 + w)\bar\kappa,$$

$$\text{Triple Stasis:} \quad - \quad \eta = 2 - (1 + w)\bar\kappa, \quad \gamma = 1. \qquad (8.1)$$

Note that in the case of triple stasis, we are restricting our attention to Branch A because Branch B does not yield a full stasis.

The constraint equations in Eq. (8.1) are all very similar to each other. Indeed, if we temporarily disregard the absence of the w-term within the constraint for $M\gamma$ stasis, *we see that these equations all become identical if* $\gamma = 1$.

There are also other commonalities between these different forms of stasis. In general, a matter-dominated universe has $\bar\kappa = 2$ while a radiation-dominated universe has $\bar\kappa = 3/2$. By contrast, within the context of our general-w model for vacuum energy, a universe dominated by vacuum energy has $\bar\kappa = 2/(1 + w)$. It therefore follows that our different mixed-component stases have restricted ranges for $\bar\kappa$ given by

$$M\gamma \text{ Stasis:} \quad 3/2 < \bar\kappa < 2,$$

$$\Lambda M \text{ Stasis:} \quad 2 < \bar\kappa < 2/(1 + w),$$

$$\Lambda\gamma \text{ Stasis:} \quad 3/2 < \bar\kappa < 2/(1 + w),$$

$$\text{Triple Stasis:} \quad 3/2 < \bar\kappa < 2/(1 + w). \qquad (8.2)$$

However, substituting these results into the corresponding equations in Eq. (8.1) we find in each case that

$$\eta > 0. \qquad (8.3)$$

Of course, this condition has already been stated throughout this paper on the basis of other consistency constraints [see, e.g., Eqs. (2.23), (3.24), (4.7), and (6.50)]. However, the condition in Eq. (8.3) is yet another commonality between our different forms of stasis.

The fact that all of our stases have the same basic constraints on their fundamental parameters suggests that they all populate different limiting regions of a common "phase space." We shall now demonstrate that this expectation is correct.

To do this, let us begin by considering the largest and most comprehensive of our stases, namely the triple stasis of Sec. VI. In Fig. 19, we display the phase diagram for triple stasis within the $(w_\triangle, \xi)$-plane for several different values of w. The results in the top panel correspond to the choice $w = -0.7$, while the results shown in the three panels at the bottom of the figure correspond to the choices $w = -0.9$ (left panel), $w = -0.5$ (middle panel), and $w = -0.25$ (right panel). The color of each point within each panel has been assigned according to the abundance-map palette shown on the far right, with the relative levels of blue, green, and red indicating the values of the stasis abundances $\bar\Omega_\Lambda$, $\bar\Omega_M$, and $\bar\Omega_\gamma$, respectively. The gray region on the left side of each panel is physically inaccessible, since self-consistency requires $w_\triangle > w$. Likewise the shaded region with $\xi < \xi_{\min}$ lies outside our regime of validity for $\epsilon_{\text{dec}} = 0.05$. The dashed black vertical line with $w_\triangle = 0$ corresponds to universes with $\bar\kappa = 2$, as shown in Fig. 14. Points to the right of this line correspond to universes with $\bar\kappa < 2$, whereas points to the left correspond to universes with $\bar\kappa > 2$. Such universes respectively correspond to the situations illustrated in the upper and lower panels of Fig. 15.
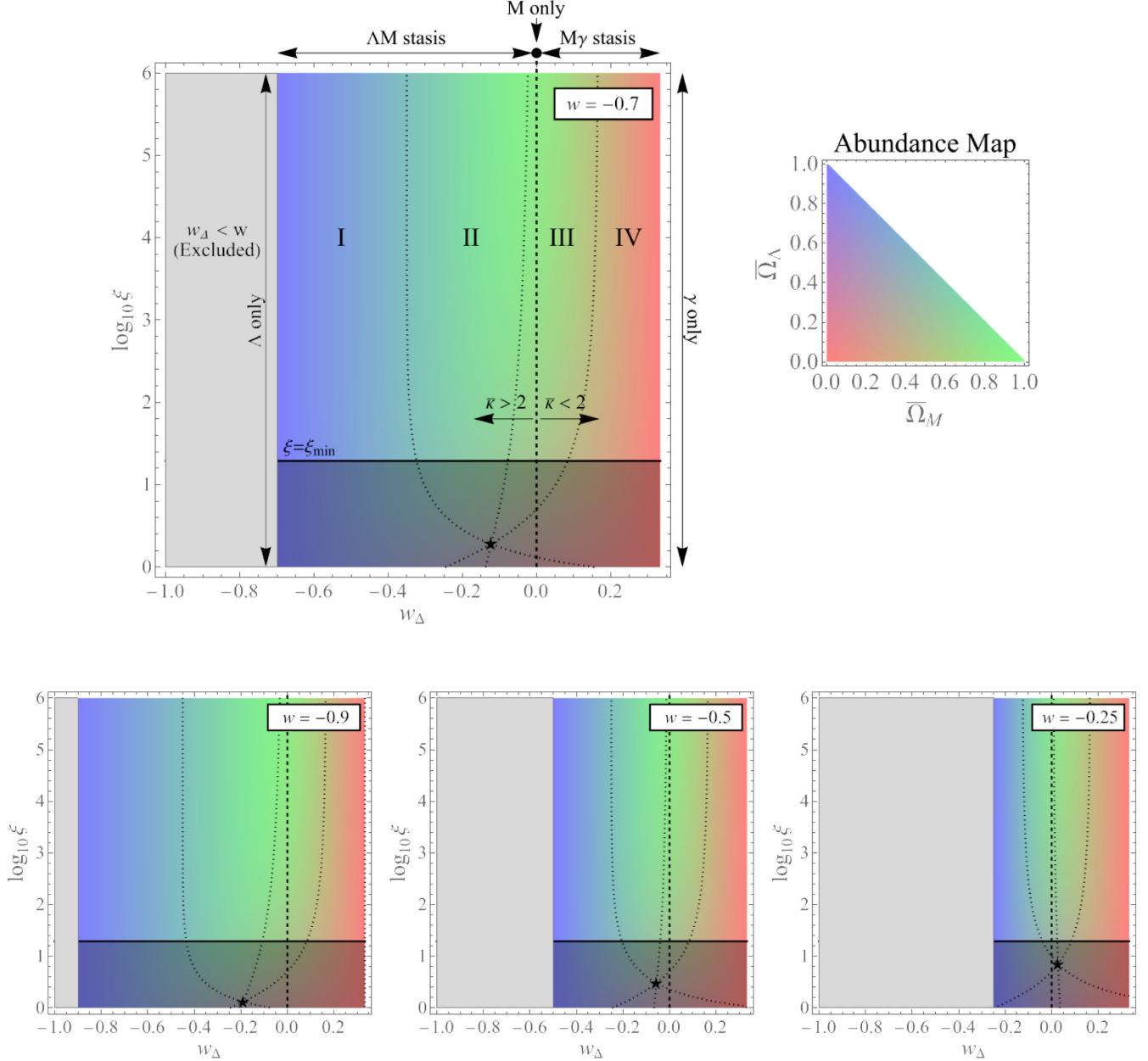
FIG. 19. "Phase diagrams" for triple stasis within the $(w_\triangle, \xi)$-plane for $w = -0.7$ (top panel) and for $w = -0.9$, $w = -0.5$, and $w = -0.25$ (corresponding to the three panels along the lower row). Working within the full exponential-decay framework, we have assigned the color of each point within the $(w_\triangle, \xi)$-plane according to the abundance-map palette shown on the top right, with the relative levels of blue, green, and red indicating the values of the stasis abundances $\bar{\Omega}_\Lambda$, $\bar{\Omega}_M$, and $\bar{\Omega}_\gamma$, respectively. The gray region on the left side of each panel is physically inaccessible, since self-consistency requires $w_\triangle > w$. Likewise the shaded region with $\xi < \xi_{\min}$ lies outside our regime of validity for $\epsilon_{\text{dec}} = 0.05$. The dashed black vertical line with $w_\triangle = 0$ corresponds to universes with $\bar{\kappa} = 2$, as shown in Fig. 14, while points to the left (respectively right) of this line correspond to universes with $\bar{\kappa} > 2$ (respectively $\bar{\kappa} < 2$), as shown in the upper (respectively lower) panel of Fig. 15. The points within Regions I through IV exhibit triple stases with $\bar{\Omega}_\Lambda > \bar{\Omega}_M > \bar{\Omega}_\gamma$, $\bar{\Omega}_M > \bar{\Omega}_\Lambda > \bar{\Omega}_\gamma$, $\bar{\Omega}_M > \bar{\Omega}_\gamma > \bar{\Omega}_\Lambda$, and $\bar{\Omega}_\gamma > \bar{\Omega}_M > \bar{\Omega}_\Lambda$, respectively. By contrast, along the edges of this plane, our triple-stasis solutions reduce to simpler stasis solutions: either to a pairwise ΛM stasis (as discussed in Sec. III and shown along the upper edge with $w_\triangle < 0$), or to a pairwise $M\gamma$ stasis (as discussed in Sec. II and shown along the upper edge with $w_\triangle > 0$), or to universes with only vacuum energy (as shown along the left edge), radiation (as shown along the right edge), or matter (as indicated at the top point with $w_\triangle = 0$). All universes along the vertical $w_\triangle = 0$ line are effectively matter-dominated (as illustrated in Fig. 14), with counterbalancing abundances of vacuum energy and radiation; however, as we move up this line towards greater values of ξ, these other abundances maintain their ratio but shrink to zero, leaving behind a universe consisting only of matter as $\xi \to \infty$. The star represents the location of the "triple point" at which $\bar{\Omega}_\Lambda = \bar{\Omega}_M = \bar{\Omega}_\gamma$. This figure therefore encapsulates and illustrates the relationships between the different versions of stasis discussed in this paper.

The points within the Regions I through IV in each panel of Fig. 19 exhibit triple stases with $\bar{\Omega}_\Lambda > \bar{\Omega}_M > \bar{\Omega}_\gamma$, with $\bar{\Omega}_M > \bar{\Omega}_\Lambda > \bar{\Omega}_\gamma$, with $\bar{\Omega}_M > \bar{\Omega}_\gamma > \bar{\Omega}_\Lambda$, or with $\bar{\Omega}_\gamma > \bar{\Omega}_M > \bar{\Omega}_\Lambda$, respectively. By contrast, along the edges of this plane, our triple-stasis solutions reduce to simpler stasis solutions: either to a pairwise ΛM stasis (as discussed in Sec. III and shown along the upper edge with $w_\triangle < 0$), or to a pairwise $M\gamma$ stasis (as discussed in Sec. II and shown along the upper edge with $w_\triangle > 0$), or to universes with only vacuum energy (as shown along the left edge), radiation (as shown along the right edge), or matter (as indicated at the top point with $w_\triangle = 0$). All universes along the vertical $w_\triangle = 0$ line are effectively matter-dominated (as illustrated in Fig. 14), with counterbalancing abundances of vacuum energy and radiation; however, as we move up this line towards greater values of ξ, these other abundances maintain their ratio but shrink to zero, leaving behind a universe consisting only of matter as $\xi \to \infty$. Thus, as anticipated, we see that this figure encapsulates and illustrates the relationships between the different versions of stasis discussed in this paper.

As we remarked at the beginning of this section, the constraint equation for $M\gamma$ stasis in Eq. (8.1) is slightly different from the others in that it does not depend on w. This, of course, makes sense since w is the equation-of-state parameter for the vacuum energy, and $M\gamma$ stasis does not involve vacuum energy. However, at a purely algebraic level, we observe that the form of the $M\gamma$ constraint equation does match the others but has an "effective" $w = 0$. Requiring $w = 0$ in turn implies that $w_\triangle \geq 0$, and we see from Fig. 19 that this is indeed precisely the region to which the $M\gamma$ stasis is restricted.

Finally, we note that each of the phase diagrams shown in Fig. 19 exhibits a "triple point"—i.e., a point at which the abundances of vacuum energy, matter, and radiation are equal during stasis. The location of this triple point in each panel is indicated by a star. Indeed, we observe that regardless of the form of X, the conditions under which the expressions for $\bar{\Omega}_\Lambda$, $\bar{\Omega}_M$, and $\bar{\Omega}_\gamma$ in Eqs. (6.58) and (6.59) coincide are

$$w_\triangle = \frac{1 + 3w}{9}, \qquad X = \frac{4 - 6w}{10 + 3w}. \qquad (8.4)$$

The latter condition can be solved for any given form of X in order to obtain the value of ξ at the triple point. This value of ξ increases monotonically with w, as can be seen by comparing the results shown in the different panels of Fig. 19, and can become as large as $\xi \sim \mathcal{O}(50)$ as w approaches zero for both the form of X in Eq. (6.52) and the form of X in Eq. (6.61).

IX. BEYOND STASIS

In addition to the stasis phenomenon discussed in previous sections, there are also *variants* of this

phenomenon in which only some—but not all—of the features associated with stasis are retained. Depending on which features are retained, we can obtain a variety of scenarios which may be exceedingly interesting in their own rights on both theoretical and phenomenological grounds. In general, it is critical to study such variants because there exist many real-world effects which may push our system beyond some of the assumptions we have made when constructing our above models of stasis. Understanding how robust the stasis phenomenon is when faced with such perturbations is therefore of profound importance for understanding the emergence of stasis within realistic models of physics.

A. Quasi-stasis

Stasis, of course, refers to an epoch in which our abundances remain absolutely fixed as functions of time. However, it is possible to obtain a *quasi-stasis* situation in which our abundances do experience a nonzero time dependence, but in which this time dependence is extremely suppressed. Within such scenarios, all of the leading power-law growth that would appear in the usual cosmology is still absent—just as in ordinary stasis— but a weak, quasilogarithmic time dependence remains. Depending on the rate of change associated with this residual time evolution, such quasi-stasis solutions may effectively serve as (and in fact be phenomenologically indistinguishable from) true stasis solutions over relevant cosmological timescales.

It is easy to see how such a quasi-stasis might arise. As we have seen, each of our pairwise stases is essentially unavoidable: for any choices of fundamental scaling exponents $(\alpha, \gamma, \delta, w)$ within the specified ranges, our system necessarily evolves into a stasis configuration, with the relevant stasis abundances remaining absolutely constant as functions of time. Indeed, only the values of these stasis abundances depend on our underlying parameter choices.

For *triple* stasis, by contrast, a new possibility opens up. Because an additional constraint equation arises—in particular, that in Eq. (6.36) which is needed in order to ensure that our two pumps are compatible with each other—not every choice of $(\alpha, \gamma, \delta, w)$ leads to a successful triple stasis. Indeed, as we have seen in Sec. VI, only those choices which place our system along Branch A in Fig. 9 lead to a full, triple stasis.

This observation implies that it is possible to choose values for $(\alpha, \gamma, \delta, w)$ [or equivalently for $(\gamma, \bar{\kappa})$] for which we do *not* obtain a triple stasis along Branch A. Amongst these, however, there are two classes of special cases that are worthy of note. Such special cases yield situations in which our abundances do not remain constant, but evolve exceedingly slowly. (Indeed, this slow evolution replaces the stasis phenomenon itself, and exists independently of any features related to the *approach* to stasis.) The first

class of such solutions consists of those lying along Branch B in Fig. 9. Indeed, we recall from Sec. VI that these solutions satisfy both of our scaling constraints in Eqs. (6.34) and (6.35), but simply fail to satisfy the second constraint in Eq. (6.48) that ensures that these solutions avoid a logarithmic instability. By contrast, the second class consists of solutions which do not lie along either Branch A or Branch B, but whose underlying parameters place it *relatively close to Branch A*. In such cases, our system does not satisfy our overall scaling relations. However, our system does satisfy these relations *approximately*, and therefore we once again expect a highly suppressed time evolution for the abundances. This situation might easily arise, for example, if our system originally lay along Branch A *at tree level*—and thus had $\gamma = 1$ at tree level— but then radiative corrections altered the scaling relations for our decay widths in such a way as to introduce a small correction for γ, pushing the effective value of this exponent slightly away from $\gamma = 1$.

This quasi-stasis phenomenon is illustrated in Fig. 20. In this figure, we plot the abundances Ω_Λ (blue), Ω_M (cyan), and Ω_γ (magenta) as functions of $\mathcal{N}$ for a true stasis (solid lines), a quasi-stasis with $\gamma = 0.95$ (dashed lines)
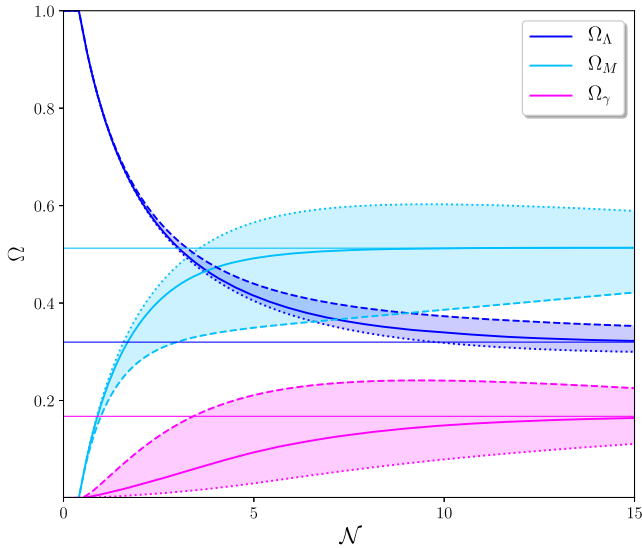

FIG. 20. Stasis versus quasi-stasis: the abundances Ω_Λ (blue), Ω_M (cyan), and Ω_γ (magenta), plotted as functions of $\mathcal{N}$ for a true stasis (solid lines) and two nearby quasi-stases, one with $\gamma = 0.95$ (dashed lines) and the other with $\gamma = 1.05$ (dotted lines). All curves are evaluated within the framework of an exponential decay for the matter-radiation transition, with $(\alpha, \delta, w) = (1, 2, -0.8)$ taken as benchmark values. Corresponding curves for all other quasi-stases with $0.95 < \gamma < 1.05$ and the same (α, δ, w) benchmark values lie within the shaded bands. In each case we see that variations in γ induce deviations from true stasis, but in each case the abundances Ω_i nevertheless remain relatively constrained to lie near these stasis values, with time evolutions that continue to be significantly suppressed. The closer γ is to unity, the more closely the Ω_i curves trace the true stasis values.

and a quasi-stasis with $\gamma = 1.05$ (dotted lines). Working within the framework of an exponential decay for the matter-radiation transition, we have taken $(\alpha, \gamma, \delta, w) = (1, 1, 2, -0.8)$ for the true stasis. Corresponding curves for all quasi-stases with $0.95 < \gamma < 1.05$ for the same choices of these other parameters lie entirely within the shaded bands delimited by the dashed and dotted curves. Indeed, the closer γ is to unity, the more closely the Ω_i curves track those obtained for a true stasis. These results illustrate that stasis is robust against departures from the $\gamma = 1$ criterion, and that the universe indeed experiences a period of approximate stasis even when γ is not exactly unity.

B. Oscillatory stasis and braiding

In our discussions of stasis, we have implicitly assumed that Δm—the characteristic mass spacing between the states in our ϕ_ℓ towers—is sufficiently small that the continuum limit we have employed, e.g., in Eqs. (2.17) and (3.8) remains a valid approximation across the entire tower. However, it is also interesting to consider what happens when Δm is larger and discretization effects become important. For concreteness, in what follows we shall focus on the case of a matter/radiation stasis, though we emphasize that similar phenomena arise in the other realizations of stasis that we have discussed in this paper as well.

As a general rule of thumb, discretization effects become important in a matter/radiation stasis of the sort discussed in Sec. II when the timescale associate with the depletion of the abundance of a particular state ϕ_n within the tower— i.e., its lifetime τ_n—is short in comparison with the characteristic time interval $\tau_{n-1} - \tau_n$ between the lifetimes of successively decaying states within the tower at time $t = \tau_n$. This characteristic time interval between the lifetimes of successively decaying states in the tower is essentially the reciprocal of the density of states $n_\tau(\tau_n)$ per unit lifetime, evaluated at $\tau = \tau_n$. In general, this density of states is given by

$$n_\tau(\tau) = \frac{1}{\gamma\delta}\left(\frac{m_0}{\Delta m}\right)^{1/\delta}(\Gamma_0\tau)^{-1/\gamma}\left[(\Gamma_0\tau)^{-1/\gamma} - 1\right]^{1/\delta-1}\frac{1}{\tau}, \quad (9.1)$$

which reduces to the approximate result in Eq. (6.31) in the regime in which $\tau \ll \tau_0$. Thus, we expect discretization effects to become important when $n_\tau^{-1}(\tau) \gtrsim \tau$, or in other words, when

$$\gamma\delta\left(\frac{\Delta m}{m_0}\right)^{1/\delta}(\Gamma_0\tau)^{1/\gamma}\left[(\Gamma_0\tau)^{-1/\gamma} - 1\right]^{1-1/\delta} \gtrsim 1. \quad (9.2)$$

In general, the quantity on the left side of Eq. (9.2) depends nontrivially on τ. Thus, depending on the values of δ, γ, Γ_0, and the ratio $\Delta m/m_0$, it is possible that discretization effects will be evident only within certain ranges of τ. Indeed, for sufficiently small $\tau \ll \Gamma_0^{-1}$, the condition in Eq. (9.2) reduces to

$$\gamma\delta\left(\frac{\Delta m}{m_0}\right)^{1/\delta}(\Gamma_0\tau)^{1/\gamma\delta} \gtrsim 1. \qquad (9.3)$$

This implies that discretization effects typically become increasingly important at late times. More specifically, they become important at timescales $\tau \gtrsim \tau_{\text{disc}}$, where we have defined

$$\tau_{\text{disc}} \equiv \Gamma_0^{-1}(\gamma\delta)^{-\gamma\delta}\left(\frac{\Delta m}{m_0}\right)^{-\gamma}. \qquad (9.4)$$

Since we are assuming that $\gamma > 0$, we observe that τ_{disc} decreases as Δm increases. Thus, as the characteristic scale of the mass splittings between the tower states increases, discretization effects become important at earlier and earlier times. Indeed, in situations in which $\tau_{N-1} \gtrsim \tau_{\text{disc}}$, these effects are important throughout the entire time interval during which which the tower states are decaying. Conversely, in situations in which $\tau_0 \ll \tau_{\text{disc}}$, the effects are nominally negligible throughout this entire time interval and the universe effectively remains in a true stasis. We may therefore determine a rough threshold for Δm above which above which discretization effects become important prior to the end of stasis by setting $\tau_{\text{disc}} \to \tau_0$ in Eq. (9.4). This threshold is

$$(\Delta m)_* \equiv (\gamma\delta)^{-\delta}m_0. \qquad (9.5)$$

In reality, however, we emphasize that discretization effects *always* come into play at times $t \sim \tau_0$, when the longest-lived states in the tower are decaying and the second term in the square brackets in Eq. (9.2) can no longer be neglected. Indeed, such discretization effects are evident during the last few e-folds of the matter/radiation stasis illustrated in the left panel of Fig. 1.

In Fig. 21, we illustrate the impact that these discretization effects have on the evolution of the abundances Ω_M and Ω_γ, as well as on the expansion rate. In the left panel, we plot these abundances (solid curves) as functions of time for the parameter choices $\alpha \approx 1.13$, $\delta = 4$, $\gamma = 9$, and $\bar\Omega_M = 3/4$. The corresponding constant abundances $\bar\Omega_M$ and $\bar\Omega_\gamma$ which would be obtained for a true stasis with the same values of α, δ, and γ are indicated by the dotted horizontal lines. In the middle panel, we show the corresponding abundance curves for the parameter choices $\alpha \approx 2.32$, $\delta = 4$, $\gamma = 9$, and $\bar\Omega_M = 1/2$.

We see from the left and middle panels of Fig. 21 that the net impact of discretization effects on the abundances of our cosmological components is to give rise to an quasi-oscillatory behavior wherein Ω_M and Ω_γ both vary around fixed central values—values which correspond to the respective stasis values $\bar\Omega_M$ and $\bar\Omega_\gamma$. We shall refer to the variant of stasis wherein this phenomenon is manifest as "oscillatory" stasis in what follows. The results shown in the left panel Fig. 21 are representative of the more general case in which these central values are different. By contrast, the results shown in the middle panel exemplify the special case in which $\bar\Omega_M = \bar\Omega_\gamma = 1/2$, with the abundance curves exhibiting a "braiding" phenomenon in which they mutually oscillate around the same central value. The results shown in both panels also illustrate that the effective period $T_{\text{osc}}(t)$ of the "oscillations" in an oscillatory stasis is in general not constant. Indeed, at any given time t, this effective period is simply the time interval $T_{\text{osc}}(t) \sim n_\tau^{-1}(t)$ between the decays of successive tower states, and $n_\tau(t)$ is in general time dependent.
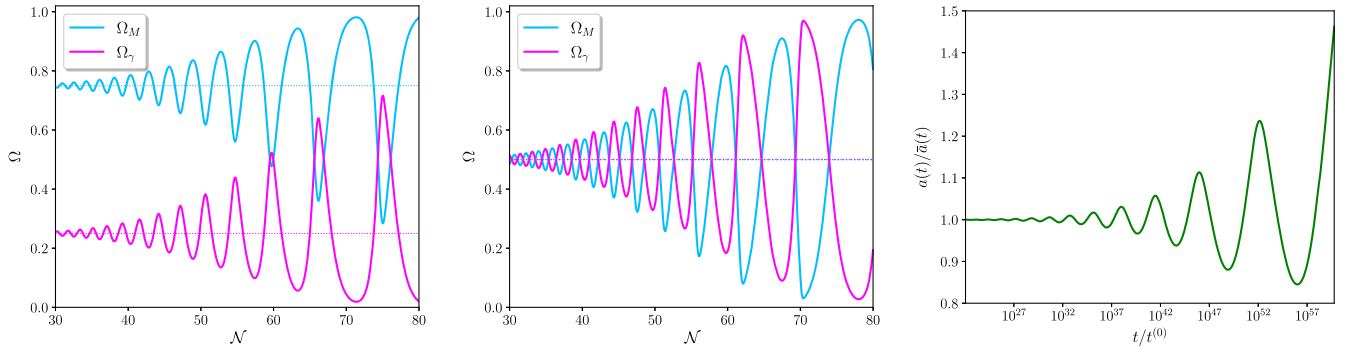

FIG. 21.   Pairwise oscillatory stasis involving matter and radiation. In the left panel, we plot Ω_M (solid cyan curve) and Ω_γ (solid magenta curve) as functions of time for the parameter choices $\alpha \approx 1.13$, $\delta = 4$, $\gamma = 9$, which imply $\bar\Omega_M = 3/4$ and $\bar\Omega_\gamma = 1/4$. The dotted horizontal cyan and magenta lines respectively indicate the corresponding constant abundances $\bar\Omega_M$ and $\bar\Omega_\gamma$ which would be obtained for a true stasis with the same values of α, δ, and γ. In the middle panel we show the abundance curves obtained for the parameter choices $\alpha \approx 2.32$, $\delta = 4$, $\gamma = 9$, which imply $\bar\Omega_M = \bar\Omega_\gamma = 1/2$. These parameter choices exemplify the special case in which $\bar\Omega_M = \bar\Omega_\gamma$ and in which the abundances Ω_M and Ω_γ exhibit a "braiding" phenomenon, mutually oscillating around the same central value. In the right panel, we plot as a function of time the ratio of the scale factor $a(t)$ to the corresponding value $\bar a(t) \sim t^{\bar\kappa/3}$ that the scale factor would have in a true stasis for the same parameter choices as in the middle panel. We emphasize that similar oscillatory phenomena can also arise for the other realizations of stasis that we have considered in this paper.

The variation of the abundances during a period of oscillatory stasis implies that κ is also not constant during such a period; rather, κ experiences a quasi-periodic oscillation as the universe expands. This behavior is illustrated in the right panel of Fig. 21, where we plot the ratio of the scale factor $a(t)$ during a period of oscillatory stasis to the corresponding value $\bar{a}(t) \sim t^{\bar{\kappa}/3}$ which would be obtained during a period of true stasis for the same parameter choices as in the middle panel. This behavior implies that as the universe expands, its *average* rate of growth remains consistent with a fixed time-and-stasis-averaged value of $\langle w \rangle$. However, the universe "reverberates" as it expands, with pulsing periods of faster and slower expansion.

The results shown in Fig. 21 also indicate that oscillatory stasis, when it arises, can potentially persist for a significant number of *e*-folds of cosmic expansion. In situations in which $\Delta m \gtrsim (\Delta m)_*$, the expression for $\mathcal{N}_s$ in Eq. (2.24) represents the total number of *e*-folds of expansion associated with both true stasis *and* oscillatory stasis. For $\tau_{N-1} \gtrsim \tau_{\rm disc}$, as discussed above, true stasis is never achieved and the number of *e*-folds $\mathcal{N}_{\rm osc}$ of oscillatory stasis is given by Eq. (2.24) as well. By contrast, for $\tau_{N-1} \lesssim \tau_{\rm disc} \lesssim \tau_0$, oscillatory stasis begins roughly when $t \sim \tau_{\rm disc}$ and ends when the last state in the tower decays. Thus, we have

$$\mathcal{N}_{\rm osc} \approx \log\left(\frac{a(\tau_0)}{a(\tau_{\rm disc})}\right). \tag{9.6}$$

Approximating $a(\tau_0)$ and $a(\tau_{\rm disc})$ with their corresponding time-averaged values $\bar{a} \sim \tau_0^{\bar{\kappa}/3}$ and $\bar{a} \sim \tau_{\rm disc}^{\bar{\kappa}/3}$, and using Eq. (2.9) in order to express $\bar{\kappa}$ in terms of the constant matter abundance $\bar{\Omega}_M$ that would be obtained for a true stasis with the same values of α, γ, and δ, we find that

$$\mathcal{N}_{\rm osc} \approx \frac{2\gamma}{4 - \bar{\Omega}_M} \log\left(\frac{\Delta m}{(\Delta m)_*}\right). \tag{9.7}$$

Once again, we emphasize that while this approximate expression for $\mathcal{N}_{\rm osc}$ decreases to zero continuously as $\Delta m \to (\Delta m)_*$, discretization effects in fact always come into play at times $t \sim \tau_0$.

The quasi-oscillatory behavior we have described here may have observable consequences. For example, this behavior could potentially affect the growth of both scalar and tensor perturbations in the early universe in distinctive ways. One particularly interesting possibility is that resonance effects could arise as a consequence of these oscillations. While $T_{\rm osc}(t)$ is in general time dependent during oscillatory stasis, an alignment of this timescale with other relevant timescales even during a single cycle of "oscillation" could potentially have consequential effects. Indeed, such single-cycle resonances are know to have a significant impact on cosmological dynamics in other

contexts (see, e.g., Ref. [24]), and it is certainly conceivable that they could have observable consequences in the context of oscillatory stasis as well. We leave the investigation of such possibilities for future work.

C. Stasis unrealized

Finally, there is another unique behavior which is potentially associated with stasis but which does not result in a stasis configuration. Depending on the underlying model parameters, it may happen that our system begins heading *toward* a stasis configuration as the result of the attractor behavior associated with stasis, but never fully reaches this destination because our level-by-level transitions reach the bottom of the tower before the stasis is fully realized. This can then result in abundances whose time evolution begins to slow over many *e*-folds (as appropriate for the approach to stasis), but then grow again as another poststasis dynamics comes into play. This phenomenon may also have important phenomenological implications, and represents one of the few ways in which a pairwise stasis may ultimately be avoided.

X. DISCUSSION AND CONCLUSIONS

Cosmic stasis—a phenomenon in which the abundances of multiple cosmological energy components remain effectively constant across extended cosmological eras despite cosmological expansion—arises naturally in many extensions of the Standard Model. In Ref. [1], for example, it was shown that a pairwise stasis involving matter and radiation can arise from the decays of a tower of unstable particles with a broad spectrum of lifetimes and cosmological abundances. In this paper, we have extended this prior analysis and demonstrated that cosmic stasis is a more general phenomenon which can also arise in the presence of other cosmological energy components with other equations of state. These include, as we have seen, cosmological systems involving vacuum energy. In such cases, the transition from overdamped to underdamped oscillation of a homogeneous scalar field provides a natural mechanism for the transfer of energy from vacuum energy to matter, thereby allowing a tower of such scalar fields with a broad spectrum of masses to give rise to a pairwise stasis involving vacuum energy and matter. We have also shown that a direct transfer of energy density from vacuum energy to radiation can, under certain conditions, give rise to a pairwise stasis involving vacuum energy and radiation. Moreover, we have shown that it is even possible for a *triple* stasis to arise in which the abundances of vacuum energy, matter, and radiation all simultaneously remain constant despite cosmic expansion. Indeed, this last result is highly nontrivial and does not emerge simply as the result of the existence of the previous pairwise stases. We further demonstrated that all of these types of stasis are dynamical attractors within their corresponding cosmological systems.

Thus, as long as these systems satisfy the basic conditions under which stasis can develop, all of these systems will ultimately flow toward the stasis state, irrespective of their initial conditions.

As indicated above, one of the keys to our analysis in this paper has been the use of the overdamping/underdamping transition as a means of transferring energy density from vacuum energy—or more generally from a cosmological energy component with an effectively constant equation-of-state parameter $-1 < w < 0$—to matter. This in and of itself represents a significant broadening of the scope of cosmological scenarios which give rise to stasis to include those involving higher-dimensional axion or axionlike fields [25,26] as well as scenarios involving realizations of the string axiverse [27].

Of course, there are a number of additional subtleties involved in modeling the overdamping/underdamping transitions within the context of a concrete model. As discussed in Sec. III, the equation-of-state parameter w_i for a given field ϕ_i exhibits a transition from the value $w_i \approx -1$ within the overdamped regime to the asymptotic time-averaged value $w_i \approx 0$ within the underdamped regime. However, this transition is not an abrupt one. Moreover, the manner in which each w_i evolves as it undergoes this transition—and even the timescale over which these transitions occur—depend sensitively on the properties of the scalar potential. Nevertheless, it can be shown [28] that stasis indeed arises in such contexts, even when all of these complications are taken into account and even for quite simple, well-motivated potentials.

It is conceivable that a stasis epoch could naturally arise in other BSM scenarios as well. These might include, for example, cosmologies involving a kination component with $w = 1$, other cosmological energy components with $w > 1/3$, or even a cosmological energy component with a time-varying equation-of-state parameter $w(t)$. Moreover, it is also conceivable that stasis could arise in cosmologies involving spatial curvature ($w = -1/3$), cosmic strings ($w = -1/3$), or domain walls ($w = -2/3$). Such cosmologies can also involve other energy components with effectively constant equation-of-state parameters within the range $-1 < w < 0$, such as we have considered in this paper, but which transfer their energy density to other cosmological components via different mechanisms. In order for this to occur, our analysis indicates that the pump terms associated with these mechanisms would need to exhibit an appropriate $P \sim 1/t$ scaling behavior during stasis. In some cases this may be nontrivial, especially if we further demand that such pump terms emerge naturally within the context of BSM physics.

Given the possibility that cosmological energy components beyond vacuum energy, matter, and radiation could conceivably have constituted a significant fraction of the total energy density of the universe at early times, another obvious extension of our analysis would be to investigate whether and under what conditions a stasis epoch involving *more* than three components might arise. What additional conditions would then have to be satisfied? In order to answer this question, history can be our guide. For each of the pairwise-stasis scenarios that we examined in Secs. II, III, and IV, the system of equations that we obtained for our stasis abundances was overconstrained. However, since some of these equations happened to be redundant, we were nevertheless able to obtain self-consistent solutions for these abundances. By contrast, for the triple-stasis scenario that we examined in Sec. VI, no such redundancies arose within the corresponding system of equations. We were therefore able to obtain a series of constraints that led to unique solutions for our stasis abundances.

Given this pattern, it is natural to expect that a *quadruple* stasis would lead to an *underconstrained* system of constraints. We would then expect to find not a unique set of stasis abundances but rather a *line* of possible solutions. In such cases, the particular stasis abundances towards which the system evolves would presumably depend on initial conditions. We would likewise expect this pattern of increasingly underconstrained solutions for the stasis abundances to continue as we introduce additional energy components into the mix. Of course, these observations are predicated on the manner in which additional pumps for energy transfer are introduced as the number of additional energy components is increased.

In this connection, we note [in complete analogy with the discussion below Eq. (4.16)] that another way of introducing a fourth energy component would be to establish a triple stasis between three of the components and then ensure that the fourth component functions as a mere *spectator*—i.e., that it have an equation-of-state parameter which exactly matches the stasis average $\langle w \rangle$ determined by other three, and that it experience no energy transfers with the other components and thereby remain inert. As a result, the dynamics of the underlying triple stasis would not be disturbed, and we would once again expect to obtain a line of potential solutions for the four stasis abundances in which the abundance of the fourth component is arbitrary and the abundances of the other three decrease to compensate but remain in the same ratios as they had prior to the introduction of the fourth component.

From a model-building perspective, the realizations of stasis that we have discussed in this paper all involve towers comprising large numbers of individual states. However, as we have repeatedly emphasized, such towers arise naturally in many extensions of the SM. For example, scenarios involving additional, compactified spacetime dimensions naturally give rise to towers of Kaluza-Klein (KK) resonances. Other examples of towers of states which emerge naturally in BSM scenarios include the towers of closed-string resonances which appear in Type I string theories and the towers of hadronlike resonances which appear in theories involving confining hidden-sector gauge groups.

Moreover, black holes effectively transfer their energy densities from matter to radiation as they evaporate. As a result, a population of primordial black holes (PBHs) with an extended mass spectrum can also thereby give rise to an extended period during which the abundances of matter and radiation remain effectively constant [2,3]. Such PBHs can thereby furnish an additional concrete model of matter/radiation stasis [3]. Indeed, this realization of stasis is rather exotic when compared with those we have studied in this paper; since heavier black holes evaporate more slowly than lighter ones, the transitions from matter to radiation proceed *upward* through the tower rather than downward.

Within the context of such BSM scenarios, there is often a straightforward relationship between the properties of the stasis epoch and the parameters of the underlying particle-physics model which gives rise to it. For example, in realizations of stasis in which the ϕ_ℓ fields are the KK resonances associated with an extra spacetime dimension of radius R, the masses m_ℓ of the KK states span the range from R^{-1} to some fundamental cutoff scale μ such as the string or GUT scale. In such realizations of stasis, the range of lifetimes for the ϕ_ℓ fields—and therefore the duration of the stasis epoch—depends crucially on the hierarchy between R^{-1} and μ. As a result, in situations in which the stasis state has $\langle w \rangle < -1/3$ (causing the universe to undergo accelerated expansion during stasis), the size of the comoving horizon today would in a very real sense be the manifestation of this hierarchy of energy scales. Indeed, within such scenarios, the large number of e-folds of expansion experienced by our universe across its history might actually be the manifestation of a hierarchy in the size of an otherwise unseen compactified dimension!

In all of our stasis realizations involving the decays of the ϕ_ℓ states, the resulting cosmological dynamics is essentially determined by the corresponding masses m_ℓ and decay widths Γ_ℓ. Moreover, we have assumed that for all ϕ_ℓ these widths are dominated by decays to effectively massless particles outside the tower which behave like radiation throughout the stasis epoch. However, within certain realizations of such stases there may be *multiple* states $\phi_\ell^{(j)}$ at each level ℓ—states which share the same mass m_ℓ and decay width Γ_ℓ. At tree level, the resulting cosmological dynamics will be largely independent of the manner in which each energy density ρ_ℓ for each ℓ might be partitioned among such degenerate states. Indeed, at tree level such a collection of degenerate states essentially functions as a single state whose total energy density ρ_ℓ is the sum of the contributions from its constituents. At loop level, however, the cosmological dynamics is in general sensitive to such degeneracies. For example, the renormalization of the masses m_ℓ and couplings which give rise to each Γ_ℓ would depend on these degeneracies since all of these states can run independently within the loops. Thus the scaling of the decay widths would ultimately depend on such degeneracies.

Moreover, in situations in which the $\phi_\ell^{(j)}$ states decay to the same species of radiation particle at tree level, loop-level diagrams will generically give rise to decay processes in which heavier ϕ_ℓ states decay into lighter $\phi_{\ell'}$ states with $m_{\ell'} < m_\ell$. For decay processes in which the resulting daughter particles are significantly lighter than the parents, these daughters will be produced with significant boosts as seen within the cosmological background frame. These boosts will therefore result in nontrivial phase-space distributions for the lighter $\phi_{\ell'}$ particles. The presence of potentially significant velocities for these states can also increase their corresponding equation-of-state parameters from $w_\ell = 0$ (consistent with our original assumption of cold matter) to anywhere within the range $0 < w_\ell < 1/3$. These phase-space distributions will also thereafter evolve nontrivially during the stasis epoch due to cosmological redshifting effects [29]. Thus, if loop-level effects are significant, they could in principle have a non-negligible effect on the cosmological dynamics involved in establishing and sustaining stasis.

Issues regarding the degeneracies of states at each mass level may be particularly relevant for string-theoretic realizations of stasis. In general, perturbative string-theory spectra contain many kinds of states, including not only KK states (and winding states if the string is closed) but also string oscillator states. All of these states come in infinite towers. For example, the infinite towers of oscillator states have masses which scale as $\alpha' m_\ell^2 \sim \ell$ where α' is the Regge slope, or equivalently $\sqrt{\alpha'} m_\ell \sim \ell^\delta$ with $\delta = 1/2$. However, at each level ℓ the number n_ℓ of oscillator states grows *exponentially*: $n_\ell \sim e^{\sqrt{\ell}} \sim e^{\sqrt{\alpha'} m_\ell}$. This can have a number of interesting consequences. For example, in string theory these states will generally have different spins (even though they share the same mass); they will therefore couple differently to lighter states and potentially have different decay widths. Second, this growth in the number of states at each mass level ultimately leads to the famous Hagedorn phenomenon [30] wherein various thermodynamic quantities experience divergences at a critical temperature T_c—a temperature beyond which the theory is believed to transition to a different phase with different underlying degrees of freedom. It may therefore be these new degrees of freedom that are relevant for understanding the dynamical properties of the early universe, at least for $T > T_c$. But even when $T < T_c$, there remains the issue of how the total abundances Ω_ℓ might scale as functions of ℓ across the tower, given that the densities of oscillator states are growing exponentially. This issue was studied in some detail for one cosmological production mechanism in Ref. [7], but many other production mechanisms are possible. Indeed, like all predictions of abundances Ω_ℓ across our tower, this is ultimately a model-dependent question which depends on the particular production mechanism envisaged. We also emphasize that in general, string oscillator states have mass splittings Δm on the order

of the string scale. Such states can therefore potentially support a stasis at intermediate energy scales below the Planck scale only within the context of low-scale string theories, with $M_{\text{string}} \equiv 1/\sqrt{\alpha'} \ll M_{\text{Planck}}$.

Of course, even if the string scale is situated near the Planck scale (implying that the excited oscillator states are therefore near the Planck scale as well), large-volume compactifications can lead to KK towers populating intermediate scales. Such KK states can therefore support a stasis at intermediate scales, even though they emerge in a string context. Indeed, within such string theories, these KK states will likely be the only part of the perturbative string spectrum whose towers are lighter than the string scale. Moreover, their degeneracies will not experience exponential growth.

It is not only the abundances and decay widths of our states that might be affected by model-specific concerns; the same may also be true of their *masses*. For example, throughout this paper we have assumed that the fields ϕ_ℓ have masses which scale according to Eq. (2.13). However, interactions of these fields with other fields in the theory may lead to radiative corrections for these masses. For KK towers stemming from a single large flat extra dimension, such radiative corrections were studied in Refs. [31,32]. In some cases, it was found [32] that the overall scaling structure of these KK masses is actually preserved under such one-loop radiative corrections—indeed, in these cases the radiative corrections can simply be bundled into "renormalizations" of the overall parameters m_0 and Δm without changing the form of Eq. (2.13). By contrast, in other cases, the one-loop radiative corrections were found to distort these scaling relations altogether. In either case, however, one generally finds that these radiative corrections are exceedingly small.

Moreover, in particle-physics realizations of stasis in which the ϕ_ℓ are coherently oscillating scalar fields, effects of this sort can affect not only the masses of these fields but also other aspects of the scalar potential [33]. Indeed, at points in field space where the ϕ_ℓ fields are significantly displaced from their vacua, loop corrections can have significant impacts on the shape of the potential. For example, these impacts have been studied within the context of large-field inflation models, where the resulting modification of the potential can in turn lead to modified predictions for inflationary observables [34–40]. One intriguing possibility that can arise in certain situations as a result of such corrections is that coherent oscillations of the ϕ_ℓ fields can in fact behave at early times like matter or radiation—or potentially even like a perfect fluid with $w > 1/3$. Thus, in realizations of stasis involving fields of this sort, there might exist mechanisms which transfer energy density from matter or radiation to vacuum energy, rather than the other way around. We leave the investigation of such possibilities for future work.

The existence of an early period of stasis throughout the cosmological timeline can have a number of phenomenological consequences. Indeed, the modification of the expansion history alone relative to that of the standard cosmology can affect the evolution of density perturbations, the spectrum of gravitational waves, and predictions for cosmic-microwave-background (CMB) observables. Moreover, such a modification can also have an impact on a variety of out-of-equilibrium processes, including those which play a crucial role in the production of dark matter or the generation of a baryon asymmetry in many BSM scenarios. Indeed, many of these possibilities were discussed in detail in Ref. [1] within the context of cosmologies involving an epoch of pairwise matter/radiation stasis. However, since these effects arise generically in any cosmological scenario involving a nonstandard expansion history, they also pertain to cosmologies involving the alternative types of stasis that we have examined in this paper.

One of the main motivations for this work has been to demonstrate that an epoch of cosmic stasis can in principle arise in universes containing nontrivial abundances of vacuum energy. This prompts the question as to whether such a stasis epoch could potentially give rise to a period of cosmic inflation, similar to those discussed in Refs. [41–45], with a duration sufficient to address the horizon and flatness problems. In typical inflationary scenarios, the extraordinary degree of large-scale homogeneity and isotropy that we observe in our universe is attributed to an epoch of rapid cosmological expansion wherein the energy density is dominated by a perfect fluid with equation-of-state parameter $w < -1/3$. However, such a period of rapid expansion could also be the result of an epoch of cosmic stasis in which a tower of states which behave like vacuum energy coexists with matter and/or radiation, provided that $\langle w \rangle < -1/3$. Moreover, since such a stasis epoch concludes when the last of these vacuum-energy states transfers its energy to matter or radiation, a graceful exit from inflation occurs naturally in this context.

In these respects, inflationary stasis scenarios of this sort have a great deal in common with so-called warm-inflation scenarios [46–48] in which radiation is produced throughout the inflationary epoch due to dissipative effects and in which thermal fluctuations, rather than quantum fluctuations, represent the dominant contribution to primordial density perturbations [49,50]. Indeed, during the slow-roll phase of warm inflation—as in a vacuum-energy/radiation stasis—Ω_γ remains approximately constant due to a transfer of energy density from vacuum energy to radiation which counteracts the effect of cosmic expansion [21,22]. However, there are also fundamental differences between these scenarios. In warm inflation, the vacuum-energy component vastly dominates the energy density of the universe during the slow-roll phase, and H therefore remains approximately constant. While vacuum energy is continually being transferred to radiation during this phase, it is not transferred at a rate that is sufficiently large in order to have a significant impact on Ω_Λ. Thus, the backreaction

of ρ_γ on H plays no essential role and can be neglected. By contrast, during an epoch of vacuum-energy/radiation stasis, Ω_Λ and Ω_γ during inflation can *both* be non-negligible—and indeed even $\mathcal{O}(1)$—and the backreaction of ρ_γ on H is incorporated fully, with H inversely proportional to t.

Of course, whether a given stasis scenario of this sort constitutes a viable model of inflation ultimately depends on whether the spectrum of scalar and tensor perturbations that it yields are consistent with observation (for a recent review, see, e.g., Refs. [51,52])—and in particular with the properties of the CMB. The evolution of these perturbation spectra during an epoch of inflationary stasis would be highly nontrivial, with significant roles potentially played not only by the quantum fluctuations of each individual ϕ_ℓ field which contributes to Ω_Λ, but also by thermal fluctuations within the radiation bath. Moreover, the collective behavior of the ϕ_ℓ fields and the value of $\langle w \rangle$ to which they dynamically give rise during stasis would affect the manner in which both scalar and tensor perturbations evolve. Investigating the perturbation spectra which can arise in inflationary stasis scenarios—spectra which may exhibit not only distinctive features at high frequencies but also characteristic patterns of non-Gaussianities—is the subject of ongoing work.

Regardless of the initial spectrum of perturbations that is generated during inflation, the presence of a stasis epoch within the cosmological timeline can alter the subsequent evolution of these perturbations. The time at which perturbations associated with a particular wave number k enter the horizon depends on the expansion history. Moreover, once the perturbations associated with a given k enter the horizon, the manner in which $H(t)$ scales with t can have a significant impact on their subsequent evolution. For example, perturbations in the density of matter are known to grow much more rapidly during a period of early matter domination than they do during a radiation-dominated epoch [53–55]. This enhanced growth can have important consequences for structure on small scales and can lead to the formation of black holes [55,56] or ultracompact mini halos [53,57]. The growth of such perturbations can also be either enhanced or suppressed during an epoch wherein the universe is dominated by a cosmological component with a constant equation-of-state parameter, depending on the value that that equation-of-state parameter takes [58]. The spectrum of density perturbations can therefore be substantially modified in cosmologies which include a stasis epoch. The effects of cosmic stasis on the growth of such perturbations and the resulting implications for small-scale structure are currently under study [59].

The modification of the cosmological history in scenarios involving a stasis epoch in general affects not only the evolution of density perturbations, but also the evolution of

the primordial contribution to the stochastic gravitational-wave background. These effects were investigated in detail in Ref. [3] for a particular realization of matter/radiation stasis involving the evaporation of a population of primordial black holes with an extended mass spectrum, as described above. However, since the effects on the stochastic gravitational-wave background during such a stasis epoch stem ultimately from the modification of the expansion history, these effects are generic and arise in any modified cosmology which involves such an epoch. The net effect on the gravitational-wave background in any particular realization of stasis depends on both the value of $\langle w \rangle$ during the stasis epoch itself and the value of the equation-of-state parameter during any other epochs which are included in the cosmological scenario in question—such as, for example, an epoch of early matter domination which might immediately precede an epoch of matter/radiation stasis.

We see, then, that cosmological stasis appears to be a robust and rather ubiquitous phenomenon within a variety of BSM-motivated cosmological scenarios. In this paper, we have concentrated on the internal theoretical mechanics of the stasis phenomenon itself. However, given these results, it becomes even more urgent to further flesh out the detailed particle-physics models which give rise to stasis and to perform quantitative analyses of the phenomenological signatures to which these models lead. In this Conclusions section we have sketched various ideas along both of these directions. Indeed, as we have indicated, many of these ideas are actively being pursued and will be discussed in future publications. However, we anticipate that many additional directions beyond those discussed here will also provide fertile terrain for future research.

[1] K. R. Dienes, L. Heurtier, F. Huang, D. Kim, T. M. P. Tait, and B. Thomas, Phys. Rev. D **105**, 023530 (2022).

[2] J. D. Barrow, E. J. Copeland, and A. R. Liddle, Mon. Not. R. Astron. Soc. **253**, 675 (1991).

[3] K. R. Dienes, L. Heurtier, F. Huang, D. Kim, T. M. P. Tait, and B. Thomas, arXiv:2212.01369.

[4] K. R. Dienes, L. Heurtier, F. Huang, T. M. P. Tait, and B. Thomas (to be published).

[5] K. R. Dienes and B. Thomas, Phys. Rev. D **85**, 083523 (2012).

[6] K. R. Dienes and B. Thomas, Phys. Rev. D **85**, 083524 (2012).

[7] K. R. Dienes, F. Huang, S. Su, and B. Thomas, Phys. Rev. D **95**, 043526 (2017).

[8] K. R. Dienes, J. Fennick, J. Kumar, and B. Thomas, Phys. Rev. D **97**, 063522 (2018).

[9] A. Albrecht, P. J. Steinhardt, M. S. Turner, and F. Wilczek, Phys. Rev. Lett. **48**, 1437 (1982).

[10] L. F. Abbott, E. Farhi, and M. B. Wise, Phys. Lett. **117B**, 29 (1982).

[11] L. Kofman, A. D. Linde, and A. A. Starobinsky, Phys. Rev. D **56**, 3258 (1997).

[12] M. L. Bellac, *Thermal Field Theory*, Cambridge Monographs on Mathematical Physics (Cambridge University Press, Cambridge, England, 2011).

[13] E. A. Calzetta and B.-L. B. Hu, *Nonequilibrium Quantum Field Theory* (Oxford University Press, New York, 2009).

[14] J. Berges, arXiv:1503.02907.

[15] D. Boyanovsky, R. Holman, and S. P. Kumar, Phys. Rev. D **56**, 1958 (1997).

[16] D. Boyanovsky and H. J. de Vega, Phys. Rev. D **70**, 063508 (2004).

[17] J. Bros, H. Epstein, and U. Moschella, Ann. Henri Poincare **11**, 611 (2010).

[18] D. Boyanovsky and R. Holman, J. High Energy Phys. 05 (2011) 047.

[19] A. Berera, I. G. Moss, and R. O. Ramos, Rep. Prog. Phys. **72**, 026901 (2009).

[20] M. Bastero-Gil and A. Berera, Int. J. Mod. Phys. A **24**, 2207 (2009).

[21] V. Kamali, M. Motaharfar, and R. O. Ramos, Universe **9**, 124 (2023).

[22] A. Berera, Universe **9**, 272 (2023).

[23] M. S. Turner, Phys. Rev. D **28**, 1243 (1983).

[24] K. R. Dienes, J. Kost, and B. Thomas, Phys. Rev. D **100**, 083516 (2019).

[25] K. R. Dienes, E. Dudas, and T. Gherghetta, Phys. Rev. D **62**, 105023 (2000).

[26] K. R. Dienes and B. Thomas, Phys. Rev. D **86**, 055013 (2012).

[27] A. Arvanitaki, S. Dimopoulos, S. Dubovsky, N. Kaloper, and J. March-Russell, Phys. Rev. D **81**, 123530 (2010).

[28] K. R. Dienes, L. Heurtier, F. Huang, T. M. P. Tait, and B. Thomas (to be published).

[29] K. R. Dienes, F. Huang, J. Kost, S. Su, and B. Thomas, Phys. Rev. D **101**, 123511 (2020).

[30] R. Hagedorn, Nuovo Cimento Suppl. **3**, 147 (1965).

[31] H.-C. Cheng, K. T. Matchev, and M. Schmaltz, Phys. Rev. D **66**, 036005 (2002).

[32] S. Bauman and K. R. Dienes, Phys. Rev. D **85**, 125011 (2012).

[33] S. Coleman and E. Weinberg, Phys. Rev. D **7**, 1888 (1973).

[34] L. Covi, D. H. Lyth, and L. Roszkowski, Phys. Rev. D **60**, 023509 (1999).

[35] L. Covi and D. H. Lyth, Phys. Rev. D **59**, 063515 (1999).

[36] M. S. Sloth, Nucl. Phys. **B748**, 149 (2006).

[37] M. S. Sloth, Nucl. Phys. **B775**, 78 (2007).

[38] V. N. Senoguz and Q. Shafi, Phys. Lett. B **668**, 6 (2008).

[39] N. Bostan and V. N. Şenoğuz, J. Cosmol. Astropart. Phys. 10 (2019) 028.

[40] L. Heurtier and F. Huang, Phys. Rev. D **100**, 043507 (2019).

[41] A. A. Starobinsky, Phys. Lett. **91B**, 99 (1980).

[42] A. H. Guth, Phys. Rev. D **23**, 347 (1981).

[43] A. D. Linde, Phys. Lett. **108B**, 389 (1982).

[44] A. D. Linde, Phys. Lett. **129B**, 177 (1983).

[45] V. F. Mukhanov and G. V. Chibisov, JETP Lett. **33**, 532 (1981).

[46] A. Berera and L.-Z. Fang, Phys. Rev. Lett. **74**, 1912 (1995).

[47] A. Berera, Phys. Rev. Lett. **75**, 3218 (1995).

[48] A. Berera, M. Gleiser, and R. O. Ramos, Phys. Rev. Lett. **83**, 264 (1999).

[49] A. N. Taylor and A. Berera, Phys. Rev. D **62**, 083517 (2000).

[50] L. M. H. Hall, I. G. Moss, and A. Berera, Phys. Rev. D **69**, 083525 (2004).

[51] A. Achúcarro et al., arXiv:2203.08128.

[52] A. S. Chou et al., in Snowmass 2021 (2022), arXiv:2211.09978.

[53] A. L. Erickcek and K. Sigurdson, Phys. Rev. D **84**, 083503 (2011).

[54] J. Fan, O. Özsoy, and S. Watson, Phys. Rev. D **90**, 043536 (2014).

[55] J. Georg, G. Şengör, and S. Watson, Phys. Rev. D **93**, 123523 (2016).

[56] A. M. Green, A. R. Liddle, and A. Riotto, Phys. Rev. D **56**, 7559 (1997).

[57] G. Barenboim and J. Rasero, J. High Energy Phys. 04 (2014) 138.

[58] K. Redmond, A. Trezza, and A. L. Erickcek, Phys. Rev. D **98**, 063504 (2018).

[59] K. R. Dienes, L. Heurtier, D. Hoover, F. Huang, A. Paulsen, T. M. P. Tait, and B. Thomas (to be published).